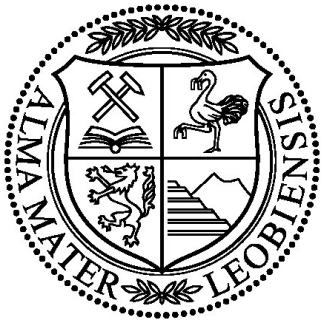

University of Leoben

Department Mineral Resources Engineering
Chair of Mineral Processing

DIPLOMARBEIT

Material flow analysis of a Seawater Magnesia Process with particular Focus on Silicate Phases

Master Thesis of:
Michael Paul Messner

Supervision of the University:
Ass.Prof. Dipl.-Ing. Dr.mont. Andreas Böhm

Supervision of RHI AG:
Dipl.-Ing. Dr. rer. nat. Christoph Piribauer

Leoben, February 2016

AFFIDAVIT

I declare in lieu of oat, that I wrote this thesis and performed the associated research myself, using only literature cited in this volume.

EIDESSTATTLICHE ERKLÄRUNG

Ich erkläre an Eides statt, dass ich diese Arbeit selbstständig verfasst, andere als die angegeben Quellen und Hilfsmittel nicht benutzt und mich auch sonst keiner unerlaubten Hilfsmittel bedient habe.

Datum Unterschrift

ABSTRACT

To meet the requirement of a process description with focus on silica impurity distribution on material streams of a seawater magnesia production plant of RHI Normag AS in Norway, a detailed investigation was performed. Aside from the preparation of a material balance for silica bearing mineral phases, proposals for their removal with respect to magnesia losses should be given. A sampling campaign covering one week of production provided the data base. Samples of slurries and solids were transported to Leoben, further processed at the Chair of Mineral Processing (Montanuniversität Leoben) and prepared for chemical and mineralogical analysis. Based on the assays and the accompanying mineralogical investigation, a chemical mineralogical phase model of every material stream as well as a material balance was created. Further processing steps were carried out to characterize the separation efficiency and show up enrichments of impurities in the feed of purification steps. With the finished balance it was possible to follow the way of silicate bearing mineral phases through the process. Together with the characterisation of the purification efficiency and SiO_2 distribution on size classes in the feed streams, using the Henry Reinhardt charts, the results of the thesis describe the prevailing process conditions at the time of sampling and serve as basis for further optimization.

KURZFASSUNG

Zur Prozessbeschreibung einer Produktionsanlage für Magnesia aus Meerwasser bei RHI Normag AS in Norwegen, wurden detaillierte Untersuchungen durchgeführt mit dem Schwerpunkt die Verteilung der SiO_2 haltigen Mineralphasen auf die Stoffströme darzustellen. Ziel war es neben der Erstellung einer Stoff- und Mineralbilanz, Vorschläge für die Entfernung der Verunreinigungen mit geringstem MgO Verlust zu erarbeiten. Datenbasis bildete eine einwöchige Probenahmekampagne vor Ort. Die Trübe- und Feststoffproben wurden nach Leoben transportiert und im Labor des Lehrstuhls für Aufbereitung verarbeitet und für die chemische und mineralogische Analyse vorbereitet. Auf Basis der chemischen Analysen und unterstützender mineralogischer Untersuchungen wurde ein chemisch-mineralogisches Phasenmodell für die einzelnen Materialströme und in weitere Folge eine Materialbilanz erstellt. Die Stoffbilanz erlaubt den Weg der SiO_2 haltigen Mineralphasen durch den Prozess zu verfolgen. Die Trenneffizienz der Reinigungsschritte sowie der Anreicherung von Verunreinigungen wurden mit Hilfe von Teilungskurven dargestellt. Zusammen mit der Darstellung der Verwachsungsverhältnisse der silikatischen Verunreinigungen im Aufgabegut mit Hilfe des Henry Reinhardt Schaubildes, beschreiben die Ergebnisse der Diplomarbeit die vorherrschenden Prozessbedingungen zum Zeitpunkt der Probenahme und dienen als Grundlage für zukünftige Optimierungsschritte.

AKNOWLEDGMENTS

I would like to express the deepest appreciation to my supervisor Prof. Andreas Böhm, who always found a moment of time for my concerns during the preparation of this thesis, for the patience and especially for his continuous input of mineral processing expertise.

Furthermore I would like to thank RHI AG for sponsoring and giving me the opportunity to write my master thesis about a processing topic in one of their plants. Therefore special thanks to Dr. Christoph Piribauer for his general supervision, the implementation of the chemical/mineralogical analysis and his assistance during the stay in Norway.

My sincere thanks also goes to the Chair of Mineral Processing for giving me access to the laboratory and research facilities, particularly to Prof. Helmut Flachberger for the initiation and the support on the way.
I thank the laboratory staff and participants in my survey, who shared their precious time during sample processing. Special thanks to Anna Balloch for her helping hand with the sieve analysis.

Last but not least I would like to thank my family, my parents Paul and Reinhild who guaranteed a basic prerequisite for my studies and always gave me helpful advice and my loved Patricia who pushed me forward and encouraged me throughout my studies and in my life in general.

TABLE OF CONTENTS

LIST OF FIGURES

LIST OF TABLES

1 Introduction

1.1 General Introduction

Magnesia is a very important industrial material. Magnesium oxide (MgO) or also called periclase does not occur in greater amounts naturally. The term periclase normally refers to the mineral, but it can be also used for synthetic magnesium oxide. Its main production volume is used in the refractories industry for the construction and maintenance of steel and other furnaces. Magnesia can be employed as grained material, in the form of refractory bricks or as chemical addition in the manufacturing of chrome olivine and other refractories [1]. The industrial importance of magnesia is due to its high degree of refractoriness, reasonable hydration resistance and good chemical stability in basic environments at elevated temperatures. Magnesium hydroxide, also called brucite is another industrial material used as magnesium source for the refractory industry. Brucite occurs naturally in bigger deposits and is therefore often directly mined. For higher product quality requirements magnesium hydroxide is produced synthetically. Because of its flame retardant properties, brucite is mainly employed as additive in coatings and as filling material. Nevertheless a big part of synthetic magnesium hydroxide is calcined to magnesia. Currently, magnesia for refractory materials is produced from natural magnesite by calcination or from seawater and magnesium-rich brines by precipitation of magnesium hydroxide with bases like lime from limestone or dolomite [3]. In seawater, magnesium is the third most abundant element behind sodium and chlorine and has an average concentration of approximately 1300 ppm. With an average content of 1.3 kg per ton seawater, a reliable magnesium source for the process of precipitation was found and used since the early 1930s. Besides magnesium some of the other major constituent ions are sulfate, calcium and potassium.

Table 1: Composition of Seawater [4]

Element	Abundance [ppm]	Principal Species
Cl	19353	Cl^-
Na	10760	Na^+
Mg	1294	Mg^{2+}, $MgSO_4$
S	812	SO_4^{2-}
Ca	413	Ca^{2+},
K	387	K^+
Br	67,3	Br^-
C	28	HCO_3^-,H_2CO_3, CO_3^{2-}
Sr	8	Sr^{2+}, $SrSO_4$
Br	4,6	$B(OH)_3$, $B(OH)_2O^-$
Si	3	$Si(OH)_4$, $Si(OH)_3O^-$
F	1,3	F-, MgF_2
salinity of seawater is ~ 3,5%		

Table 2: Composition of dolomite from XRF

Element	Abundance [%]
Na_2O	0,02
MgO	40,16
Al_2O_3	0,10
SiO_2	1,89
P_2O_5	0,01
SO_3	0,11
K_2O	0,01
CaO	57,47
TiO_2	0,01
Cr_2O_3	0,01
Fe_2O_3	0,20
ZrO_2	0,01
total	99,99

Production of magnesia from seawater is a well-known industrial process. A significant portion of the world magnesia supply is produced by precipitation. High availability of inexpensive starting materials and great purity of the product makes precipitation from seawater magnesia an economically significant process [2]. This process is continuous, with constant feeding of raw materials and manufacturing of a product. It involves the extraction of dissolved magnesium from seawater by precipitating magnesium hydroxide with lime or dolomite lime. The precipitate is then washed, purified and calcined to form magnesia [3]. The use of dolomite lime or so called dolime holds some advantages over the use of high-calcium lime from limestone, in that half the volume of seawater is required per ton of magnesia since half of the magnesia is derived from dolime [4]. Precipitating magnesia from seawater and dolomite lime is a way of producing a high quality product, because of the consistency of the process and very little variation in the product composition. Magnesia from seawater is therefore often preferred to magnesias from magnesite. Nevertheless, the raw materials must be carefully controlled, because the purity of the dolomite is crucial for the purity of the end product magnesia. Depending on the application, industrially produced magnesia can be found in different types varying in their physicochemical properties. Calcining conditions, characterised by temperature, significantly influence the pore volume and therefore the reactivity. The three main types are caustic calcined magnesia (CCM), “dead burned” or sintered magnesia and fused magnesia. While caustic magnesia is carefully burned around 800°C, sinter magnesia is calcined at higher temperatures up to 2000°C. Fused magnesia is produced at temperatures over the melting point of periclase at 2800°C in the electric arch furnace. Especially in the case of fused magnesia, it is obvious that a product with such a high input of energy needs a raw material with a minimum in unfavourable impurities. A refractory product with high melting point can only be produced by manufacturing magnesia with great purity. The major contaminants in the final product derived from raw materials are SiO_2, Al_2O_3, Fe_2O_3 as well as CaO and $CaCO_3$. Because some impurities significantly influence the quality of the refractory product by lowering the solidus temperature, it is important to keep the total input low and remove them at certain steps during the production process. Since most of the impurities origin from dolomite associated minerals, knowledge about their chemical and mineralogical properties is essential. Also seawater can add impurities to the process, which can occur either as solids, like sand and fine silt, or as in the case of boron and bicarbonate in a dissolved state.

1.2 Objective

The focus of this master thesis lies on silica contamination of the magnesia production at a seawater magnesia plant of RHI Normag AS in Porsgrunn, Norway. The plant is located at the peninsula of Herøya industry park, which is also home of several other industrial producers. The site is close to the sea, so supply of seawater is guaranteed and dolomite is shipped from a quarry. Freshwater is pumped from nearby lakes, which assures a constant supply. Especially due to the production line for high quality fused magnesia, it is from great interest to achieve a minimum in silica contamination. In the actual process used in Porsgrunn, the dolomite is purified from silicates in the dry as well as in the wet process line. Nevertheless the produced

quality could have a lower silica contamination. In this thesis the way of silicate bearing mineral phases through the production process shall be investigated. The results shall form the basis for the creation of a balance model, which describes the silica material flows in the plant. The efficiency of selected silica separation systems shall be described. Based on the results, possible technical solutions for further silica reduction should be discussed.

1.3 Summary

In the preparatory phase all available information about the seawater magnesia process was collected and evaluated. Therefore available literature was studied and a first material balance model was created by reviewing flow charts of the process. Additionally several meetings were performed to collect more information about the situation in the plant. In the next step a sampling campaign was planned. Based on the first material balance model, sampling points for material streams were identified and the sampling conditions specified. At the beginning of June, 2015 a ten day trip to the plant in Porsgrunn, Norway was carried out. The sampling program was performed in a one week sampling period. At each sampling point in the dry (raw dolomite drying and calcining) and wet process (slaking, $Mg(OH)_2$ precipitation and purification) single samples were taken and combined to daily bulk samples. After finishing the sampling campaign, the material was packed and sent to the laboratory of the Chair of Mineral Processing in Leoben, Austria. The sampling campaign is described in chapter 4.

In the next step, the sample material was processed to create samples for the chemical/mineralogical analysis. Therefore the samples were divided, filtrated and washed free of soluble components for the analysis. Besides, the content of solid and soluble components was measured. To illustrate enrichments of impurities in material streams by Henry Reinhardt diagrams, the feed of purification steps was investigated. Therefore raw dolomite (feed dry process), slaked dolime (feed wet process) as well as underflow of the primary thickener (feed cyclones) were separated in grain size classes by screening and sedimentation methods and every size class chemically analysed. To evaluate the separation efficiency of purification aggregates in the wet process, partition numbers were used. The data was created by wet screening.

In a short mineralogical investigation the assumptions for the SiO_2 bearing mineral phases, quartz and mica (phlogopite-annite series) were verified by microscopy techniques. Therefore stereo as well as transmitted light microscopy was used. Additionally an EDX analysis was performed by RHI. The data supported the assumption, since mineral phases with properties according to the proposed ones (quartz and mica) were found. Details on the composition of the mica phase as well as the transferring equation are given in chapter 6 and Appendix C.

With the results of the chemical analysis in a first step, the content of SiO_2 bearing mineral phases was calculated. Then a balance model was created by combining results from chemical and mineralogical assay and measured flow rates from process data. Therefore three single balances were first calculated individually and subsequently combined. With this model it was

possible to illustrate the material flows through the plant beginning at the feed of dolomite and finishing with the filter cake of the vacuum filters. For verification an alternative overall equalization calculus was performed which was not successful (not included in the thesis).

According to the material balance, with progress of the process the content of quartz as well as mica is reduced. Overall, the process is more efficient in reducing quartz (99,95% reduction) than mica (81,02% reduction). The chemical and mineralogical analysis of vacuum filter cake as final product of the balance supports this result, since mica is the dominant impurity. The separation efficiency interpreted from partition numbers (Chapter 7.3 and Appendix H) shows a separation grain size for the sand separator of 235 µm which seems reasonable for the used technique (rake classifiers) and is in good agreement with the SiO_2 distribution on the size classes of the feed stream (mixer / reactor overflow) depicted in the Henry Reinhardt chart, given in chapter 7.4. For the cyclone system a separation grain size of 210 µm was found, which seems to be too high. By using the mass distribution of separation products from the balance in combination with the Henry Reinhardt diagram, a lower separation grain size of 85 µm is found. Overall the Henry Reinhardt charts show an enrichment of mica in the fines (<360 µm) of dolomite while quartz and mica are equally distributed over the size classes. In the wet process an enrichment of SiO_2 as well as mica and quartz is found in the coarse fraction of slaked dolime (>200 µm) and primary thickener underflow (>25 µm).

Since the main purpose of the sampling campaign of this thesis was to obtain material stream data of the whole process for creation of the silicate balance, no detailed sampling campaign of single apparatus was performed. Based on the problems in balancing large mass streams by means low contents (<2 m-%) and the rather large variance of assay data, further sampling campaigns should be concentrated on smaller balance areas (e.g. the cyclone system) for improved insight.

Nevertheless the cyclone system doesn't seem to work ideal, since a high separation grain size indicates problems in the performance. According to the accumulation of mica in the vacuum filter cake combined with the enrichment of mica in the coarse fraction of the cyclone feed, wet screening could be considered as alternative process.

2 Process Description

The production of magnesia from seawater is in general a simple and well known process. Because of their sufficient availability, seawater and carbonate rock like dolomite are used as raw materials for the production process of magnesia. Additionally low raw material costs and the high quality of the final product make seawater and dolomite to an eligible source of MgO. In Figure 1 an overview of the caustic calcined as well as fused magnesia production process in Porsgrunn is illustrated. For better understanding, the seawater process is divided into a dry process, which is mainly calcination of dolomite and a wet process with the precipitation of magnesium hydroxide, separation of impurities and filtration. Figure 2 visualises the process as flow diagram in single steps starting with homogenised dolomite and ending with the vacuum filter pulp as feed for the final calcination in the rotary kiln. In the following paragraphs, the single steps are described more in detail.

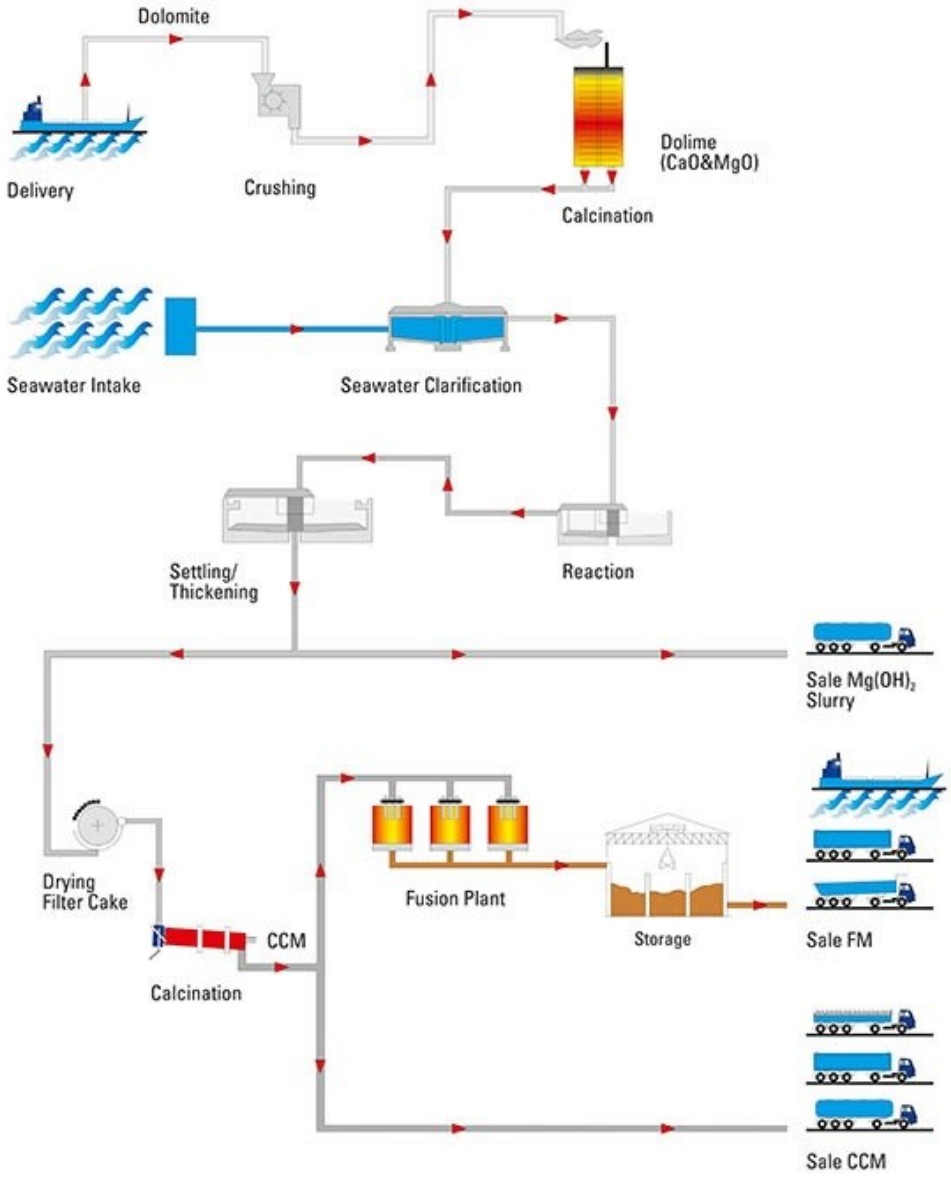

Figure 1: Seawater process at RHI Normag AS [8]

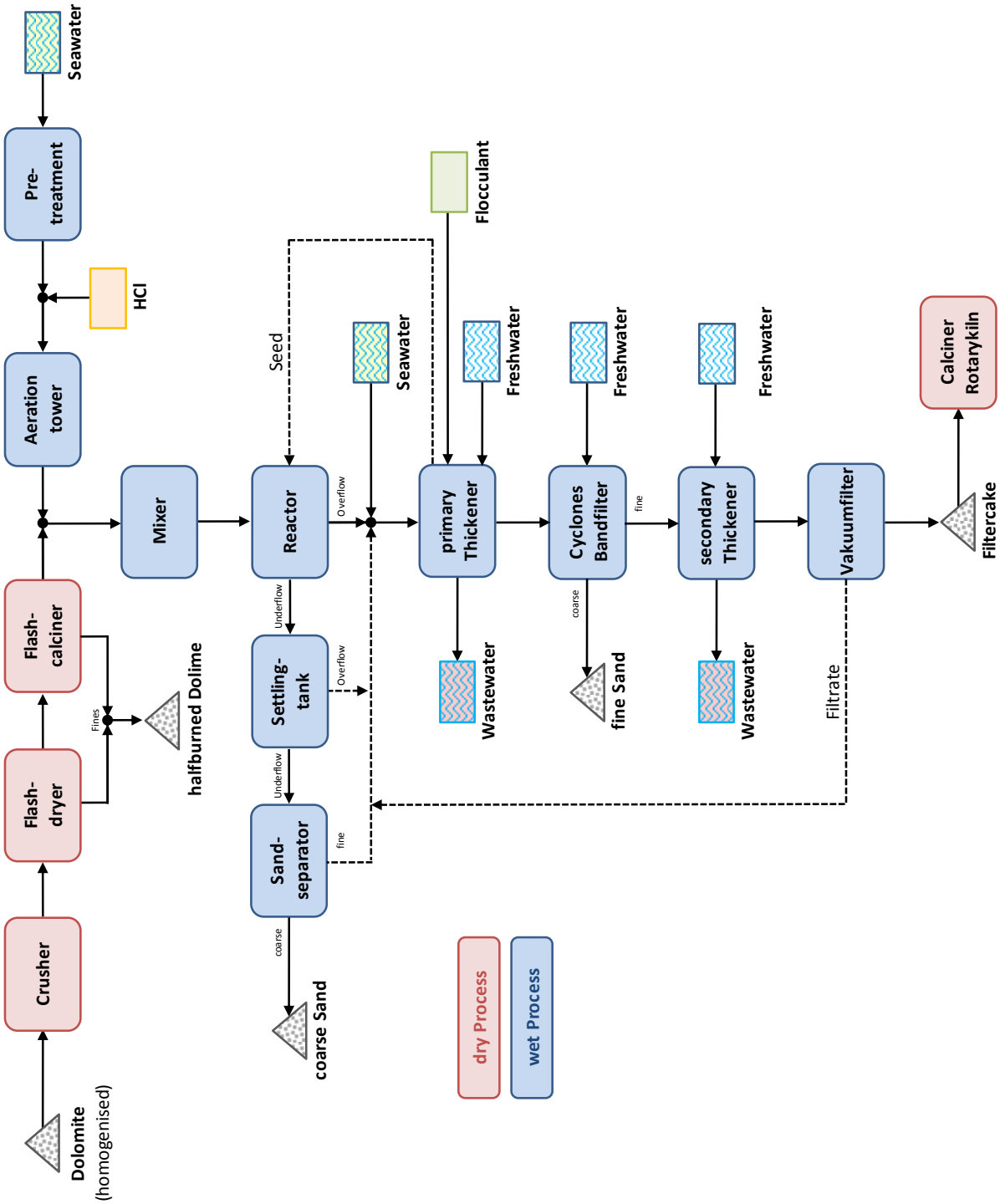

Figure 2: Process flow diagram

2.1 Dry Process

2.1.1 Drying

In a first step as preparation for the wet process, already selectively mined, crushed and homogenised dolomite is dried and calcined. The material is first pre-screened at 13 mm mesh size. The fine material <13 mm is forwarded to the flash dryer, while the coarse material is crushed in an opened circuit by a cone crusher and then added to the fines. Since liberated silica impurities are enriched in the fines, fine material is removed after drying by air classification on the top of the flash dryer. The fines from this classification step are later in the process mixed with fines from the calcination process. Coarse dry and dedusted dolomite is sieved on a 2mm screen. The fraction <2 mm is fed to the calciner. The coarse fraction is crushed in a cone crusher and then added to the flash dryer feed.

2.1.2 Calcining

Dolomite is calcined in a flash calciner at approximately 1000°C. According to the reaction equation (1), the product of the calcination process is dolomite lime or so called dolime. The carbonate dolomite releases CO_2 and dolime which mainly consists of CaO and MgO remains. At this point it is necessary to mention that the calcination temperature has an essential influence on the slaking ability of the calcined product with water and therefore also on the following precipitation reaction in the wet process. It is important to produce dolime of correct reactivity. If dolomite is burned at too high temperatures, the reaction with water is slow and high amounts of unreacted dolime can be found in the waste material. On the other side, if dolomite is burned at too low temperatures, the reactivity is bad and raw material is lost unreacted as waste material. This could also result in a carbonate impurity in the final product. Another problem with high calcination temperatures and impurities like SiO_2, Al_2O_3 and Fe_2O_3 in dolomite is the possible formation of calcium silicates and calcium aluminoferrite. While slaking, insoluble hydrates could be formed, which remain as insoluble impurities.

$$CaMg(CO_3)_{2\,(s)} \rightleftharpoons MgO \cdot CaO_{\,(s)} + 2CO_{2\,(g)} \qquad \text{(1) Calcination of dolomite}$$

The product of the flash calciner is pneumatically transferred to silos for further use as dolime in the wet process. Fine material that results from dedusting during the calcination process is mixed with the fines from the flash dryer. This so called “half burned” dolime is dumped as waste material.

Figure 3: Calciner in Porsgrunn [9]

2.2 Wet Process

In the wet process the precipitation and purification is performed in several steps. Therefore dolime has to be first slaked and then mixed in an additional step with more seawater. Slaking is done in the mixer, which is actually a feeding pipe in the centre of the reactor/hydro separator. Dolime is fed to the mixer/reactor from storage silos. By adjusting the weight, the feed is precisely controlled. In the plant in Porsgrunn three hydroseparators are installed, whereby two of them (Hydroseperator A and C) are in use. In principle a hydroseparator is a cylindrical tank with agitator and rakes. It is very similar to a circular thickener, except for a smaller diameter. It is mainly used to separate coarse, fast settling particles from the mixture. The rakes move coarse particles to the centre of the hydro separator, where they are removed. These are mainly unreactive agglomerations like non- or over calcined residuals of dolomite and silica bearing mineral phases like quartz and mica.

Figure 4: Overflow hydro separator

2.2.1 Slaking

The hydrating/slaking reaction is very fast and exothermic. As described in reaction equation (2), CaO from dolime reacts with water to form calcium hydroxide $Ca(OH)_2$, which raises the pH-value of the mixture to approximately 12,5. Magnesium oxide is nearly insoluble in water and remains as MgO, while $Ca(OH)_2$ is dissolved. When dolomite is calcined at high temperatures, a layer of "dead burned" MgO is formed on the surface of the particle [1]. Even if some parts of MgO react with water and form hydroxide, it is instantly precipitated at the surrounding pH conditions. In principle the slaking process dissolves soluble and disperses insoluble parts of dolime, more precisely MgO in a very fine grained suspension.

$$MgO{\cdot}CaO_{(s)} + H_2O_{(l)} \rightleftharpoons MgO_{(s)} + Ca(OH)_{2\,(aq)} \qquad \text{(2) Hydration of dolime}$$

2.2.2 Precipitation

In the hydro separator the first part of magnesium precipitates from seawater. According to reaction equation (3), magnesium ions in seawater react with calcium hydroxide from the solution and form magnesium hydroxide. Because of its poor solubility at the surrounding pH conditions $Mg(OH)_2$ precipitates and forms a suspension of fine crystals, while calcium ions remain in solution. Since the process is done in an excess of dolime, so called "over liming", there is still calcium hydroxide available to precipitate magnesium ions. Therefore the overflow of the hydro separator is mixed with additional seawater in a chute on the way to the primary thickener. This process of secondary precipitation is called "seawater washing".

$$Ca(OH)_{2\,(aq)} + \begin{matrix} MgSO_{4\,(aq)} \\ Mg_2^{+}{}_{(aq)} \\ MgCl_{2\,(aq)} \end{matrix} \rightleftharpoons Mg(OH)_{2\,(s)} + \begin{matrix} CaSO_{4\,(aq)} \\ Ca_2^{+}{}_{(aq)} \\ CaCl_{2\,(aq)} \end{matrix} \qquad \text{(3) Precipitation}$$

For precipitation of magnesium hydroxide, the reaction conditions can significantly influence the properties of the precipitate, which has a direct impact on further production steps. Adding seed crystals to fresh slaked dolime by inserting slurry from the primary thickeners, nuclei for $Mg(OH)_2$ crystal growth are allocated. This step helps to form bigger crystals, which will produce a precipitate with improved settling and filtration properties. Also diluting seawater for seawater washing with used process water supports the formation of larger crystals.

2.2.3 Seawater Pretreatment

Seawater cannot be used without pre-treatment in the process. Before it is fed to the process, fine sand and silt are removed in settling tanks. Additionally to solid impurities, seawater contains naturally calcium bicarbonate, which can react with $Ca(OH)_2$ from slaked dolime and form insoluble calcium carbonate, as seen in reaction equation (4). This would lead to a lime contamination in the final product.

$$Ca(HCO_3)_{2\,(aq)} + Ca(OH)_{2\,(aq)} \rightleftharpoons 2CaCO_{3\,(s)} + 2H_2O_{\,(l)} \quad \text{(4) Precipitation of calcium carbonate}$$

To prevent this effect, seawater is degassed. Acid is added to lower the pH-value to approximately 4, which results in a release of carbon dioxide. Therefore seawater is mixed with hydrochloric acid and fed to an aeration tower. Here CO_2 gas is removed from sprinkled seawater by a counter current of air. As seen in reaction equation (5), after seawater degassing only calcium chloride, which is originally present in seawater remains.

$$Ca(HCO_3)_{2\,(aq)} + 2HCl_{\,(aq)} \rightleftharpoons CaCl_{2\,(aq)} + 2CO_{2\,(g)} + 2H_2O_{\,(l)} \quad \text{(5) Seawater degassing}$$

2.2.4 Sand Separator

From the hydro separator, two material streams are generated. Fine material is found in the overflow, while coarse material settles and is therefore found in the underflow. These coarse particles are further processed to remove contaminations from the product. Therefore the reactor underflow is fed to a settling tank. The overflow of the settling tank is combined with the overflow of the reactor, while the underflow is periodically, about three to four times a day, fed to a sand separator. In the sand separator material is separated in two stages by settlement and is removed by rakes. The working principle is similar to a screw classifier. The sand is then dumped as waste material, while the overflow is fed back to the reactor.

Figure 5: Sand separator I/ rake classifier

Figure 6: Sand separator II

2.2.5 Primary Thickener

After seawater washing, the material is split into two streams and fed to two primary thickeners (A and B). The large area (diameter appr. 38 m; surface appr. 1100 m^2 per thickener) and the capacity is needed to provide enough settling area and time for compaction of magnesium hydroxide precipitate before it is removed. For faster sedimentation an organic flocculant is added. The primary thickener is additionally to thickening also a washing stage for the precipitate. Freshwater, which is added continuously serves as wash water to remove soluble components which are mainly salt from seawater and calcium hydroxide. It is important to remove any excess of $Ca(OH)_2$, because of the high pH-value it can react again with CO_2 from air and precipitate as calcium carbonate. This would result in a carbonate contamination in the final product, as seen in reaction equation (6). The overflow of the primary thickener leaves the system as wastewater and the underflow is fed to the cyclones. A small part of the underflow is fed back to the reactor as seeding material, to gain bigger $Mg(OH)_2$ crystals.

$$Ca(OH)_{2\,(aq)} + CO_{2\,(g)} \rightleftharpoons CaCO_{3\,(s)} + H_2O_{\,(l)} \qquad (6)$$ Precipitation of calcium carbonate

Waste water from the process still contains a small amount of magnesium, which is lost. The pH-value is due to calcium hydroxide high, which would make neutralisation necessary. Since most of the other companies at Herøya Industry Park produce acid waste water, it is discharged through the waste water system.

2.2.6 Cyclone System

The combined underflow of the primary thickeners A and B is fed to the cyclone system. Cycloning is done in 5 steps with 68 cyclones in a circuit as shown in Figure 8. At every pump sump of the cyclones freshwater is added, which has the effect of reducing the solid concentration and is an additional washing step. The sixth step is only a dewatering step of coarse material before the material is fed to a band filter, as seen in Figure 9. While the filter cake is dumped as waste material, the filtrate is recycled with the water from the sixth step to the seawater washing. The fine product of cycloning is fed to the secondary thickener. Cycloning is done to remove impurities that were not removed by the sand separator.

Figure 7: Cyclone system I

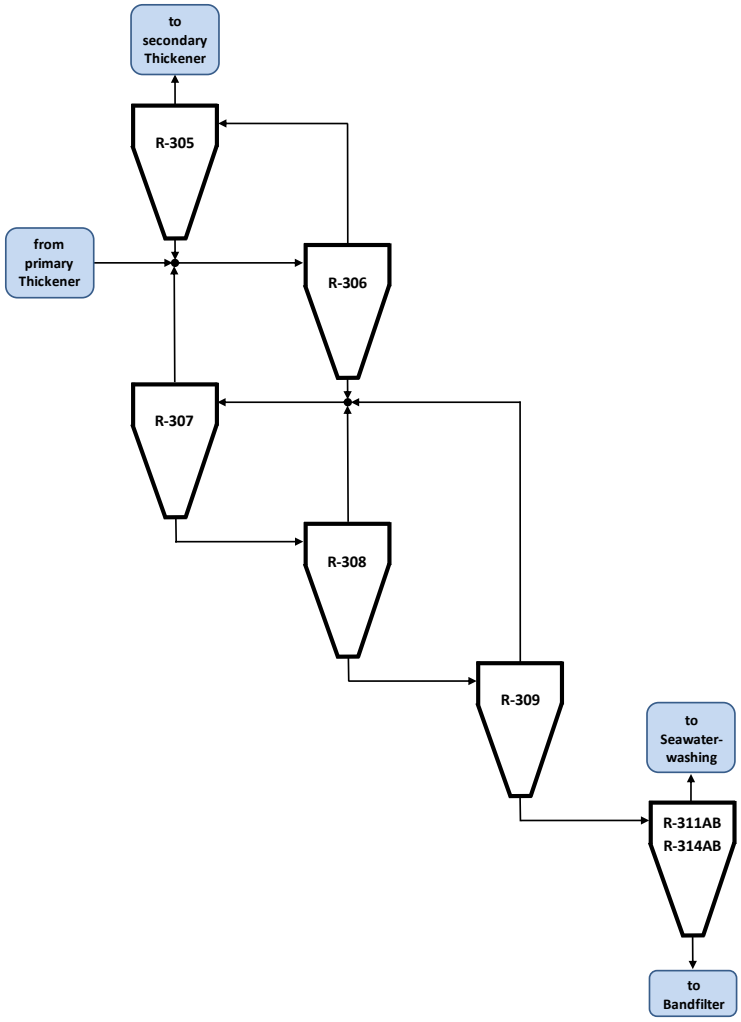

Figure 8: Cyclone system II

Figure 9: Band filter and dewatering cyclones

2.2.7 Secondary Thickener

Similar to the primary thickener, material in this step is not only thickened, but also washed with fresh water again. The overflow of the secondary thickener leaves the system as wastewater, while the underflow reports to the vacuum filters for further dewatering.

2.2.8 Filtration

The pulp of the secondary thickener is first steam heated and then filtered on large vacuum filters. Those vacuum filters are rotary drum filters without washing zone. Since magnesium hydroxide precipitate is very difficult to filter, the filter cake has still a high water content of around 50%. The consistence of the filter cake is paste like and sticky, therefore permanent washing of the conveyor belt is necessary to prevent blockages. For handling the pulp and because of the following calcination step, a minimum water content is aspired. The washing water from cleaning the conveyor belt is collected and fed together with the filtrate of the vacuum filters as process water to the seawater washing stage. The filter cake is fed as main product to the rotary kiln for calcination.

Figure 10: Filter cake

2.3 Calcination

Just for completeness the calcination of the magnesia is mentioned shortly. After filtering the filter cake is directly fed to the rotary kiln. There it first gets dried and at higher temperatures in the oven, the actual calcination step takes place. According to reaction equation (7), the magnesium hydroxide forms magnesium oxide which is as caustic calcined magnesia (CCM) a final product of the production process.

$$Mg(OH)_{2\,(s)} \rightleftharpoons MgO_{\,(s)} + H_2O_{\,(g)} \qquad (7)$$ Calcination of magnesium hydroxide

In general the process of magnesia precipitation from seawater with dolime can be described with previously mentioned steps. Since this thesis is mainly dealing with silicate contaminations, the focus lies in the reduction of those contaminations. There are three points in the process, where waste material is removed, the fines of the flash dryer and flash calciner in the dry process and in the wet process the sand separator sand and the coarse material of the cyclone system.

3 Impurities

Magnesia precipitated from seawater is in comparison to magnesia from other mineral sources from higher quality. Nevertheless impurities from raw materials as well as contaminations from the production process can be found. Because of its use in the refractory industry, some of the impurities have a significant influence on the properties of the final product. Therefore raw materials have to be selected carefully and their quality controlled frequently. The main impurities are SiO_2, Al_2O_3, Fe_2O_3 as well as CaO, $CaCO_3$ and boron. This thesis is focussed on contaminations by silica, nevertheless for completeness, the other impurities are shortly mentioned.

3.1 Impurities from Dolomite

Impurities originating from the dolomite ore are mainly based on silica. The contaminating mineral phases contain SiO_2 in the form of quartz and mica group phyllosilicates especially phlogopite $KMg_3AlSi_3O_{10}(F,OH)_2$ and annite $KFe_3AlSi_3O_{10}(OH,F)_2$ (see chapter 6 Mineralogical Investigation). Also sulphide minerals like pyrite may occur accessorily. Both, quartz and mica stay inert during slaking and are enriched in the waste material of the purification steps but remain to some extent also in the product.
Apart of the chemical and mineralogical composition of dolomite, calcination conditions are also critical for the production of a dolime suitable for subsequent reaction with seawater. Dolime produced initially from dolomite must be of good reactivity, as any uncalcined dolime will not react with seawater and remain as a contamination in the product, while overburning would result in poor slaking ability because the reactivity of dolime is too low for sufficient reaction with seawater. Correct calcination of dolomite significantly reduces the quantity of material being removed by the classification systems in the wet process and therefore going to waste [1][4].

Another problem of high calcination temperatures is the formation of calcium silicate and calcium aluminoferrite, which once hydrated with water form insoluble impurities. These contaminations can appear while using dolomite with high natural SiO_2, Al_2O_3 and Fe_2O_3 levels when directly calcined.

3.2 Impurities from Seawater

Even when seawater is very stable in its composition, it can contain contaminations and has to be treated before it is used for slaking dolime. Seawater is slightly alkaline with a pH about 8 and buffered by the carbonate system by exchanging CO_2 gas with the atmosphere. It naturally contains calcium bicarbonate which can react with $Ca(OH)_2$ from slaked dolime and precipitate as insoluble calcium carbonate which leads to a lime contamination in the final product. To prevent this effect, seawater is degassed with hydrochloric acid in an aeration tower.

Silica impurities in seawater can originate from fine suspended particles like silt and sand. Although seawater inlets are sited in sheltered areas, some very fine sand is inevitably drawn into the system and in heavy storms silica contamination can rise [1].

Boron is found in seawater in the form of non-dissociated orthoborate acid. Because of its properties as flux agent, the level of boron has to be reduced, especially when the magnesia product is used for the refractory industry. Precipitated magnesium hydroxide has a high capacity for absorbing boron. By rising the pH-value with an excess of lime, so called “over liming”, the absorption effect can be reduced on expense of lime contamination.

4 Sampling Campaign and Material Balance

The main objective of the sampling campaign was to collect sample material of the sweater magnesia process to describe the material streams by means of a material balance. This balance shall make the way of silicate bearing mineral phases through the production process traceable and shall especially reveal their behaviour in purification steps. To realize this idea, a first simplified flowsheet for the whole process had to be created in the preparatory phase. Therefore detailed flowsheets and descriptions of the seawater magnesia plant were examined (for flowsheets see Appendix A). The overall process was simplified to the first balance model, based on material streams. This model was presented and accepted by RHI. The model contained, as shown in Figure 11, all essential production steps of the plant including single apparatus and process groups. It starts with the feed of raw materials and ends with the feed of the rotary kiln. The material balance serves primarily to understand the material flows but also as calculation basis for further characterisation of single apparatus.

According to the first material flow balance model, the sampling campaign was planned. Therefore the sampling points were defined (and agreed in a meeting) and a sampling procedure was elaborated, which had to balance theoretical requirements on optimal sampling and technical possibilities in the plant. All ingoing and outgoing material streams of the balance had to be analysed for their chemical and mineralogical properties. Therefore it was on one hand crucial to take a sufficient sample mass for the performance of those measurements and on the other hand most representative samples had to be taken. Since the variations in the material stream compositions were not known and therefore the confidence limits couldn't be determined, the sample masses and numbers had to be estimated. To perform the sampling campaign with respect to all principles of accurate sampling, attendance was paid to the sampling mass, grain size and the homogeneity of the material. The most critical sample was dolomite, since it had a grain size up to 13mm. The sample mass for a bulk sample was estimated to be 12,6 kg made of three 4,2 kg single samples, according to chemical analysis of a dolomite sample from a previous project (see Appendix F). Since all other samples had a smaller grain size, the sample masses needed to be the same or less. The number of samples that could be taken each day per sampling point was limited, since sampling of twenty-five sampling points in the whole plant was only possible in two cycles during one shift. The evaluation of the material stream homogeneity and therefore the exact place and way of sampling was done on site.

Some material streams had a solid content in a range of some mass percent, so sample volumes up to ten litres were planned. It was therefore decided to use plastic canisters up to 25 litres for liquid and 5 litre buckets for solid samples. To perform the sampling campaign, a 10 day stay in Porsgrunn was arranged. It was organised, that after finishing the sampling campaign, the samples were sent to the laboratory of the Chair of Mineral Processing in Leoben for further analysis. The chemical and mineralogical measurements were planned to be done at the RHI Technology Centre. In Porsgrunn a stuff member organised the sample containers and material for sampling.

The sampling campaign was performed in a period of one week (11.-17. June, 2015). At the dry process, samples were taken on the first, sixth and seventh day because of a calciner standstill. This interruption nevertheless had no influence on the wet process, where sampling was done in a daily interval. In general at every sampling point two single samples were taken per day at a time distance of four to five hours and combined to a bulk sample. Samples from freshwater and seawater were taken daily only once.

In Table 3 the planned minimum sample mass of every sampling point is listed. In the following paragraphs, the sampling points are illustrated. The flow charts of the process, attached in Appendix A, include the exact position of the sampling points. The process data of the production process, including feeding rates of material streams are saved on a server for a longer period of time. Since data could be checked from Leoben, data collection was not done during the sampling campaign.

Table 3: Sampling points

name	indication	quantity per day
1DOL	feed dolomite <13mm	20 kg
3DOLG	dolomite coarse	20 kg
4DOLIME	dolime / feed wet process	10 kg
20INT	dolomite feed sieve	10kg
21HB	dolomite fines halfburned dolime fines	1kg
6SW	feed seawater	0,5 l
7OHSA	overflow hydroseperator A	10 l
7OHSC	overflow hydroseperator C	10 l
8UHSA	underflow hydroseperator A	1 l
8UHSC	underflow hydroseperator C	1 l
23U8M	underflow 8m tank	1 l
9SSS	sand from sand separator	1 kg
11FPT	feed primary thickener	10 l
12OPTA	overflow primary thickener A	1 l
12OPTB	overflow primary thickener B	1 l
13UPTA	underflow primary thickener A	5 l
13UPTB	underflow primary thickener B	5 l
14FW	freshwater for prim. thickener freshwater for cyclones	0,5 l
15FST	feed sec. thickener	10 l
16FBF	feed cyclones bandpassfilters	5 l
17CBF	filtercake bandpassfilter	1 kg
18UST	underflow sec. thickener	1 l
19CVF	filtercake vacuumfilter	1 kg
22FVF	filtrate vacuumfilter	1 l
24OST	overflow sec. thickener	1 l

4.1 Balance Model for Sampling Campaign

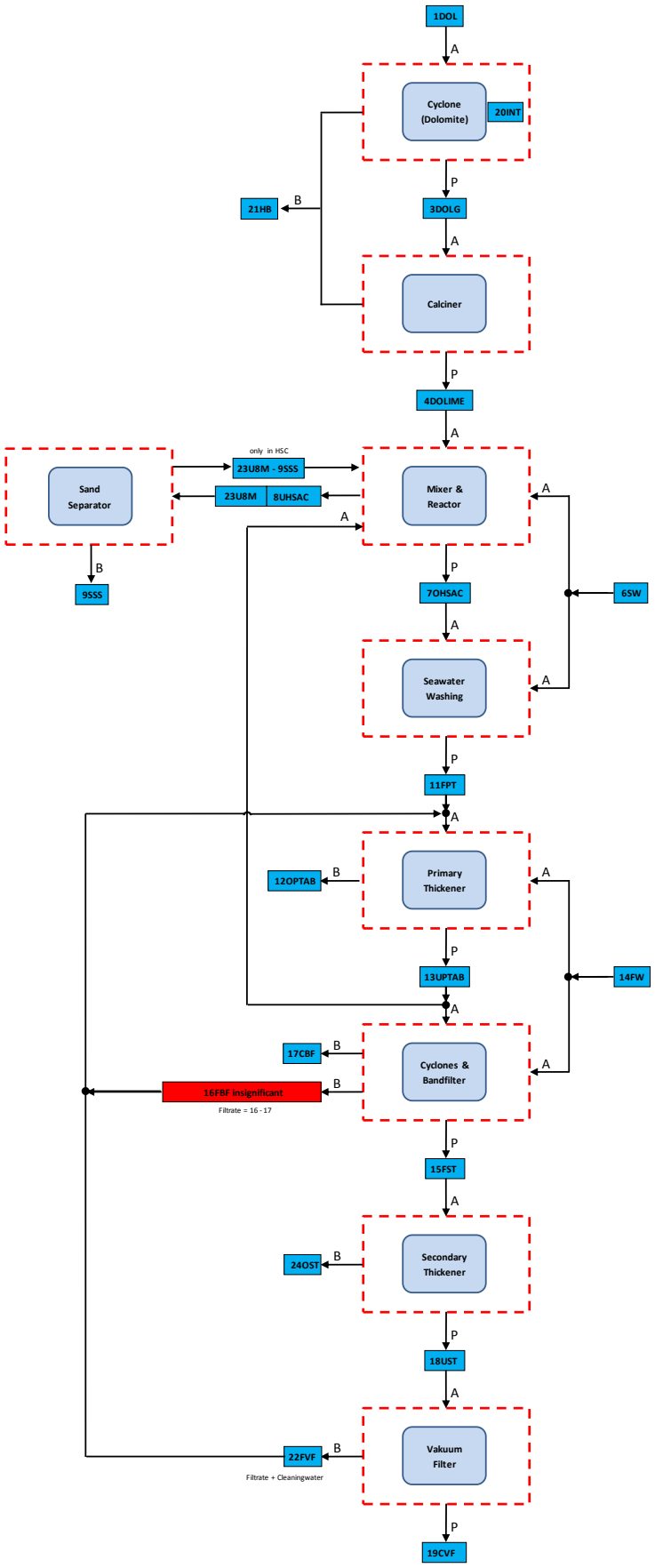

material flow		
1DOL	feed Dolomite <13mm	
3DOLG	Dolomite coarse	
4DOLIME	Dolime / feed wetprocess	
20INT	Dolomite feed sieve	
21HB	Dolomite fines	halfburned
	Dolime fines	
6SW	feed seawater	
7OHSA	overflow hydroseperator A	
7OHSC	overflow hydroseperator C	
8UHSA	underflow hydroseperator A	
8UHSC	underflow hydroseperator C	
23U8M	underflow 8m tank	
9SSS	sand from sand separator	
11FPT	feed primary thickener	
12OPTA	overflow primary thickener A	
12OPTB	overflow primary thickener B	
13UPTA	underflow primary thickener A	
13UPTB	underflow primary thickener B	
14FW	freshwater for prim. thickener	
	freshwater for cyclones	
15FST	feed sec. thickener	
16FBF	feed cyclones bandpassfilters	
17CBF	filtercake bandpassfilter	
18UST	underflow sec. thickener	
19CVF	filtercake vacuumfilter	
22FVF	filtrate vacuumfilter	
24OST	overflow sec. thickener	

Figure 11: Material balance for the sampling campaign

4.2 Sampling Points

Figure 12: Sampling point 1DOL I

Figure 13: Sampling point 1 DOL II

The sample material of raw dolomite (1DOL) was taken at the transfer point between two conveyer belts after a storage silo (Figure 12). It was possible to pass through the whole material stream with a bucket in the maintenance hole (Figure 13). Three buckets with around 4 kg sample were taken. The internal material stream (20 INT) was taken after de dusting of dried dolomite in the air classifier. At the calcination tower, a sampling point was already established (Figures 14 and 15). Two bucket with around 4 kg sample material were taken with the sampling device.

Figure 14: Sampling point 20 INT I

Figure 15: Sampling point 20 INT II

Figure 16: Sampling point 21 HB

Figure 17: Sampling point 3 DOLG

Coarse dried and de dusted dolomite (3DOL) was sampled at a conveyor belt scale (Figure 17). One bucket with around 4 kg sample was taken from several places of the material stream. A sample of the fines from dedusting of dolomite and the calciner (21 HB) was taken before they were dumped as waste material (Figure 16). One bucket was filled with a sample from the falling material stream.

Figure 18: Sampling point 4 DOLIME calciner I

Figure 19: Sampling point 4 DOLIME calciner II

Figure 20: Sampling point 4 DOLIME silo I

Figure 21: Sampling point 4 DOLIME silo II

Calcined dolomite (4 DOLIME) was sampled at two different places in the process. Beneath the calciner, a sampling point was already installed (Figure 18). Two buckets of material were taken with the sampling device (Figure 19). Because of the calciner standstill from day one to five, samples were taken directly from the feeding silo scale besides the wet process (Figures 20 and 21). Two buckets were filled up from the falling material stream with a sampling spoon with a total cross cut of around 10 cm.

Figure 22: Sampling point 6 SW and 14 FW

Samples from seawater (6 SW) and Freshwater (14 FW) were taken from preinstalled sampling points in the wet plant (Figure 22). The water was let run for a while, so for sure actual process water was taken.

Figure 23: Sampling point 7 OHSC

The overflows of hydro separators A and C (7 OHSA and 7 OHSC) were sampled in the drainage of the overflow collector (Figures 23 and 24). A solid plastic bucket was fixed to a rope and let down to the material flow. Since coarse particles had already time to settle in the hydro separator, turbulence of the suspension was considered as sufficient for homogeneous samples. A 25 l canister was filled up with sample suspension.

Figure 24: Sampling point 7 OHSA

Figure 25: Sampling point 8 UHSA and B I

Figure 26: Sampling point 8 UHSA and B II

Underflows of the hydro separators (8 UHSA and 8 UHSB) were sampled at the end of the feeding pipes of the 8 m tank (Figures 25 and 26). Material was taken with a sampling spoon with a total cross cut of around 10 cm, before both streams mixed up. A 5 l canister was filled up from each material stream. Because of the flowing speed, homogeneity was expected to be given.

Figure 27: Sampling point 9 SSS

Figure 28: Sampling point 23 U8M

Material from the 8 m tank was taken at the feeding tube of the sand separator (Figure 28). A 5 l canister was filled with sample material. Sand separator sand was sampled before it was dumped as waste material (Figure 27). By fixing a 5 l canister to an extension rod, the whole falling material stream could be sampled.

Figure 29: Sampling point 11 FPT

Figure 30: Sampling point 15 FST

Feed of the primary thickener (11 FPT) was taken after seawater washing in an opened gutter (Figure 29). For sampling a bucket was let down to the material stream fixed to a rope. Sample homogeneity was expected due to the turbulence of the flowing material. A 25 l canister was filled up with sample material of several buckets. Feed of the secondary thickener (15 FST) was taken from a preinstalled sampling point beneath the cyclone system (Figure 30). A 25 l canister was filled up with sample material.

Figure 31: Sampling point 12 OPTA

Figure 32: Sampling point 12 OPTB

Overflows of the primary thickener (12 OPTA and 12 OPTB) were sampled in the drainage of the overflow collector (Figures 31 and 32). A 5 l canister of each overflow was filled with sample material.

Figure 33: Sampling point 13 UPTA

Figure 34: Sampling point 13 UPTB

The underflows of primary thickeners A and B (13 UPTA and 13 UPTB) were taken from the seed crystal feeding of the reactor (Figures 33 and 34). A tube for sampling was preinstalled. A 25 l canister was filled up to the half with sample material. Feed of the band filter (16 CBF) was sampled at the feeding tube of the last dewatering cyclone (Figure 35). A 5 l canister was filled with sample material. Band filter cake (17 CBF) was sampled before it was dumped as waste material (Figure 36). The material was taken from the whole cross-section of the filter band. Sample material was stuffed in a 5 l canister.

Figure 35: Sampling point 16 FBF

Figure 36: Sampling point 17 CBF

Figure 37: Sampling point 18 UST

Figure 38: Sampling point 19 CVF

Underflow of the secondary thickener (18 UST) was taken from a preinstalled sampling point (Figure 37). A 5 l canister was filled with material. Filter cake of the vacuum filters (19 CVF) was sampled directly from the conveyor belt (Figure 38). Therefore material was taken from different points of the material stream and stuffed in a 5 l canister. The vacuum filter filtrate (22 FVF) was taken from a collection tank (Figure 39). A 5 l canister was filled with sample material. Overflow of the secondary thickener (24 OST) was taken from the drainage of the overflow collector (Figure 40). A 5 l canister was filled with sample material.

Figure 39: Sampling point 22 FVF

Figure 40: Sampling point 24 OST

5 Processing and Analysis

In a first step, the sample material that was sent from Norway to Leoben had to be prepared for chemical analysis. Sample processing and preparation was performed in the laboratory of the Chair of Mineral Processing and the final chemical analysis was done at the RHI Technology Center in Leoben. For analysis of the elementary composition X-ray fluorescence spectroscopy was available. Additionally to the elementary composition, loss of ignition, carbon and sulphur content and the mineralogical composition were determined. The mineralogical composition was measured via X-ray diffractometry. Therefore and for the general analysis it was necessary to prepare homogeneous solid samples.

Solid samples from the dry process were first dried at 105°C in a drying furnace. Except of raw dolomite, which was used for particle size analyses, samples for chemical analysis were prepared without further processing. Since the grain size of the samples was already very small, the material was first homogenised and then split with a riffle divider to get a sample for chemical analysis. Liquid samples of seawater, freshwater and clear water of the thickeners were taken without any further processing since no suspended particles were contained. The remaining samples of the material had to be homogenised before sample splitting, because solid components settled to the bottom of the transport canisters. To do so, splitting was performed during intense mixing with an agitator after homogenisation. The sample material was sucked into a glass bottle that was attached to a vacuum pump. Depending on the size of the glass bottle, around 500 to 1000 grams of suspension were taken. Then the suspensions were filtered and the filter cake washed with distilled water before drying at 105°C. The salt content of the filtrate was measured by evaporation of the liquid. The salt content was later needed to calculate a correct phase model of the single material streams. After drying, the solid sample material was homogenised and samples for the chemical analysis were prepared.

Since it was planned to investigate the distribution of impurities over size classes by Henry-Reinhardt charts, the samples had to be classified before doing chemical analysis. Therefore the samples were separated into size classes. Since the information about enrichments is of special interest at the feed of a purification step, samples of those material streams were chosen. For the dry process, raw dolomite was taken from the feed of the calciner. Therefore raw dolomite samples were separated into 16 particle size classes between 0 to 25 mm by manual screen analysis. The material size classes bigger than 1 mm were crushed smaller than 1 mm in a rotor beater mill before samples of all classes were homogenised and prepared for chemical analysis.

As feed of the wet process the composition of slaked dolime was calculated from wet sieve analysis of sand separator sand and the overflow of the hydro separators. Since the grain size was smaller than 2 mm, the material of both samples was separated into seven size classes between 0 and 2 mm, which were then prepared for chemical analysis.

Additionally the underflow of the primary thickener was separated into six grain size classes by wet sieving and six grain size classes <25µm by sedimentation as feed of the cyclone system. While wet sieving is a relative simple method of separation, sedimentation of a bigger amount of sample is more sophisticated with respect to preparation, work and time. The procedure of sample preparation by sedimentation is described in Appendix G.

During the process of sample preparation it turned out, that the measurement program of daily samples would result in too many measurements. Therefore it was agreed with RHI to combine some of the samples to weekly samples. Process data from the RHI server was evaluated for the days of the sampling period. In Table 4, the average values which were available for calculating are shown.

Table 4: Process data

material stream	type	amount	unit
feed dolomite	dry	19,317	t/h
feed dolime	dry	8,976	t/h
cake vacuum filter	wet	21,278	t/h
underflow prim. thickener	wet	48,727	m^3/h
		54,588	t/h
feed seawater / slaking	wet	1411,038	m^3/h
feed seawater / seawater washing	wet	399,452	m^3/h
feed freshwater / sec. thickener	wet	554,226	m^3/h
feed freshwater / cyclones	wet	149,667	m^3/h
pulp feed cyclones	wet	48,727	m^3/h

Table 5: Solid content

material stream	g_{solid} [%]
7OHSAC	2,60
9SSS	64,70
8UHSAC	4,38
23U8M	3,07
11FPT	2,05
13UPTAB	18,41
15FST	6,83
16FBF	4,37
17CBF	55,40
18UST	25,21
19CVF	47,53
22FVF	0,26

6 Mineralogical Investigation

For a comprehensive evaluation of the material flows and for understanding the processing problems, not the total chemical SiO_2 content but the source of SiO_2 and its distribution on the silicates is crucial to know. To identify the types of minerals and to obtain a qualitative overview of the separation of the minerals during the process, the mineralogical investigation was confined to the product streams and the feed stream. The simplified flow sheet is depicted in Figure 41.

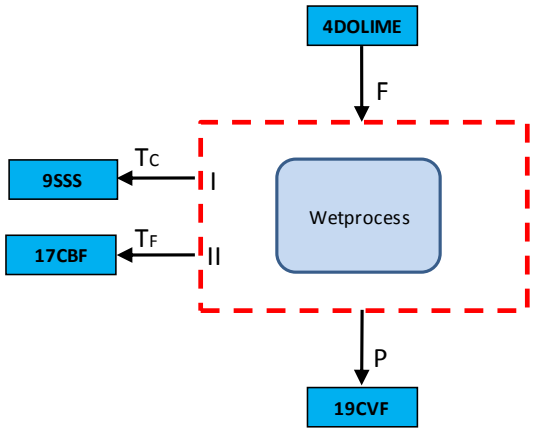

Figure 41: Balance for mineralogical investigation

As the total SiO_2 content is in the range of some percent for most of the samples, the samples used for microscopy were prepared by acid digestion in hot hydrochloric acid (35%). All the magnesium hydroxide and lime constituents are digested, while the silicates are enriched in the non-digestible residuals.

From washed SiO_2 containing residuals, grain mounts were produced by embedding the particles in liquids of defined refractive index in case of transmitting light microscopy (Reichert-Jung, Polyvar Weitfeld Photomikroskop). Liquids of a refractive index between 1,52 and 1,54 were used to elaborate the mineral refractive index using the Becke line.

The plane particles were observed by the stereomicroscope Leica MZ16 with 61 mm working distance and digital camera. The stereo microscope reveals transparent, sharp edged particles of conchoidal fracture and flaky particles, less transparent and nacre luster.

Applying the systematic investigations common at the polarizing microscope on grain mounts of acid insoluble residue from vacuum filter cake, the following observations were made.

For the transparent particles:

- anisotropic behaviour between crossed polarizers
- refractive index between 1,52-1,53
- uniaxial optically negative character
- first order interference colours

For the flaky minerals:

- Anisotropic behaviour
- Biaxial and intermediate birefringence
  (observed by the numerous bright interference colours)

These observations confirm the mineralogical composition given from RHI mineralogists in preparatory meetings stating, that the main pollutant minerals are quartz and mica. In the case of mica it was the phlogopite-annite series.

6.1 Optical Microscopy

In Figures 42 to 47 the acid insoluble residue is shown with the stereoscopic microscope. It is easily seen in Figure 43 that the sand separator sand contains different types of coarse particles. On one hand there are quartz grains and in contrast there are flaky, layer shaped particles indicating mica. Additionally there are opaque greyish rocky grains that could indicate the presence of uncalcined dolomite.

The sand of the cyclones shows a similar picture but it is much finer, and less greyish minerals are visible. Like in the sand separator sand, quartz grains and flaky, layer shaped particles can be observed.

The residue of dolime shows as expected all of the mineral phases mentioned for the sand separator sand and the cyclones sand. The main product of the wet process, filter cake of the vacuum filters, is as seen in Figure 45 too fine for stereoscopic microscopy. This sample was therefore examined in transmitted-light (Figures 46 and 47). The sample preparation was done by embedding the material in a chinolin-based mixture. Overall there were several mineral phases present in the sample, but three dominating phases could be found. The minerals of a refractive index smaller than 1,53 could be identified as quartz. Rounded, optical isotropic grains with refraction index >1,53 were identified as MgO. This statement is confirmed by the corroded surface due to acid leaching. MgO could be originated from dolime. The third dominant mineral phase was a bigger brownish, shapeless aggregate which was interpreted as mica sheets.

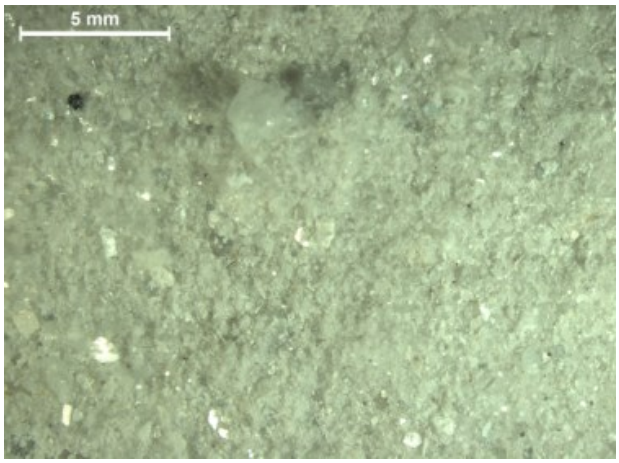

Figure 42: Residue of dolime

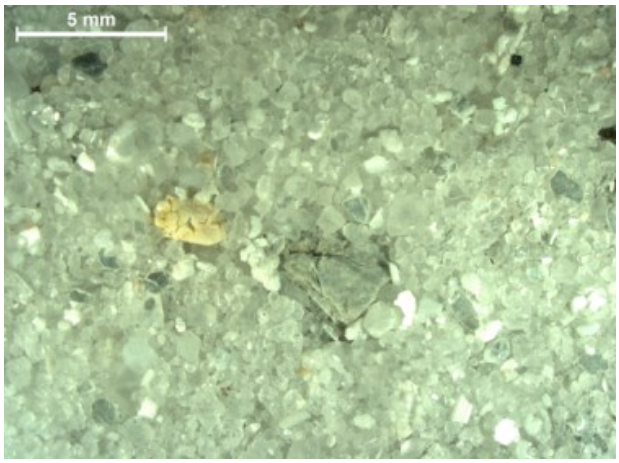

Figure 43: Residue of sand separator sand

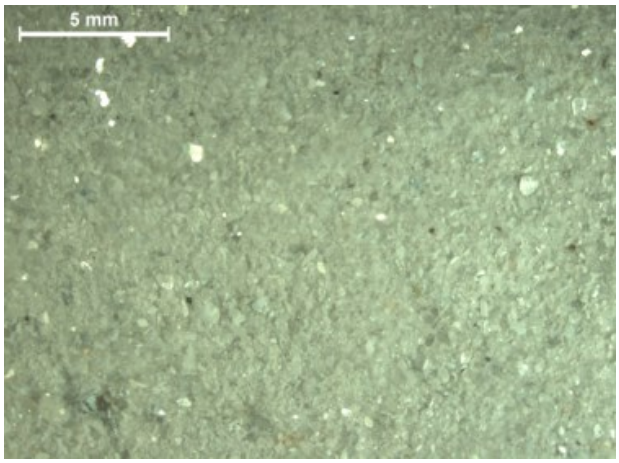

Figure 44: Residue of cylone sand

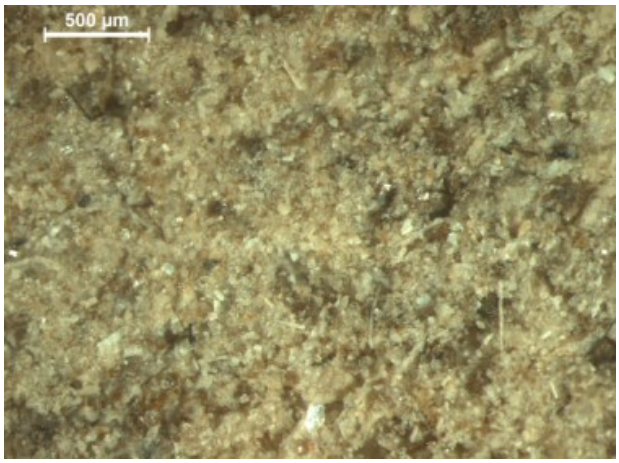

Figure 45: Residue of vacuum filter pulp I

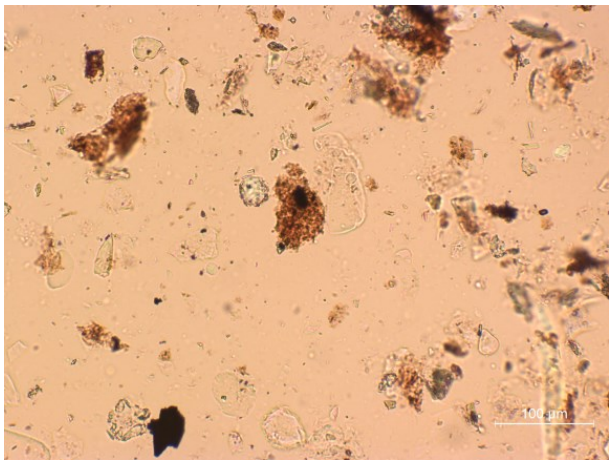

Figure 46: Residue of vacuum filter pulp II

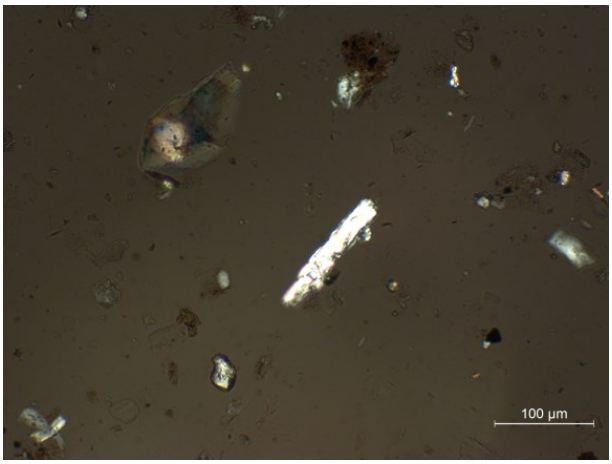

Figure 47: Residue of vacuum filter pulp III

6.2 Electron Microscopy and EDX-Analysis

In addition to stereoscopic and transmitted-light microscopy, the residue of vacuum filter pulp was analysed in an electron microscope with energy dispersive X-ray spectroscopy. In Figures 48 to 50 measurement spots on the sample are shown. Table 5 summarizes the elementary composition of each measurement spot. In general it can be observed that the amount of silica in the phases from Figure 48 spot 1 and 3, Figure 49 spot 1,3 and 4 and Figure 50 spot 3 and 4 is quite high, which indicates the presence of quartz. Some phases with lower silicate levels show higher amounts of aluminium, potassium, magnesium and iron together, which could indicate mica minerals in Figure 48 spot 4 and Figure 49 spot 2 and 5. Also an impurity with high iron content is indicated in Figure 50 spot 2. Overall it is difficult to make specific assumptions, because there is a lot of fine material covering the surface of the bigger grains which could affect the measurement.

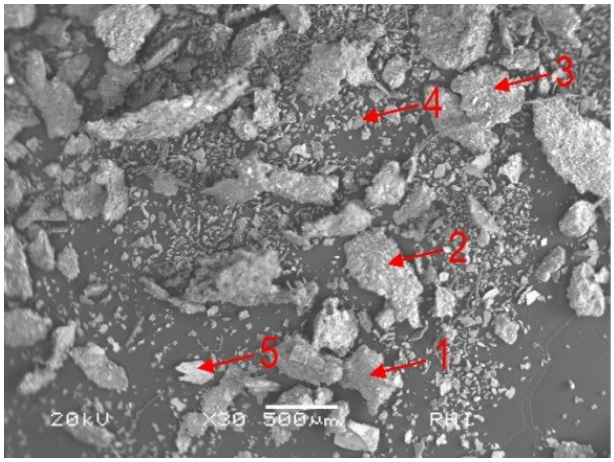

Figure 48: Residue of vacuum filter pulp IV

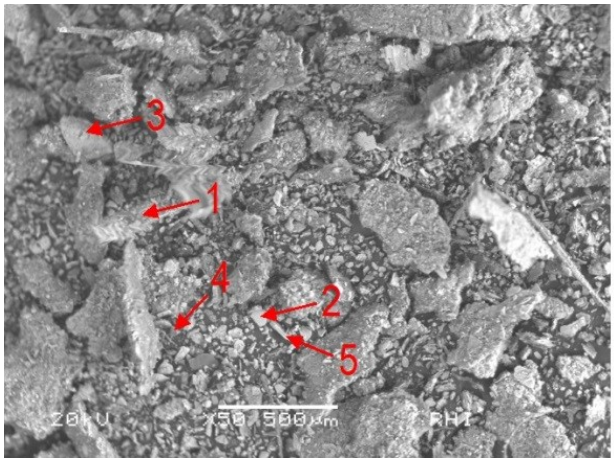

Figure 49: Residue of vacuum filter pulp V

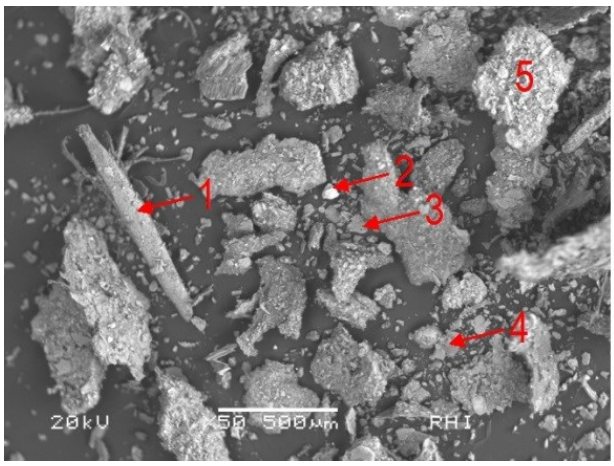

Figure 50: Residue of vacuum filter pulp VI

Table 6: EDX-analysis of acid-insoluble residue of 19CVF

Fig.	Spot	F	Na_2O [%]	MgO [%]	Al_2O_3 [%]	SiO_2 [%]	P_2O_5 [%]	SO_3 [%]	Cl	K_2O [%]	CaO [%]	TiO_2 [%]	Fe_2O_3 [%]
48	1			1,3	1,3	97			+				
	2			8,5	1,2	73,1				0,4	16,7		
	3			3,2	2,5	92,1				1,3	0,9		
	4	+	0,4	22,3	14,1	51				8,9			
	5			30,4		69,1							0,5
49	1			4,3	1,2	88,5				0,5	5,6		
	2			18,3	10,9	55,7				13,9		1,2	
	3		1,2	7,8	2,6	85,9			+	2			
	4			0,8		99,2							
	5				5,4	71,2				10,5	2,6		10,3
50	1	+		2,8	1,7	36,3	9,5	8,9		3,3	34,2		
	2			2,1		14,2		1,7	+				81,6
	3		1,2			98,3			+				
	4			3,5	3,1	89,4			+				

Overall some basic assumptions can be made from the mineralogical investigation. By optical observation coarse particles in millimetre range can be found in sand separator sand and finer grains smaller than 500 µm in sand of the cyclones. Greyish parts of a mineral phase, likely to be unreacted dolomite are present mainly in tailings of the sand separator. In the final product several fine grained mineral phases can be found, including quartz, mica and periclase. Since filter cake of the vacuum filters contains very little amounts of impurities, concentrating steps had to be done. For a detailed analysis of the mineralogical composition, it would make sense, to prepare more sample material by leaching a bigger amount of filter cake. Measuring this concentrate could give a better qualitative and quantitative impression about the mineral impurities.

7 Results and Discussion

7.1 Material Stream Composition

From the results of the chemical analysis in a first step the average elementary composition of the week samples was calculated. Then the amount of quartz and mica was determined. In Appendix B the raw data are listed and in Appendix C the calculation of quartz and mica is described in detail. The average mica content was calculated based on the aluminium-content, since all aluminium was assigned to mica. The composition of the "average mica" is derived from the elementary compositions of annit and phlogopite. The remaining silica not consumed by mica was assumed to be free quartz.

The solid and salt contents were measured for every sample during preparation for the chemical analysis. With the data of solid and soluble contents in the sample material, an overview of all sampled material streams could be created (see Appendix J, Table J-1 and J-2). In Figure 51 the total mass composition of the material streams including a separation in solid-liquid-soluble as well as quartz and mica. The total solid content is defined by the masses of quartz mica and the insoluble rest. In Figure 52 the mass content of the main components CaO, MgO, quartz and mica in the solid phase is illustrated relativized to 100%.

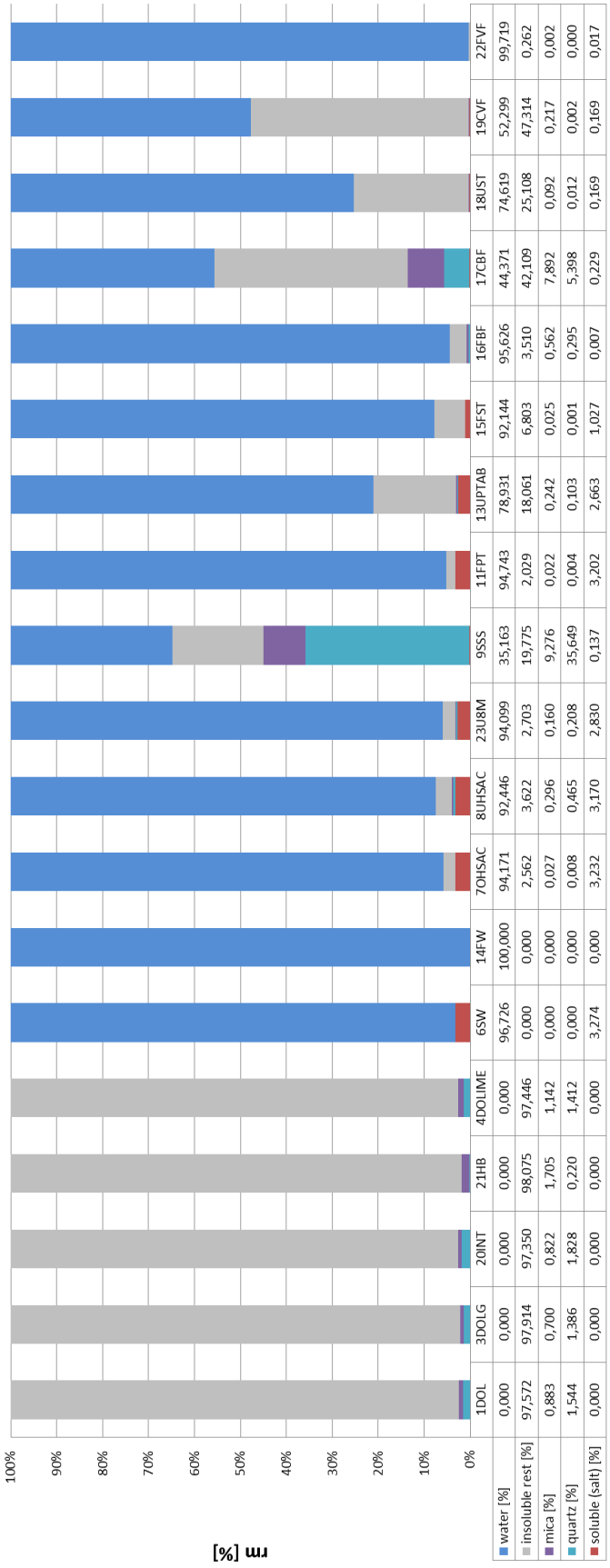

	1DOL	3DOLG	20INT	21HB	4DOLIME	6SW	14FW	7OHSAC	8UHSAC	23U8M	9SSS	11FPT	13UPTAB	15FST	16FBF	17CBF	18UST	19CVF	22FVF
water [%]	0,000	0,000	0,000	0,000	0,000	96,726	100,000	94,171	92,446	94,099	35,163	94,743	78,931	92,144	95,626	44,371	74,619	52,299	99,719
insoluble rest [%]	97,572	97,914	97,350	98,075	97,446	0,000	0,000	2,562	3,622	2,703	19,775	2,029	18,061	6,803	3,510	42,109	25,108	47,314	0,262
mica [%]	0,883	0,700	0,822	1,705	1,142	0,000	0,000	0,027	0,296	0,160	9,276	0,022	0,242	0,025	0,562	7,892	0,092	0,217	0,002
quartz [%]	1,544	1,386	1,828	0,220	1,412	0,000	0,000	0,008	0,465	0,208	35,649	0,004	0,103	0,001	0,295	5,398	0,012	0,002	0,000
soluble (salt) [%]	0,000	0,000	0,000	0,000	0,000	3,274	0,000	3,232	3,170	2,830	0,137	3,202	2,663	1,027	0,007	0,229	0,169	0,169	0,017

Figure 51: Total material stream composition

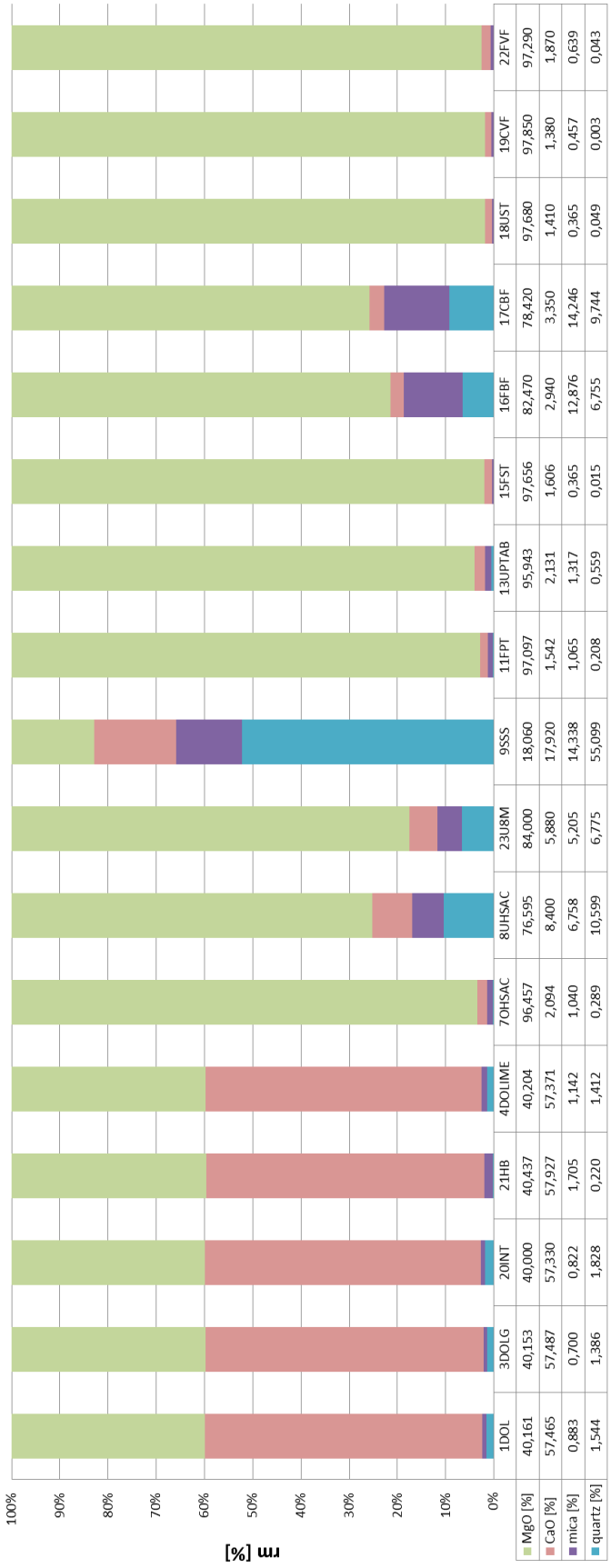

	1DOL	3DOLG	20INT	21HB	4DOLIME	7OHSAC	8UHSAC	23U8M	9SSS	11FPT	13UPTAB	15FST	16FBF	17CBF	18UST	19CVF	22FVF
MgO [%]	40,161	40,153	40,000	40,437	40,204	96,457	76,595	84,000	18,060	97,097	95,943	97,656	82,470	78,420	97,680	97,850	97,290
CaO [%]	57,465	57,487	57,330	57,927	57,371	2,094	8,400	5,880	17,920	1,542	2,131	1,606	2,940	3,350	1,410	1,380	1,870
mica [%]	0,883	0,700	0,822	1,705	1,142	1,040	6,758	5,205	14,338	1,065	1,317	0,365	12,876	14,246	0,365	0,457	0,639
quartz [%]	1,544	1,386	1,828	0,220	1,412	0,289	10,599	6,775	55,099	0,208	0,559	0,015	6,755	9,744	0,049	0,003	0,043

Figure 52: Content of main components in the solid phase

7.2 Material Balance

By combining the results of the material stream composition and process data during the sampling period, in a next step the actual material balance for the production process was created. In comparison to the first balance of the sampling campaign, which was mainly used to define sampling points, this balance is focussed on basic material streams of the three single purification steps. For calculation, those three systems were balanced in a first step individually. These steps are the calciner (I), the system mixer-reactor-sand separator (II) and the system cyclones-vacuum filter (III). The balance room includes all in- and outgoing material streams.

Variations from random sampling and analysis errors as well as imperfect equilibrium of the process from buffering effects of thickeners and silos cause variations. Therefore results of the single step balance did not fit perfectly. The single balances were linked according to the flow sheet given in figure 53 using the mass recovery. The result was used to illustrate the total SiO_2, quartz and mica material flows through the plant with their absolute (t/h) as well as relative (%) contents. The calculation is described in detail in Appendix D.

Figure 53: Material balance for SiO_2 quartz and mica

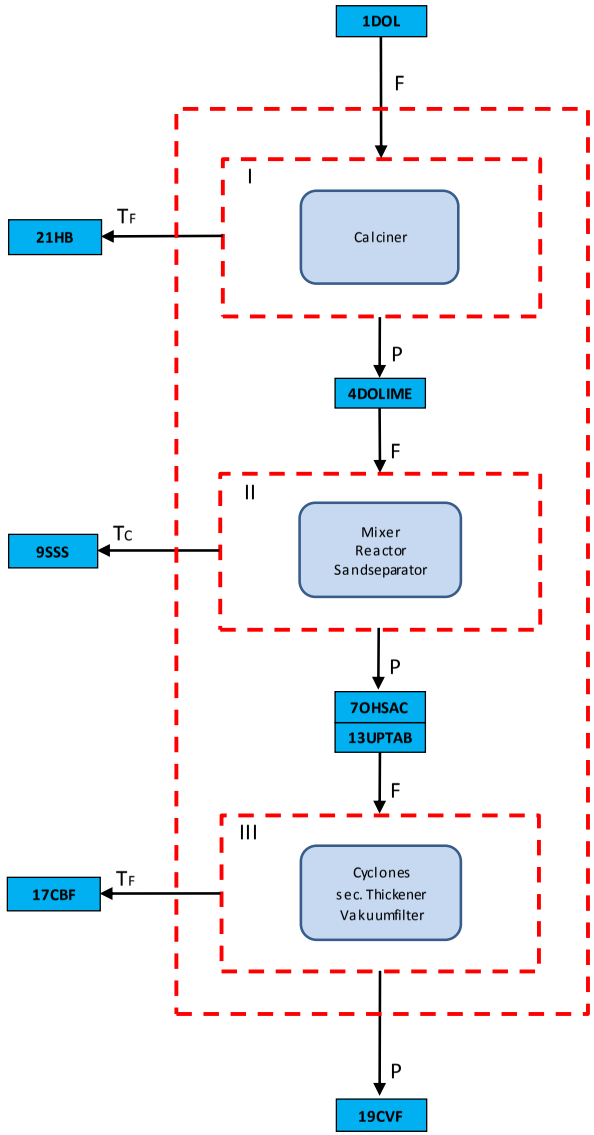

Feed total process - 1DOL

phase	I [t/h]	ri [%]
SiO_2 total	0,364	100,00
Mica	0,171	100,00
Quarz	0,298	100,00

Tailings fine, calciner - 21HB

phase	I [t/h]	ri [%]
SiO_2 total	0,198	54,32
Mica	0,068	39,95
Quarz	0,172	57,51

Feed wetprocess - 4DOLIME

phase	I [t/h]	ri [%]
SiO_2 total	0,166	45,68
Mica	0,102	60,05
Quarz	0,127	42,49

Tailings coarse, sandseparator - 9SSS

phase	I [t/h]	ri [%]
SiO_2 total	0,106	28,98
Mica	0,025	14,63
Quarz	0,096	32,15

Feed cyclones - 13UPTAB

phase	I [t/h]	ri [%]
SiO_2 total	0,061	16,70
Mica	0,092	53,63
Quarz	0,025	8,52

Tailings coarse, cyclones - 17CBF

phase	I [t/h]	ri [%]
SiO_2 total	0,051	13,90
Mica	0,059	34,65
Quarz	0,025	8,47

Product wetprocess - 19CVF

phase	I [t/h]	ri [%]
SiO_2 total	0,010	2,80
Mica	0,032	18,98
Quarz	0,000	0,05

7.3 Efficiency of Separation

Based on grain size distributions and the mass distribution of the balance model, the partition numbers (PN) and therefore the separation efficiency of purification steps in the wet process were determined. For the sand separator system, the grain size distribution of hydroseparator overflow and sand separator sand and for the cyclone system the grain size distributions of primary thickener underflow and band filter cake were used (Appendix E). The calculation is described in detail in Appendix H. In Figure 54 and 55 the separation efficiency is illustrated. For the characterisation of the separation efficiency, the grain size of PN_{50} was identified. For the sand separator a grain size of 0,235 mm and for the cyclone system a grain size of 0,21 mm was found (see Table 7). Since the separation principle in both, the sand separator and the cyclones is based on the settling velocity in the gravitational respectively centrifugal force and the analysis was done by grain size analysis via wet sieving, the results don't meet the physical principle perfectly. To check each product by sedimentation in the sedimentation bottle (Appendix G) would have been too time consuming. Nevertheless the results should fit to give an impression about the separation efficiency of the two systems.

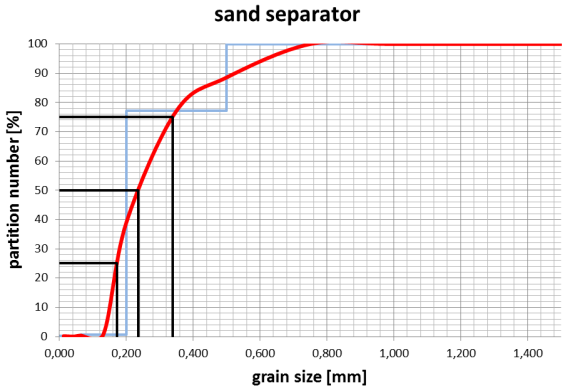

Figure 54: Partition curve sand separator

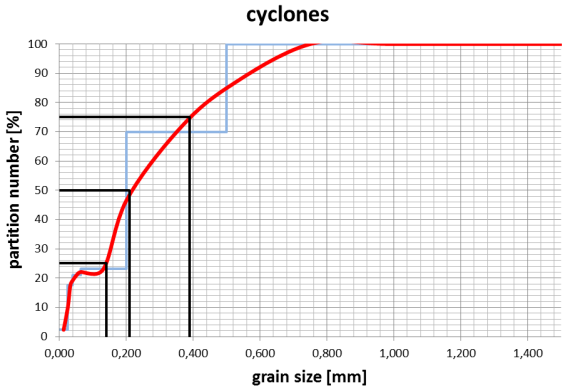

Figure 55: Partition curve cyclone system

Table 7: Separation efficiency

	type	sand separator	cyclones
partition numbers	PN_{25} [mm]	0,172	0,140
	PN_{50} [mm]	0,235	0,210
	PN_{75} [mm]	0,338	0,390
characterisation	EP	0,083	0,125
	Imp	0,353	0,595
	X	1,965	2,786

7.4 SiO_2 distribution over particle size classes visualised by Henry Reinhardt charts

To illustrate possible enrichments of SiO_2 bearing mineral phases, samples of the feed of the main purification steps were analysed for size distribution and the SiO_2 grades within the size classes. The data set allows the construction of Henry-Reinhardt diagrams (for detailed explanation and calculation see Appendix I). The size distributions were analysed by screening in case of dolomite (feed dry process), by wet screening in case of slaked dolime (feed wet process) and by a combination of wet screening and sedimentation in case of the underflow of the primary thickener (feed cyclones).

As shown in the Henry-Reinhardt diagrams for mica/SiO_2 in Figures 56 to 61, the intergrowth curve of the feed material as well as the average grade of SiO_2 bearing mineral phases in the separation products, coarse and fine, can be specified. The connection to the separation process by grain size is done via size distribution curves. Since Henry Reinhardt diagrams are based on analytical separation processes, they reflect the theoretical totally efficient separation. The results may thus be used to find an optimum separation cut size and serve to benchmark a process, but need not to correspond with actual separation processes.

The Henry-Reinhardt diagram for raw dolomite as the feed to the calciner is shown in Figure 56. It can be observed, that there is an enrichment of mica in the fines. The settings of the process are indicated with a red dashed line. This line indicates that almost 30% of the fed dolomite is removed as fines including the mica enrichment during drying and calcining. The other 70% show that the mica content is more or less equally distributed over the size classes. For dolomite, the grade of quartz and total SiO_2 is distributed equally over the size classes, so no enrichment is detectable (for diagrams see Appendix I, Figure I-5 and I-7). It can be observed, that the enrichment of mica starts with a grain size around 360µm.

Feed dry process

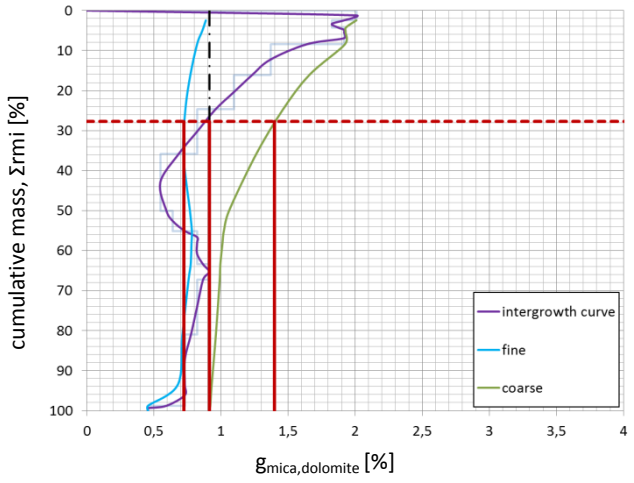

Figure 56: Henry-Reinhard diagram for mica in dolomite

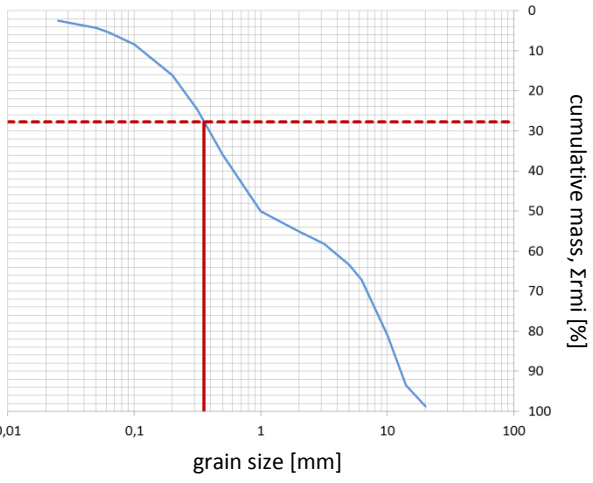

Figure 57: Cumulative mass distribution of size for dolomite

The slaked dolime as feed material of the system sand separator-mixer-reactor shows an enrichment of silica in the coarse. In Figure 58, the total amount of SiO_2 is illustrated, because quartz and mica show similar behaviour (for diagrams see Appendix I, Figure I-9 and I-11). The grain size distribution was calculated from combining the screen-analysis of sand separator sand and the overflow of the hydro separators, since it was impossible to take a sample of slaked dolime. Taking 235µm corresponding to the PN_{50} value of the sand separator (Figure 54) as the separation cut size (horizontal line) in the HR chart, around 2 % of the feed is removed as coarse material with a SiO_2 grade of around 64%. The fine product has a SiO_2 grade of around 0,8% (Figure 58). In this case, the values from balance, separation efficiency and the Henry Reinhardt charts fit very well together, since SiO_2 grades of chemical analysis with 60,65% SiO_2 in the sand separator sand and 0,69% SiO_2 in the hydro separator overflow can be found (Appendix C, Table C-2).

Feed wet process

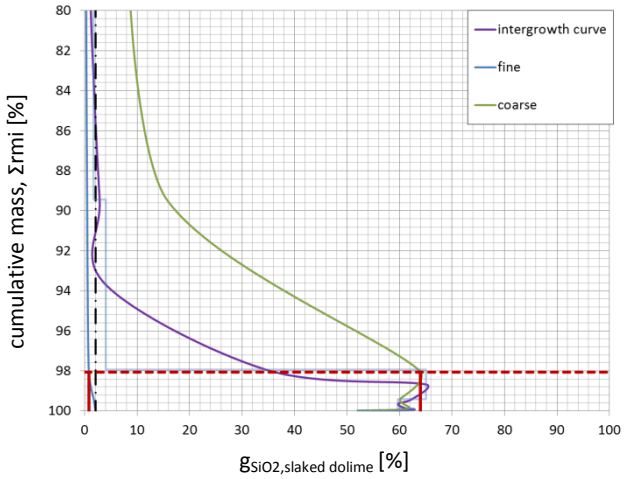

Figure 58: Henry-Reinhardt diagram for total SiO_2 in slaked dolime

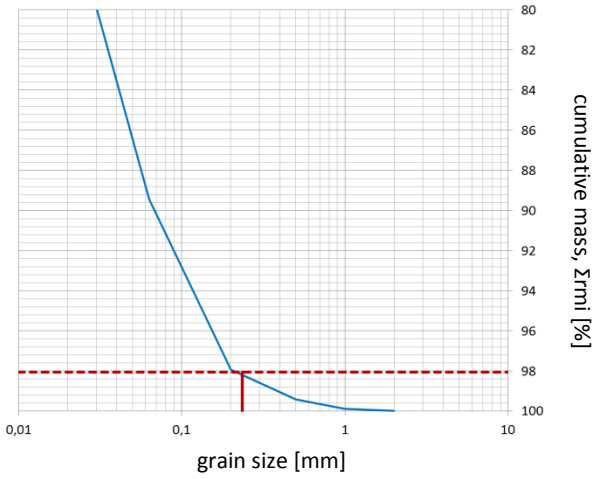

Figure 59: Cumulative mass distribution of size for slaked dolime

For the feed of the cyclones (analysis of primary thickener underflow by combination of wet screening and sedimentation analysis) an enrichment of total SiO_2 was found to be in the coarse size range. For quartz and mica similar behaviour was found (for diagrams see Appendix I, Figure I-15 and I-17). Using the mass distribution of separation products from the balance (removal of 5,9 % coarse product) to predict the separation results in the Henry Reinhardt chart, a coarse waste material containing approximately 12 % SiO_2 is found. The product reporting to the secondary thickener would contain 0,86 % SiO_2. According to the chemical analysis in the real process from the sampling campaign, cyclone sand contains around 15,3 % SiO_2, which fits more or less to the results. The feed of the secondary thickener contained 0,18 % SiO_2, which could never be reached according to the SiO_2 assays in the size

classes of the sedimentation test. The separation grain size with 85 µm found with the theoretical totally efficient separation in the Henry Reinhardt diagram differs significantly from the grain size of 210 µm found in the separation efficiency by partition numbers. Several factors including fluctuation of SiO_2 content and/ or the variation in the analysis result of low SiO_2 grades as well as problems caused by time shifts of sampling can lead to this difference. Nevertheless the enrichment of SiO_2 in the coarse size range can be illustrated.

Feed cyclones

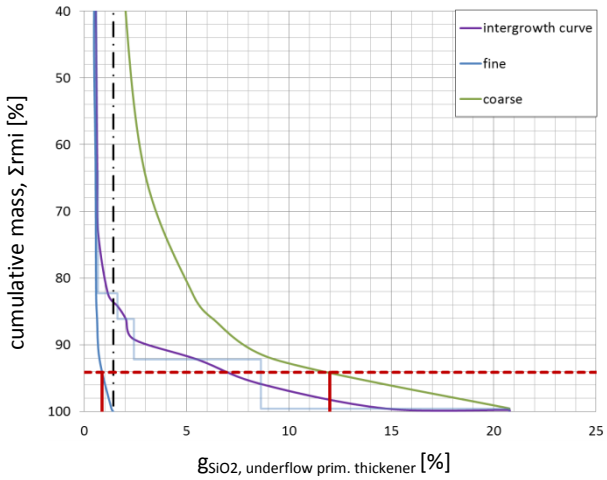

Figure 60: Henry-Reinhard diagram for total SiO_2 in underflow prim. thickener

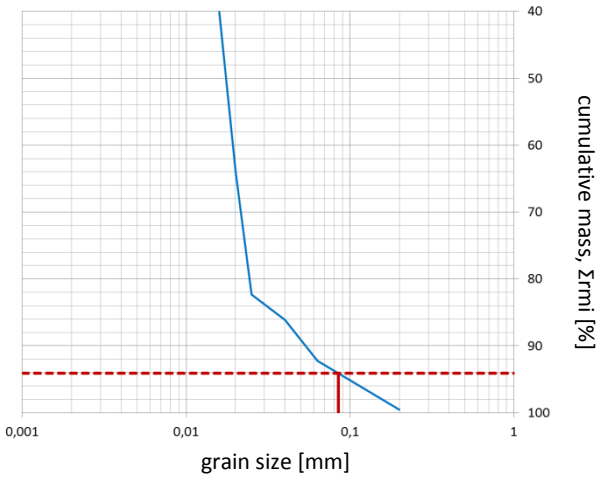

Figure 61: Cumulative mass distribution of size for underflow prim. thickener

8 Conclusions

The sampling campaign was performed within six days with two samples at every sampling point per day. Because of silos and two thickening stages, which retain material for a certain time, the plan of following the material through the process could not be performed as first thought. In the processing steps, most of the samples were prepared for chemical analysis as daily samples. Due to the big number of samples, the decision to prepare only weekly samples of some sampling points had to be taken. Because of this fact and the generally short sampling period of one week, there is no real information about the margin of variations in the process. The standard variation from chemical analysis, which varies depending on the type of sample with up to 22,65 % rel. for SiO_2 (see statistical data in Appendix B, Table B-9) gives an indication. However, these values overlap with the variations from the method of analysis by XRF. The sampling campaign and all measurements represent the prevailing situation in the time of the sampling (11.-17. June, 2015). This leads also to the point that conclusions from those measurements cannot be adopted for other raw materials. If another dolomite is used, the intergrowth conditions can be totally different and therefore the behaviour of the impurities in the process. Also the material balance is calculated with process data and adjustments during the sampling campaign. Changes in the process control are therefore not represented.

The material balance model for silica impurities was created, using the raw data from sampling. Calculating the mass distribution in the balancing areas (balance II and III) based on SiO_2 grades, a constant solid flow between the single areas was assumed. While the output of area I is the full input of area II, the difference between the output of area II to the input of area III was calculated with 12% , whereby additional precipitation through seawater washing reduces this mass difference. The calculated equilibrium is therefore no real equilibrium. For verification, an equalization calculus, which is not included in this thesis, was performed including besides SiO_2 grades also Al_2O_3, MgO and CaO and additionally to solid also the soluble contents. Balancing by this method was not successful. Perhaps due to small values for the grades, storage and retention effects by the thickeners and the high degree of recycling processes, the result didn’t reflect the reality.

Nevertheless with the balance as calculated in this thesis, by combining results from chemical assay and measured flow rates, the material flows through the plant can be illustrated beginning at the feed of dolomite and finishing with the filter cake of the vacuum filters. With progress of the process the content of quartz as well as mica is reduced, as shown in Figures 62 and 63 in total tonnage and relativized. Overall, the process is more efficient in reducing quartz (99,95% reduction) than mica (81,02% reduction). The separation efficiency from apparatus of the purification steps can be interpreted to some degree by using the partition numbers. While the separation grain size for the sand separator is with 235 µm in an acceptable area and the connection to the Henry Reinhardt diagram supports this result, the separation grain size of 210 µm for the cyclone system seems quite high. By using the mass distribution of separation products from the balance in combination with the Henry Reinhardt

diagram, a lower separation grain size of 85 µm is found. A reason for this difference may be the illustration of the theoretical totally efficient separation by Henry Reinhardt diagrams and an imperfect separation process illustrated by the partition numbers. Since in the preparatory meetings the information was given, that the cyclone system is not in the best condition, it was inspected optically. Some of the cyclones were blocked by a crust and therefore not working well, but no further investigation was done at this point.

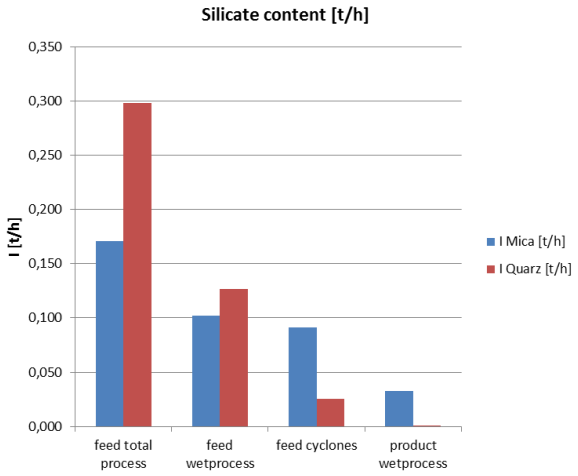

Figure 62: Reduction of impurities in total tonnage

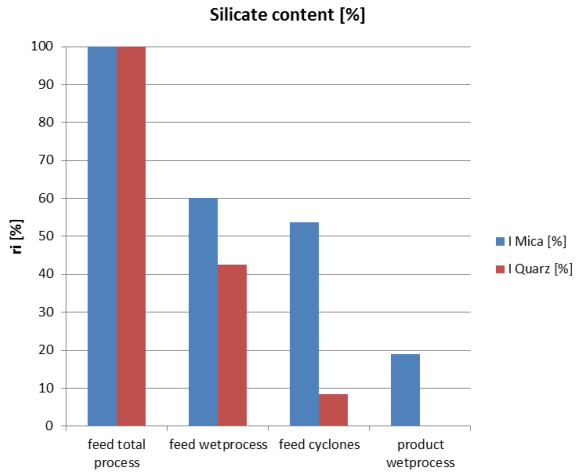

Figure 63: Reduction of impurities relativized

By investigating the samples from the purification process, enrichments of properties in the material flows were found and illustrated with Henry-Reinhardt charts. Since impurities are removed in three steps, the feed of those points was analysed. For dolomite, as feed of the calciner, an enrichment of mica was observed in the fines. With rising grain size, the concentration of mica was distributed equally. For quartz there was no enrichment observable, because it was distributed more or less equally over the grain sizes. An explanation for this could be the hardness of the minerals and the particle size of mica. Soft mica particles accumulate therefore in the fines. Since grains coarser than 360 µm include impurities equally distributed, only a part of mica can be separated by removing the fines. As shown in Henry-Reinhardt diagrams, all liberated mica is already removed by dedusting. Removing more fines would only result in a loss of dolime feed but has no beneficial effect on the composition. Investigations regarding a finer feed for the flash dryer and calciner could give an answer to the question, if finer comminution would liberate more mica which can be removed. Liberating and removing more mica can reduce the total SiO_2 content of the feed, but a finer grain size could have an impact on the calcination behaviour and quality of the produced dolime.

Because of the slaking reaction, dolime was not directly from interest for the investigation of intergrowth conditions. The composition of slaked dolime was therefore calculated from analysis of the separation products. Enrichment of quartz as well as mica can be found in coarse particle sizes. Since dolime is chemically dispersed in very fine particles during slaking,

the impurities get liberated. Based on the proposed model, 29 % of the total SiO_2 content is removed with the sand separator. Similar to slaked dolime, the primary thickener underflow shows an enrichment of quartz and mica in coarse particle sizes. The cyclone system is responsible for removing 14 % of the total SiO_2 content (Figure 53). Purification steps remove besides impurities also valuable magnesia from the process. While waste material from the sand separator includes around 18 % MgO which is according to the measurement of the total carbon content partially still dolomite, waste material from the cyclone system consists of 78 % MgO in form of magnesium oxide and magnesium hydroxide (Figure 52).

The predefinition of the SiO_2 bearing mineral phases quartz and mica was based on information from preparatory meetings and results from mineralogical measurements via X-ray diffraction. The microscopic investigation, including stereo and transmitted light microscopy as well as an EDX analysis, supported the assumption, since mineral phases with properties according to the proposed ones (quartz and mica) were found. Nevertheless for future investigations, detailed analysis of leaching residue should be performed. By leaching a bigger amount of vacuum filter cake, preferably as bulk sample of several days, enough residue material for exact analysis could be created. This leaching step could be done with strong mineral acids like hydrochloric acid to prepare an acid insoluble residue, as it was done in the thesis. The problem with strong acid leaching is that besides magnesium hydroxide also calcium and magnesium oxide as well as carbonate impurities get dissolved. Another more gentle option is leaching of $Mg(OH)_2$ with ammonium salt solutions like ammonium chloride or similar. Since only magnesium hydroxide is soluble in such a “solvent”, a residue containing all other mineral impurities and MgO could be created.

The results of this thesis should provide process data and serve as a basis for further investigations. It should give ideas how the separation efficiency of a process can be characterised and enrichments of properties are useful illustrated. For further investigations, sampling should be performed concentrated to the area of interest and if samples from more than one material stream are needed, the sampling should be done contemporary or if necessary considering the retention times of the process.

Further investigations should be carried out to obtain a deeper insight about the prevailing situation and to identify alternative processing methods. For cycloning, a detailed sampling campaign of the cyclone system should be performed. Since the main purpose of the sampling campaign of this thesis was to gain material stream data of the whole process for creation of the silicate balance, no detailed sampling campaign of the cyclone system was performed.

According to the material balance and the composition of vacuum filter cake, the remaining silicate bearing mineral phase is mainly mica (Figure 63 and Figures 51-52). According to this and the fact, that silicate impurities are found in the coarse fraction of cyclone feed (Figure 60), wet screening should be considered. Nevertheless a detailed investigation specifically for wet screening should be performed.

9 References

[1] A.S.Bhatti, D. Dollimore and A. Dyer, 1984; *Magnesia from Seawater: A Review;* Clay Minerals 19, pp 865-875, 1984

[2] R.C. Carson and J. Simandl, 1993; Technical Note, *Kinetics of Magnesium Hydroxide Precipitation from Seawater using slaked Dolomite*; Minerals Engineering, Vol. 7. No 4, pp 511-517; 1994

[3] V. Martinac, M Labor & N. Petric, 2004; *Boric oxide in seawater derived magnesia, Indian Journal of Marine Sciences*, Vol. 33 (3), pp. 226-230, September 2004

[4] Mark A. Shand, 2006; *The Chemistry and Technology of Magnesia*, Published by John Wiley& Sons, Inc., Hoboken, New Jersey. 2006, ISBN: 978-0-471-65603-6

[5] J. Xiao, 2011; *Boron isotope fractionation during brucite deposition from artificial seawater*; Climate of the Past, 7, pp 693-706, 2011

[6] Unknown Author, 2011, *Manufacture of magnesium oxide from sea water*, Case study of Premier Periclase in Drogheda, Co. Louth; The Physical Sciences Initiative

[7] Deborah A. Kramer, 2008; *Magnesium Minerals and Compounds*, U.S. Geological Survey Minerals Yearbook 2008, Vol 1, pp 615-629

[8] "*Seawater process*", 08.01.2016, RHI company homepage: http://www.rhi-ag.com/linkableblob/internet_en/76584/data/Flowchart_Porsgrunn-data.jpg

[9] C. Piribauer, 2014*; Sampling points RHI NORMAG*, Internal RHI Sampling Report

[10] W. Wulandari, G. A. Brooks, M. A. Rhamdhani, and B. J. Monaghan, 2010; *Magnesium: Current and alternative production routes*, Chemeca- Australasian Conference on Chemical Engineering, Engineering at the Edge, pp. 347-357, 2010

[11] C. Henrista, J.-P. Mathieua, C. Vogelsb, A. Rulmonta, R. Clootsa, 2002; *Morphological study of magnesium hydroxide nanoparticles precipitated in dilute aqueous solution*, Journal of Crystal Growth Vol. 249, pp. 321–330, 2003

[12] T Richard Hull, Baljinder K Kandola, 2009; *Fire Retardancy of Polymers : New Strategies and Mechanisms*; RSC Publishing 2009

[13] Unknown Author, 2001, *SUMMARY OF DATA FOR CHEMICAL SELECTION - Magnesium Oxide*; Prepared by Technical Resources International; National Toxicology Program – U.S. Deartment of Health and Human Services

[14] E. Lee Bray, 2014; *MAGNESIUM COMPOUNDS*; U.S. Geological Survey, Mineral Commodity Summaries, January 2015

[15] George C. Whipple, Andrew Mayer, Jr., 1905, *The Solubility of Calcium Carbonate and of Magnesium Hydroxide and the Precipitation of these Salts with Lime Water*, Public Health Pap Rep., Vol. 31(Pt 2), pp. 151–165, 1905

[16] Böhm, A; Niiranen, K., 2016, *2D VERSUS 3D LIBERATION ANALYSIS TO CHARACTERIZE INTERGROWTH IN LD SLAGS,* Proceedings of the 28th IMPC Canada Quebec XXVIII International Mineral Processing Congress September 11-15, in press

10 Appendix

Appendix A: Flow Charts

Dry process A-1

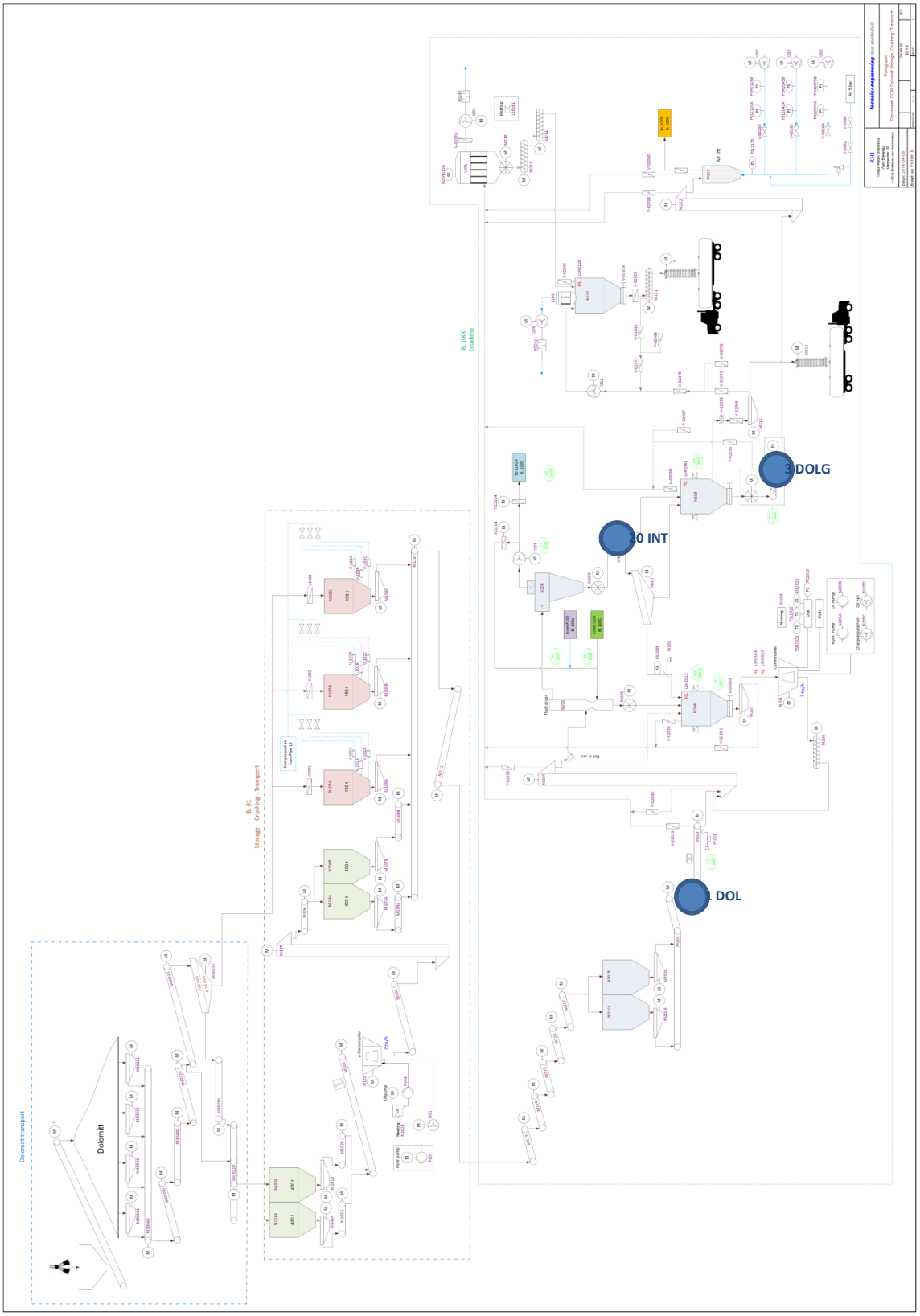

Dry process A-2

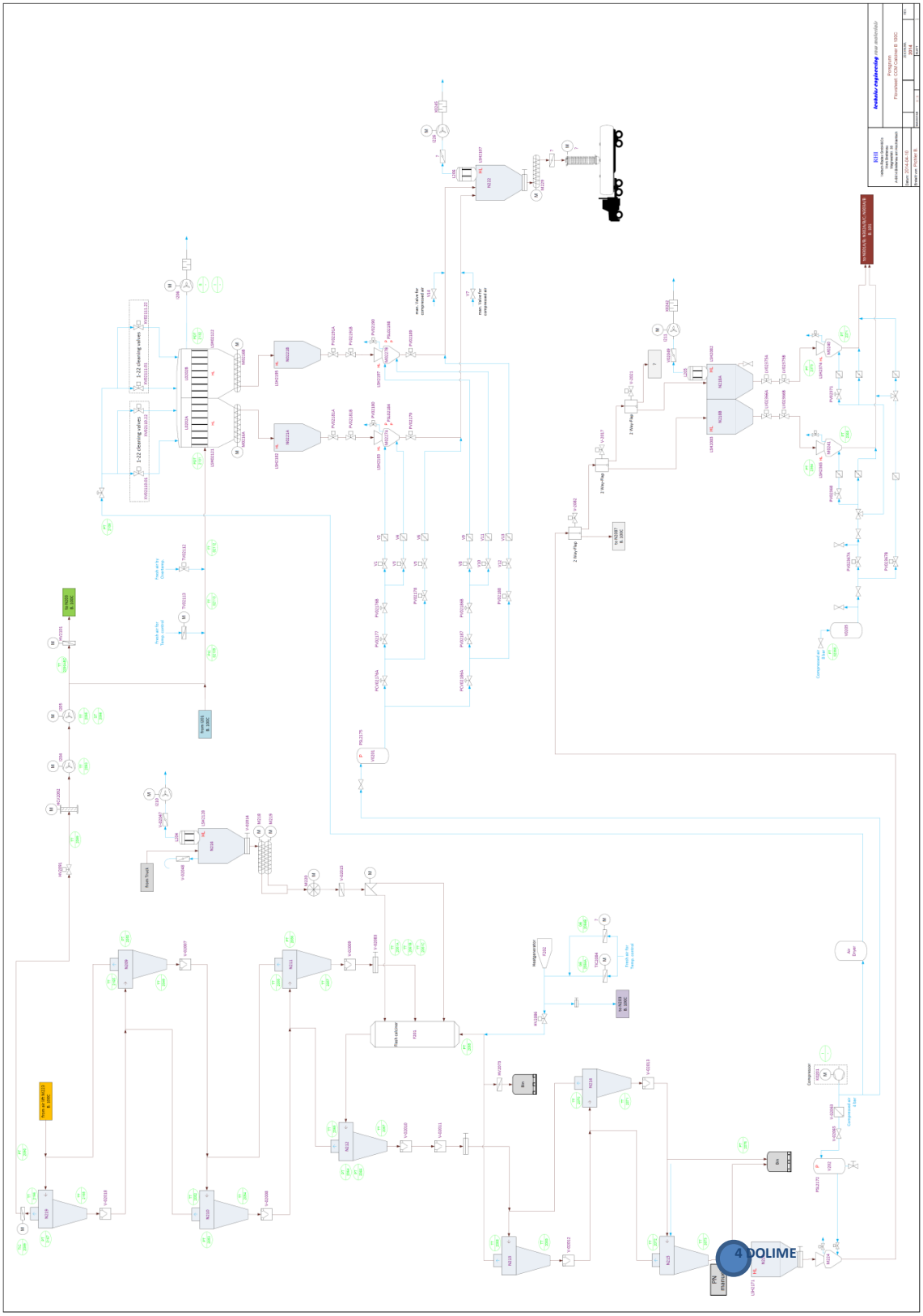

Wet process A-3

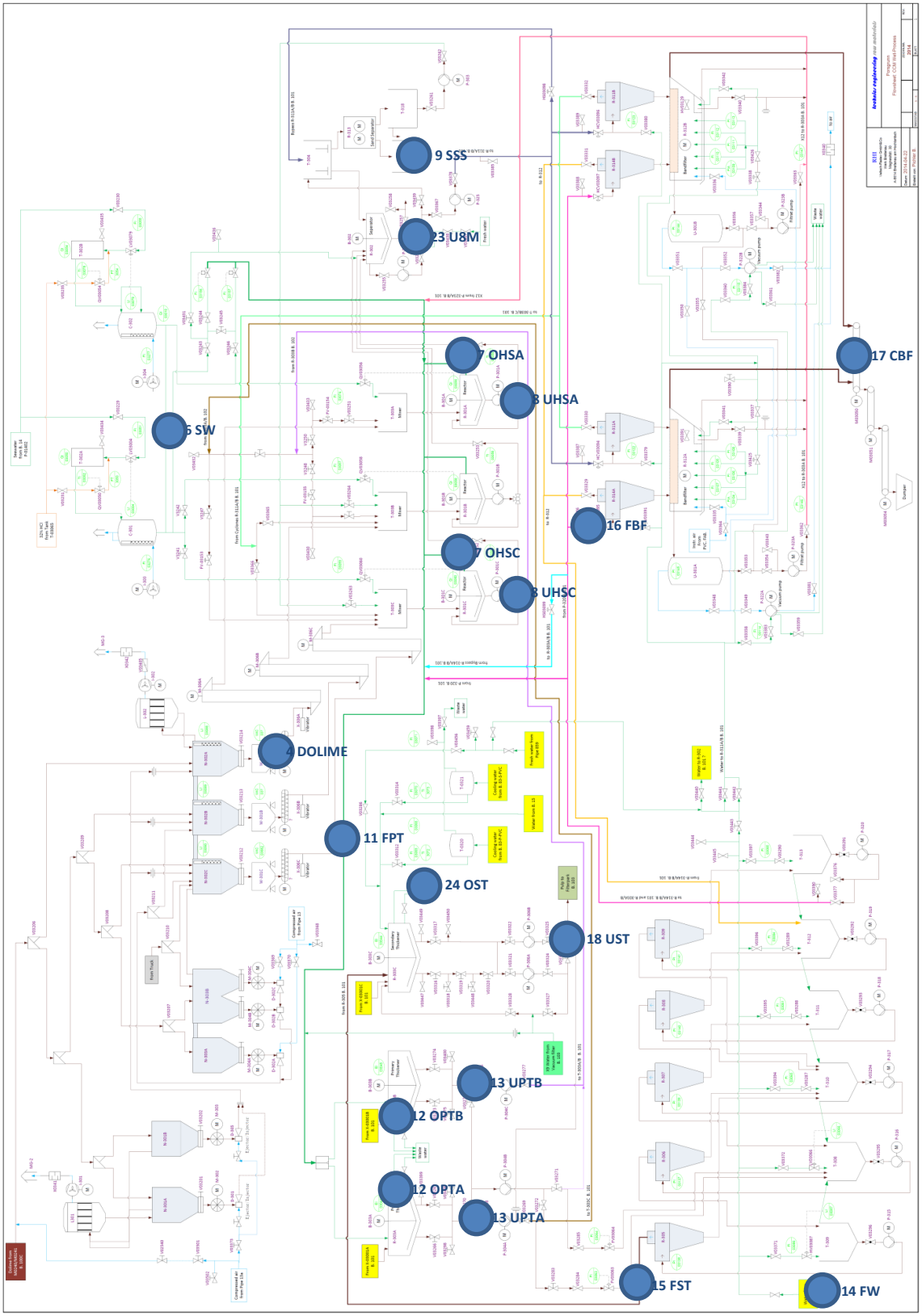

Wet process A-4

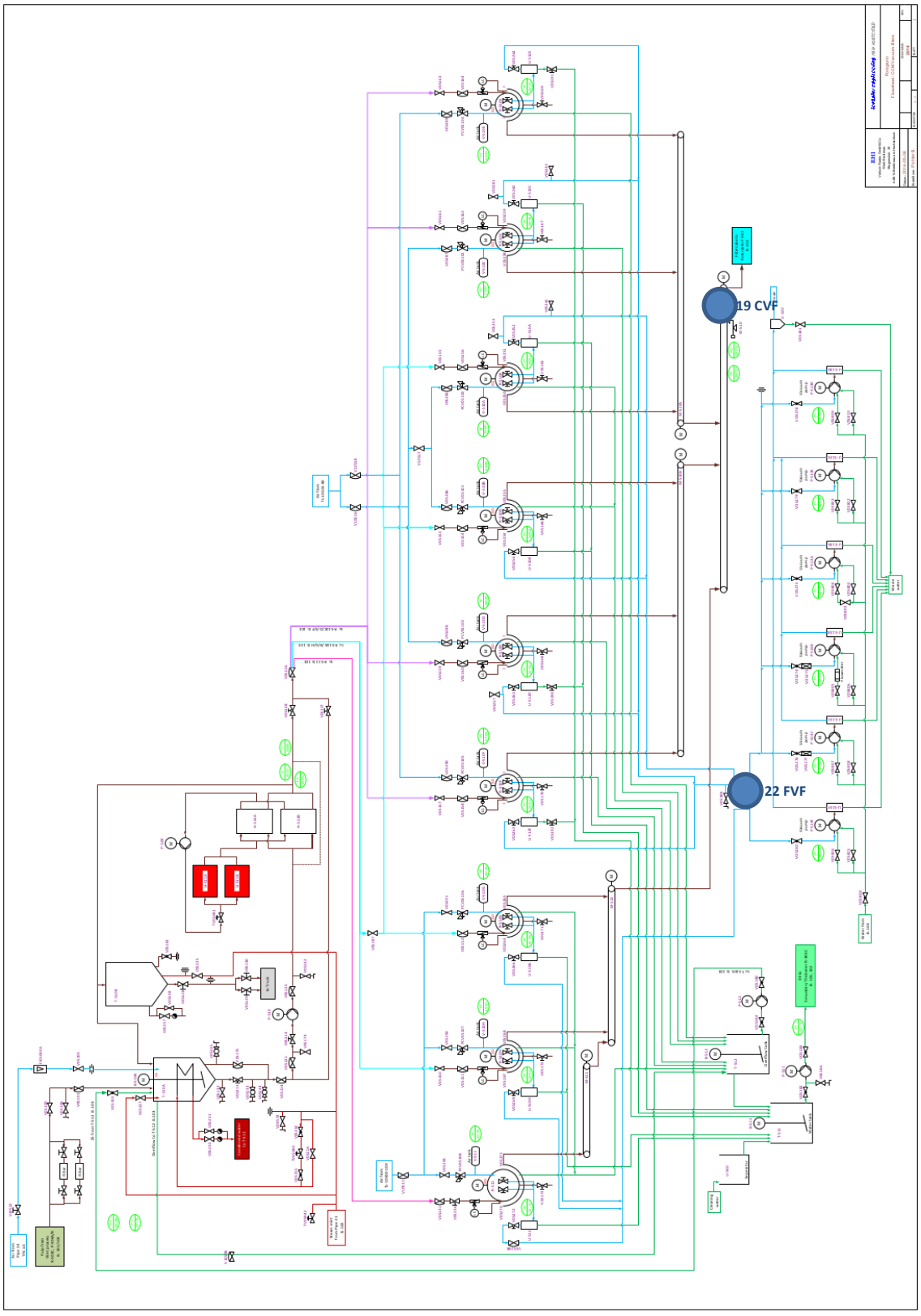

TABLE B-1: Samples for chemical and mineralogical analysis

Table B-2	Table B-3	Table B-4	Table B-5	Table B-6	Table B-7	Table B-8
1 3 DOLG1	22 11 FPT 1	39 21 HB7	56 13 UPTA1	72 SA 2	87 SAND 2000	101 S<5
2 4 DOLIME 3/1	23 13 UPTA3	40 7 OHSA1	57 17 CBF1-6	73 SA 3,15	88 HS 25	102 N 63/200
3 4 DOLIME3/2	24 13 UPTA4	41 11 FPT3	58 18 UST1-6	74 SA 5	89 HS 0	103 N 200/500
4 4 DOLIME 4/1	25 13 UPTA5	42 7 OHSA2	59 19 CVF1-6	75 SA 6,3	90 F1	104 N>40
5 4 DOLIME 4/2	26 13 UPTA6	43 7 OHSA3	60 23 U8M1-6	76 SA 10	91 F3	105 S5/10
6 4 DOLIME 5/1	27 13 UPTB3	44 7 OHSA4	61 1DOL6	77 13 UPTB1	92 F4	106 S10/20
7 4 DOLIME 5/2	28 13 UPTB4	45 7 OHSA5	62 1DOL7	78 SA 14	93 SAND 1000	107 S15/20
8 4 DOLIME 6/1	29 13 UPTB5	46 7 OHSA6	63 SA 0,025	79 SA 20	94 SAND 500	108 S20/25
9 4 DOLIME 6/2	30 11 FPT 2	47 7 OHSC1	64 SA 0,05	80 SA 25	95 SAND 200	109 S>25
10 4 DOLIME 6/3	31 13 UPTB6	48 7 OHSC2	65 SA 0,063	81 13 UPTB2	96 SAND 63	110 N<25
11 4 DOLIME 7/1	32 15 FST 1	49 7 OHSC3	66 13 UPTA2	82 8 UHSA1-6	97 SAND 25	111 N 25/40
12 3 DOLG6	33 15 FST 3	50 7 OHSC4	67 SA 0,1	83 8 UHSC1-6	98 SAND 0	112 N 40/63
13 4 DOLIME 7/2	34 15 FST 4	51 7 OHSC5	68 SA 0,2	84 16 FBF1-6	99 HS 200	
14 4 DOLIME 7/3	35 15 FST 5	52 11 FPT4	69 SA 0,315	85 22 FVF1-6	100 HS 63	
15 3 DOLG7	36 15 FST 6	53 7 OHSC6	70 SA 0,5	86 9 SSS1-6		
16 20 INT 1	37 21 HB1	54 11 FPT5	71 SA 1			
17 20 INT 6	38 21 HB6	55 11 FPT6				
18 20 INT 7		56 13 UPTA1				
19 4 DOLIME 1		57 17 CBF1-6				
20 4 DOLIME 2/1		58 18 UST1-6				
21 4 DOLIME 2/2		59 19 CVF1-6				
		60 23 U8M1-6				

TABLE B-2: Chemical and mineralogical data I

property	unit	1	2	3	4	5	6	7	8	9	10	11	12	13	14	15	16	17	18	19	20	21
total carbon																						
total carbon	%	11,16	0,27	0,23	0,31	0,18	0,19	0,22	0,23	0,25	0,21	0,25	10,96	0,20	0,17	11,13	11,12	11,09	11,17	0,20	0,32	0,24
XRD-analysis																						
Dolomite	$CaMg(CO_3)_2$	>50%	0,5-2%	0,5-2%	0,5-2%	0,5-2%	0,5-2%	0,5-2%	0,5-2%	0,5-2%	0,5-2%	0,5-2%	>50%			>50%	>50%	>50%	>50%	0,5-2%	0,5-2%	0,5-2%
Quartz, syn	SiO_2	0,5-2%									0,5-2%	0,5-2%	0,5-2%	0,5-2%	0,5-2%	0,5-2%	0,5-2%	0,5-2%	0,5-2%			
Phlogopite-1M	$KMg_3(Si_3Al)O_{10}(OH)_2$	<0,5%	<0,5%		<0,5%	<0,5%					<0,5%		<0,5%				<0,5%	<0,5%	<0,5%			<0,5%
Lime	CaO		>50%	>50%	>50%	>50%	>50%	>50%	>50%	>50%	>50%	>50%		>50%	>50%					>50%	>50%	>50%
Periclase, syn	MgO		10-50%	10-50%	10-50%	10-50%	10-50%	10-50%	10-50%	10-50%	10-50%	10-50%		10-50%	10-50%					10-50%	10-50%	10-50%
Portlandite	$Ca(OH)_2$		0,5-2%	0,5-2%	0,5-2%	0,5-2%	0,5-2%	0,5-2%	0,5-2%	0,5-2%	0,5-2%	0,5-2%		0,5-2%	0,5-2%					0,5-2%	0,5-2%	0,5-2%
loss of ignition																						
LOI	%	45,88	2,78	3,67	2,62	2,67	2,42	2,82	3,86	2,58	2,27	3,92	46,00	1,94	2,23	45,62	45,63	46,28	45,82	1,75	2,91	2,62
XRF-analysis																						
Na_2O	%	0,08	0,03	0,02	0,03	0,05	0,05	0,06	0,05	0,07	0,04	0,06	0,02	0,02	0,05	0,04	0,05	0,06	0,07	0,04	0,04	0,04
MgO	%	40,09	40,40	40,40	40,01	40,26	40,49	40,46	40,42	40,02	40,14	40,09	40,22	39,91	39,72	40,15	39,98	40,27	39,75	40,09	40,27	40,18
Al_2O_3	%	0,08	0,12	0,10	0,14	0,14	0,13	0,13	0,14	0,16	0,10	0,08	0,09	0,09	0,09	0,06	0,09	0,09	0,09	0,13	0,15	0,14
SiO_2	%	1,41	1,36	1,43	2,11	1,98	1,28	1,36	1,14	2,10	2,23	2,61	1,55	2,62	2,83	2,01	2,16	1,58	2,70	1,92	1,62	1,96
P_2O_5	%	0,01	0,01	0,02	0,02	0,01	0,01	0,02	0,02	0,02	0,01	0,02	0,01	0,02	0,03	0,01	0,00	0,00	0,01	0,01	0,01	0,02
SO_3	%	0,09	0,15	0,12	0,13	0,10	0,13	0,15	0,16	0,15	0,12	0,01	0,03	0,12	0,12	0,03	0,10	0,10	0,07	0,10	0,13	0,12
K_2O	%	0,03	0,03	0,03	0,03	0,03	0,03	0,03	0,04	0,04	0,03	0,02	0,03	0,02	0,03	0,03	0,04	0,04	0,02	0,04	0,03	0,03
CaO	%	57,22	57,68	57,65	57,09	57,22	57,67	57,56	57,78	57,20	57,13	56,93	57,84	56,99	56,94	57,40	57,32	57,60	57,07	57,45	57,51	57,27
TiO_2	%	0,02	0,01	0,01	0,01	0,01	0,01	0,01	0,01	0,01	0,01	0,01	0,01	0,01	0,01	0,01	0,01	0,01	0,01	0,01	0,01	0,02
Cr_2O_3	%	0,00	0,00	0,00	0,20	0,00	0,00	0,00	0,00	0,00	0,00	0,00	0,00	0,01	0,00	0,00	0,00	0,00	0,00	0,00	0,00	0,00
MnO	%	0,01	0,01	0,00	0,01	0,00	0,00	0,01	0,01	0,01	0,00	0,01	0,00	0,01	0,01	0,00	0,01	0,00	0,00	0,00	0,01	0,01
Fe_2O_3	%	0,18	0,20	0,21	0,21	0,20	0,19	0,20	0,21	0,21	0,18	0,16	0,18	0,18	0,16	0,22	0,21	0,21	0,18	0,20	0,21	0,20
ZrO2	%	0,77	0,00	0,00	0,00	0,00	0,00	0,00	0,01	0,00	0,00	0,00	0,01	0,00	0,00	0,02	0,03	0,03	0,02	0,01	0,00	0,00
BaO	%	0,00	0,00	0,00	0,00	0,00	0,00	0,00	0,00	0,00	0,00	0,00	0,00	0,00	0,00	0,00	0,00	0,00	0,00	0,00	0,00	0,00
HfO_2	%	0,00	0,00	0,00	0,00	0,00	0,00	0,00	0,00	0,00	0,01	0,00	0,00	0,00	0,00	0,01	0,00	0,00	0,00	0,00	0,00	0,00
total	%	100,0	100,0	100,0	100,0	100,0	100,0	100,0	100,0	100,0	100,0	100,0	100,0	100,0	100,0	100,0	100,0	100,0	100,0	100,0	100,0	100,0
LECO																						
S	%	0,007	0,050	0,060	0,050	0,050	0,050	0,070	0,060	0,050	0,040	0,030	0,006	0,040	0,040	0,004	0,010	0,008	0,008	0,040	0,040	0,030
SO_3	%	0,02	0,12	0,15	0,12	0,12	0,12	0,17	0,15	0,12	0,10	0,07	0,02	0,10	0,10	0,01	0,03	0,02	0,02	0,10	0,10	0,07

TABLE B-3: Chemical and mineralogical data II

property	unit	22	23	24	25	26	27	28	29	30	31	32	33	34	35	36	37	38
total carbon																		
total carbon	%	0,36	0,42	0,35	0,35	0,37	0,34	0,38	0,28	0,33	0,31	0,26	0,33	0,34	0,32	0,34	9,25	9,06
XRD-analysis																		
Brucite, syn	$Mg(OH)_2$	>50%	>50%	>50%	>50%	>50%	>50%	>50%	>50%	>50%	>50%	>50%	>50%	>50%	>50%	>50%		
Calcite, syn	$CaCO_3$	0,5-2%	0,5-2%	0,5-2%	0,5-2%	0,5-2%	0,5-2%	0,5-2%	0,5-2%	0,5-2%	0,5-2%	0,5-2%	0,5-2%	0,5-2%	0,5-2%	0,5-2%	2-5%	2-5%
unknown	unknown	0,5-2%	0,5-2%	0,5-2%	0,5-2%	0,5-2%	0,5-2%	0,5-2%	<0,5%		0,5-2%			<0,5%			0,5-2%	2-5%
Dolomite	$CaMg(CO_3)_2$		0,5-2%				<0,5%	<0,5%			<0,5%		<0,5%	<0,5%		<0,5%	>50%	>50%
Quartz, syn	SiO2		0,5-2%	0,5-2%	0,5-2%	0,5-2%	0,5-2%	0,5-2%		<0,5%	0,5-2%							0,5-2%
Lime	CaO																2-5%	2-5%
Periclase, syn	MgO																2-5%	2-5%
ICP-analysis																		
B_2O_3 conc.	%	0,029	0,028	0,031	0,053	0,028	0,037	0,024	0,028	0,027	0,023	0,024	0,017	0,027	0,022	0,021	0,000	0,000
loss of ignition																		
LOI	%	31,93	31,65	31,68	31,78	31,82	31,93	31,61	32,00	31,87	31,86	31,98	31,93	31,77	31,90	32,02	34,92	34,87
XRF-analysis																		
Na_2O	%	0,07	0,07	0,07	0,05	0,11	0,05	0,07	0,07	0,08	0,04	0,05	0,07	0,08	0,05	0,04	0,04	0,04
MgO	%	97,33	95,43	95,42	95,84	95,78	95,68	95,55	95,89	97,28	96,36	97,73	97,51	97,53	97,91	97,60	40,31	40,42
Al_2O_3	%	0,14	0,16	0,15	0,15	0,16	0,14	0,16	0,13	0,13	0,13	0,04	0,03	0,04	0,04	0,05	0,20	0,22
SiO_2	%	0,61	1,25	1,22	1,29	1,33	1,06	1,24	0,92	0,54	0,88	0,15	0,16	0,15	0,15	0,17	0,86	0,90
P_2O_5	%	0,01	0,02	0,02	0,02	0,03	0,02	0,03	0,02	0,02	0,02	0,00	0,01	0,01	0,00	0,01	0,05	0,05
SO_3	%	0,22	0,40	0,46	0,31	0,22	0,32	0,30	0,36	0,25	0,21	0,25	0,29	0,24	0,20	0,23	0,21	0,26
K_2O	%	0,00	0,00	0,00	0,03	0,02	0,02	0,02	0,01	0,00	0,01	0,00	0,00	0,00	0,00	0,00	0,03	0,03
CaO	%	1,38	2,37	2,36	2,06	2,09	2,47	2,33	2,36	1,45	2,07	1,52	1,69	1,72	1,43	1,67	58,07	57,83
TiO_2	%	0,01	0,01	0,01	0,01	0,01	0,01	0,01	0,01	0,01	0,01	0,01	0,01	0,01	0,01	0,01	0,01	0,01
Cr_2O_3	%	0,00	0,00	0,00	0,00	0,00	0,00	0,00	0,01	0,00	0,02	0,00	0,00	0,00	0,00	0,00	0,00	0,00
MnO	%	0,01	0,01	0,01	0,01	0,01	0,01	0,01	0,01	0,01	0,01	0,01	0,01	0,01	0,01	0,01	0,01	0,01
Fe_2O_3	%	0,20	0,25	0,24	0,21	0,21	0,20	0,25	0,21	0,19	0,23	0,21	0,19	0,19	0,18	0,18	0,20	0,22
ZrO2	%	0,01	0,02	0,02	0,01	0,02	0,01	0,02	0,00	0,03	0,01	0,02	0,02	0,01	0,01	0,02	0,00	0,01
BaO	%	0,00	0,00	0,00	0,00	0,00	0,00	0,00	0,00	0,00	0,00	0,00	0,00	0,00	0,00	0,00	0,00	0,00
HfO_2	%	0,00	0,00	0,01	0,01	0,00	0,00	0,00	0,00	0,01	0,00	0,01	0,00	0,00	0,00	0,00	0,00	0,00
total	%	100,0	100,0	100,0	100,0	100,0	100,0	100,0	100,0	100,0	100,0	100,0	100,0	100,0	100,0	100,0	100,0	100,0
LECO																		
S	%	0,000	0,120	0,140	0,080	0,080	0,140	0,120	0,120	0,000	0,110	0,070	0,070	0,090	0,050	0,080	0,080	0,080
SO_3	%	0,00	0,30	0,35	0,20	0,20	0,35	0,30	0,30	0,00	0,27	0,17	0,17	0,22	0,12	0,20	0,20	0,20

TABLE B-4: Chemical and mineralogical data III

property	unit	39	40	41	42	43	44	45	46	47	48	49	50	51	52	53	54	55
total carbon																		
total carbon	%	9,59	0,41	0,45	0,37	0,48	0,43	0,46	0,42	0,44	0,38	0,57	0,45	0,40	0,39	0,39	0,35	0,36
XRD-analysis																		
Brucite, syn	$Mg(OH)_2$		>50%	>50%	>50%	>50%	>50%	>50%	>50%	>50%	>50%	>50%	>50%	>50%	>50%	>50%	>50%	>50%
Calcite, syn	$CaCO_3$	2-5%	0,5-2%	0,5-2%	0,5-2%	0,5-2%	0,5-2%	0,5-2%	0,5-2%	<0,5%	<0,5%	0,5-2%	0,5-2%	0,5-2%	0,5-2%	0,5-2%	0,5-2%	0,5-2%
unknown	unknown	0,5-2%		0,5-2%		0,5-2%	0,5-2%	0,5-2%		0,5-2%	0,5-2%	0,5-2%	0,5-2%	0,5-2%	0,5-2%	0,5-2%	0,5-2%	
Dolomite	$CaMg(CO_3)_2$	>50%				<0,5%	<0,5%	<0,5%				0,5-2%	<0,5%	<0,5%		<0,5%		
Quartz, syn	SiO2			<0,5%	<0,5%	0,5-2%	0,5-2%	0,5-2%	0,5-2%	0,5-2%	0,5-2%	0,5-2%	<0,5%	0,5-2%		<0,5%	0,5-2%	0,5-2%
Lime	CaO	2-5%																
Periclase, syn	MgO	2-5%																
ICP-analysis																		
B_2O_3 conc.	%	0,000	0,010	0,030	0,022	0,016	0,014	0,015	0,023	0,017	0,016	0,022	0,033	0,020	0,026	0,016	0,028	0,027
loss of ignition																		
LOI	%	35,42	31,98	32,00	32,02	32,14	31,85	31,94	31,84	32,01	31,94	32,01	31,85	31,74	32,08	31,84	32,12	32,08
XRF-analysis																		
Na_2O	%	0,06	0,05	0,08	0,06	0,06	0,07	0,06	0,08	0,08	0,09	---	0,07	0,07	0,09	0,07	0,05	0,07
MgO	%	40,58	96,88	96,63	96,84	96,00	96,42	96,44	96,15	96,66	96,53	---	96,39	96,33	96,86	96,38	97,31	97,17
Al_2O_3	%	0,14	0,08	0,11	0,10	0,11	0,13	0,12	0,13	0,11	0,11	---	0,11	0,12	0,10	0,13	0,11	0,11
SiO_2	%	0,88	0,47	0,75	0,56	0,65	0,73	0,73	0,86	0,66	0,64	---	0,69	0,82	0,55	0,77	0,60	0,67
P_2O_5	%	0,05	0,01	0,02	0,01	0,02	0,02	0,02	0,02	0,02	0,02	---	0,01	0,02	0,02	0,02	0,02	0,02
SO_3	%	0,17	0,24	0,35	0,25	0,39	0,24	0,29	0,32	0,26	0,24	---	0,30	0,25	0,39	0,27	0,20	0,20
K_2O	%	0,03	0,01	0,00	0,01	0,02	0,02	0,02	0,02	0,02	0,01	---	0,01	0,02	0,00	0,02	0,00	0,00
CaO	%	57,88	1,99	1,76	1,93	2,50	2,10	2,05	2,13	1,95	2,09	---	2,15	2,10	1,70	2,07	1,46	1,50
TiO_2	%	0,01	0,01	0,01	0,01	0,01	0,01	0,01	0,01	0,01	0,01	---	0,01	0,01	0,01	0,01	0,01	0,01
Cr_2O_3	%	0,00	0,00	0,00	0,00	0,00	0,00	0,00	0,00	0,00	0,00	---	0,00	0,00	0,00	0,00	0,00	0,00
MnO	%	0,01	0,01	0,01	0,01	0,01	0,01	0,01	0,01	0,01	0,01	---	0,01	0,01	0,01	0,01	0,01	0,01
Fe_2O_3	%	0,19	0,22	0,27	0,21	0,22	0,24	0,22	0,25	0,21	0,22	---	0,21	0,22	0,26	0,22	0,21	0,22
ZrO2	%	0,00	0,02	0,01	0,01	0,00	0,01	0,02	0,01	0,01	0,01	---	0,03	0,02	0,01	0,02	0,01	0,02
BaO	%	0,00	0,00	0,00	0,00	0,00	0,00	0,00	0,00	0,00	0,00	---	0,00	0,00	0,00	0,00	0,00	0,00
HfO_2	%	0,00	0,00	0,00	0,00	0,00	0,00	0,00	0,00	0,00	0,01	---	0,00	0,00	0,00	0,00	0,00	0,00
total	%	100,0	100,0	100,0	100,0	100,0	100,0	100,0	100,0	100,0	100,0	---	100,0	100,0	100,0	100,0	100,0	100,0
LECO																		
S	%	0,070	0,080	0,000	0,080	0,110	0,040	0,060	0,070	0,070	0,050	0,060	0,040	0,040	0,000	0,040	0,000	0,000
SO_3	%	0,17	0,20	0,00	0,20	0,27	0,10	0,15	0,17	0,17	0,12	0,15	0,10	0,10	0,00	0,10	0,00	0,00

TABLE B-5: Chemical and mineralogical data IV

property	unit	56	57	58	59	60	61	62	63	64	65	66	67	68	69	70	71
total carbon																	
total carbon	%	0,40	0,72	0,58	0,54	0,89	12,59	12,71	12,41	11,23	10,58	0,41	11,43	12,68	12,58	---	---
XRD-analysis																	
Brucite, syn	$Mg(OH)_2$	>50%	>50%	>50%	>50%	>50%						>50%					
Calcite, syn	$CaCO_3$	0,5-2%	0,5-2%	0,5-2%	0,5-2%	0,5-2%						0,5-2%					
Illite 2M1	$(K,H_3O)Al_2Si_3AlO_{10}(OH)_2$	0,5-2%	0,5-2%			0,5-2%						0,5-2%					
Quartz, syn	SiO_2	0,5-2%	5-10%			5-10%		2-5%				0,5-2%					
Dolomite	$CaMg(CO_3)_2$		0,5-2%			0,5-2%	>50%	>50%									
Portlandite	$Ca(OH)_2$					0,5-2%											
unknown	unknown																
loss of ignition																	
LOI	%	36,65	28,23	32,18	32,36	30,57	46,89	46,67	46,69	46,62	46,65	35,14	46,60	46,78	46,72	46,77	46,75
XRF-analysis																	
Na_2O	%	0,04	0,13	0,04	0,02	0,06	0,05	0,00	0,00	0,01	0,03	0,05	0,03	0,01	0,00	0,01	0,01
MgO	%	95,98	78,42	97,68	97,85	84,00	40,32	39,97	40,43	40,26	40,25	96,20	40,26	40,12	40,10	40,25	40,54
Al_2O_3	%	0,16	1,56	0,04	0,05	0,57	0,10	0,09	0,22	0,20	0,21	0,16	0,21	0,15	0,12	0,09	0,06
SiO_2	%	1,13	15,26	0,19	0,18	8,79	1,54	2,47	1,31	1,38	1,53	1,03	1,63	1,80	1,98	1,47	0,92
P_2O_5	%	0,02	0,20	0,00	0,01	0,05	0,01	0,01	0,01	0,02	0,02	0,02	0,01	0,01	0,00	0,00	0,00
SO_3	%	0,43	0,01	0,36	0,24	0,22	0,09	0,14	0,13	0,17	0,10	0,25	0,13	0,12	0,16	0,09	0,08
K_2O	%	0,02	0,29	0,00	0,00	0,09	0,02	0,01	0,01	0,04	0,06	0,02	0,05	0,01	0,00	0,00	0,00
CaO	%	1,91	3,35	1,41	1,38	5,88	57,63	57,09	57,59	57,60	57,51	1,93	57,48	57,54	57,37	57,70	58,19
TiO_2	%	0,01	0,10	0,01	0,01	0,03	0,01	0,01	0,02	0,01	0,01	0,01	0,01	0,01	0,01	0,01	0,01
Cr_2O_3	%	0,00	0,00	0,00	0,00	0,00	0,00	0,01	0,00	0,00	0,00	0,00	0,00	0,00	0,00	0,16	0,00
MnO	%	0,01	0,02	0,01	0,01	0,01	0,00	0,01	0,00	0,01	0,01	0,01	0,01	0,00	0,01	0,00	0,00
Fe_2O_3	%	0,26	0,64	0,22	0,23	0,28	0,21	0,17	0,25	0,25	0,25	0,28	0,18	0,22	0,22	0,19	0,18
ZrO2	%	0,02	0,02	0,03	0,01	0,01	0,01	0,01	0,02	0,03	0,01	0,02	0,00	0,00	0,00	0,02	0,01
BaO	%	0,00	0,00	0,00	0,00	0,00	0,00	0,00	0,00	0,00	0,00	0,00	0,00	0,00	0,00	0,00	0,00
HfO_2	%	0,00	0,00	0,00	0,00	0,00	0,00	0,00	0,00	0,01	0,00	0,00	0,00	0,00	0,02	0,00	0,00
total	%	100,0	100,0	100,0	100,0	100,0	100,0	100,0	100,0	100,0	100,0	100,0	100,0	100,0	100,0	100,0	100,0
LECO																	
S	%	0,000	0,040	0,030	0,030	0,020	0,010	0,000	0,000	0,000	0,000	0,000	0,000	0,000	0,010	---	---
SO_3	%	0,00	0,10	0,07	0,07	0,05	0,03	0,00	0,00	0,00	0,00	0,00	0,00	0,00	0,03	---	---

TABLE B-6: Chemical and mineralogical data V

property	unit	72	73	74	75	76	77	78	79	80	81	82	83	84	85	86
total carbon																
total carbon	%	---	---	---	---	---	0,37	---	---	---	0,40	0,92	0,84	0,59	0,81	2,29
XRD-analysis																
Brucite, syn	$Mg(OH)_2$						>50%				>50%	>50%	>50%	>50%	>50%	5-10%
Calcite, syn	$CaCO_3$						0,5-2%				0,5-2%	0,5-2%	0,5-2%	0,5-2%	0,5-2%	0,5-2%
Illite 2M1	$(K,H_3O)Al_2Si_3AlO_{10}(OH)_2$											0,5-2%	0,5-2%	0,5-2%		0,5-2%
Quartz, syn	SiO_2						0,5-2%				0,5-2%	10-50%	10-50%	10-50%		>50%
Dolomite	$CaMg(CO_3)_2$											0,5-2%	0,5-2%	0,5-2%		5-10%
Portlandite	$Ca(OH)_2$											0,5-2%	2-5%			5-10%
unknown	unknown											0,5-2%				
loss of ignition																
LOI	%	46,70	46,60	46,61	46,66	46,52	34,93	46,49	46,70	46,87	34,39	29,58	28,83	29,46	33,75	15,87
XRF-analysis																
Na_2O	%	0,00	0,02	0,00	0,02	0,00	0,03	0,01	0,02	0,01	0,06	0,11	0,08	0,10	0,03	0,21
MgO	%	40,36	40,09	40,08	40,15	39,96	96,74	39,96	40,27	40,89	96,45	78,52	74,67	82,47	97,29	18,06
Al_2O_3	%	0,07	0,09	0,09	0,10	0,09	0,11	0,08	0,08	0,05	0,12	0,69	0,79	1,41	0,07	1,57
SiO_2	%	1,35	1,94	1,88	1,57	1,92	0,67	2,30	1,52	0,31	0,80	12,16	14,27	11,74	0,29	60,65
P_2O_5	%	0,00	0,00	0,01	0,01	0,01	0,02	0,01	0,00	0,00	0,02	0,05	0,07	0,19	0,01	0,31
SO_3	%	0,09	0,09	0,07	0,09	0,08	0,38	0,11	0,04	0,05	0,35	0,34	0,29	0,06	0,20	0,04
K_2O	%	0,01	0,00	0,00	0,01	0,01	0,01	0,01	0,00	0,00	0,01	0,24	0,19	0,37	0,00	0,31
CaO	%	57,88	57,52	57,63	57,81	57,67	1,73	57,25	57,81	58,50	1,89	7,54	9,26	2,94	1,87	17,92
TiO_2	%	0,01	0,01	0,01	0,01	0,01	0,01	0,01	0,01	0,01	0,01	0,01	0,02	0,08	0,01	0,12
Cr_2O_3	%	0,00	0,01	0,00	0,00	0,00	0,00	0,00	0,01	0,00	0,00	0,00	0,00	0,00	0,00	0,00
MnO	%	0,00	0,00	0,00	0,01	0,01	0,01	0,01	0,00	0,00	0,01	0,01	0,01	0,02	0,01	0,08
Fe_2O_3	%	0,21	0,21	0,21	0,21	0,21	0,25	0,22	0,21	0,17	0,24	0,29	0,33	0,58	0,21	0,72
ZrO2	%	0,02	0,02	0,02	0,01	0,03	0,03	0,02	0,03	0,01	0,02	0,03	0,02	0,03	0,01	0,01
BaO	%	0,00	0,00	0,00	0,00	0,00	0,00	0,00	0,00	0,00	0,00	0,00	0,00	0,00	0,00	0,00
HfO_2	%	0,00	0,00	0,00	0,00	0,00	0,00	0,00	0,00	0,00	0,00	0,00	0,00	0,00	0,00	0,00
total	%	100,0	100,0	100,0	100,0	100,0	100,0	100,0	100,0	100,0	100,0	100,0	100,0	100,0	100,0	100,0
LECO																
S	%	---	---	---	---	---	0,000	---	---	---	0,000	0,000	0,000	0,000	0,000	0,080
SO_3	%	---	---	---	---	---	0,00	---	---	---	0,00	0,00	0,00	0,00	0,00	0,20

TABLE B-7: Chemical and mineralogical data VI

property	unit	87	88	89	90	91	92	93	94	95	96	97	98	99	100
total carbon															
total carbon	%	2,73	0,94	0,97	1,39	0,88	0,75	3,30	3,51	1,60	2,00	8,10	3,00	#	0,74
XRD-analysis															
Dolomite	$CaMg(CO_3)_2$	10-50%						10-50%	10-50%	5-10%	5-10%	>50%	0,5-2%		
Quartz, syn	SiO_2	10-50%	0,5-2%					>50%	>50%	>50%	>50%	5-10%	0,5-2%		0,5-2%
Portlandite, syn	$Ca(OH)_2$	2-5%						2-5%	2-5%	0,5-2%					
Calcite, syn	$CaCO_3$	2-5%	5-10%	5-10%	5-10%	2-5%	2-5%				0,5-2%	10-50%	10-50%		5-10%
Talc-2M	$Mg_3Si_4O_{10}(OH)_2$	2-5%										0,5-2%			
Phlogopite	$KMg_3(Si_3Al)O_{10}(OH)_2$	0,5-2%	0,5-2%					2-5%	5-10%	0,5-2%	0,5-2%	2-5%			0,5-2%
Tremolite	$Ca_2Mg_5Si_8O_{22}(OH)_2$	0,5-2%						0,5-2%	0,5-2%	0,5-2%	0,5-2%	0,5-2%			
Brucite, syn	$Mg(OH)_2$	0,5-2%	>50%	>50%	>50%	>50%	>50%	0,5-2%	0,5-2%	0,5-2%	2-5%	10-50%	>50%		>50%
loss of ignition															
LOI	%	16,70	31,77	33,50	37,88	33,65	33,27	16,24	18,25	9,14	11,30	38,03	34,32	26,03	31,07
XRF-analysis															
Na_2O	%	0,67	0,09	0,04	0,06	0,06	0,05	0,28	0,22	0,21	0,28	0,10	0,06	0,21	0,05
MgO	%	18,62	92,38	94,23	93,48	95,33	96,67	15,74	18,88	10,28	13,08	40,91	70,86	64,88	91,17
Al_2O_3	%	5,24	0,37	0,16	0,10	0,05	0,03	2,14	2,02	1,45	1,59	2,15	2,14	3,41	0,52
SiO_2	%	52,00	1,71	0,27	0,36	0,18	0,18	62,75	59,70	78,26	71,48	9,17	3,98	20,19	3,49
P_2O_5	%	0,03	0,06	0,01	0,01	0,00	0,01	0,06	0,12	0,25	1,05	0,15	0,02	0,10	0,03
SO_3	%	0,19	0,19	0,33	0,34	0,70	0,28	0,00	0,13	0,00	0,00	0,28	0,45	0,95	0,26
K_2O	%	0,97	0,08	0,00	0,00	0,00	0,00	0,55	0,97	0,70	0,62	0,26	0,02	1,61	0,15
CaO	%	20,33	4,65	4,71	5,35	3,42	2,49	17,75	17,54	8,29	9,66	46,16	22,10	7,65	3,82
TiO_2	%	0,21	0,02	0,01	0,01	0,01	0,01	0,09	0,08	0,06	0,21	0,05	0,02	0,13	0,02
Cr_2O_3	%	0,03	0,00	0,00	0,00	0,00	0,00	0,01	0,02	0,03	0,01	0,00	0,00	0,00	0,00
MnO	%	0,17	0,02	0,01	0,01	0,01	0,01	0,13	0,05	0,03	0,03	0,03	0,01	0,02	0,02
Fe_2O_3	%	1,51	0,39	0,19	0,25	0,21	0,23	0,45	0,25	0,42	1,97	0,70	0,32	0,80	0,41
ZrO2	%	0,02	0,03	0,02	0,02	0,02	0,02	0,03	0,02	0,01	0,01	0,02	0,01	0,04	0,04
BaO	%	0,01	0,00	0,00	0,00	0,00	0,00	0,00	0,00	0,00	0,00	0,00	0,00	0,00	0,00
HfO_2	%	0,00	0,00	0,00	0,00	0,00	0,00	0,00	0,00	0,00	0,00	0,00	0,01	0,01	0,01
total	%	100,0	100,0	100,0	100,0	100,0	100,0	100,0	100,0	100,0	100,0	100,0	100,0	100,0	100,0
LECO															
S	%	0,060	0,000	0,000	0,070	0,010	0,030	0,060	0,050	0,030	0,050	0,070	0,090	#	0,000
SO_3	%	0,15	0,00	0,00	0,17	0,03	0,07	0,15	0,12	0,07	0,12	0,17	0,22	#	0,00

TABLE B-8: Chemical and mineralogical data VII

property	unit	101	102	103	104	105	106	107	108	109	110	111	112
total carbon													
total carbon	%		0,68		0,99		0,60	0,68	1,02		0,81	1,26	0,72
XRD-analysis													
Brucite, syn	$Mg(OH)_2$		>50%		>50%		>50%	>50%	>50%		>50%	>50%	>50%
Quartz, syn	SiO_2		5-10%		10-50%							0,5-2%	0,5-2%
Calcite, syn	$CaCO_3$		2-5%		2-5%		2-5%	5-10%	5-10%		5-10%	5-10%	5-10%
Phlogopite	$KMg_3(Si_3Al)O_{10}(OH_)2$		0,5-2%		0,5-2%								0,5-2%
Dolomite	$CaMg(CO3)_2$				2-5%								
loss of ignition													
LOI	%	40,43	30,10	29,60	30,22	38,36	33,30	33,72	33,81	35,70	33,47	34,92	31,62
XRF-analysis													
Na_2O	%	0,09	0,10	0,15	0,17	0,07	0,05	0,05	0,07	0,13	0,03	0,04	0,08
MgO	%	34,43	86,79	71,75	71,70	85,43	96,23	95,30	92,66	66,90	95,19	93,26	93,11
Al_2O_3	%	0,21	0,61	1,78	1,78	0,26	0,14	0,17	0,16	0,38	0,11	0,29	0,35
SiO_2	%	1,33	8,63	20,77	20,65	1,07	0,48	0,59	0,67	2,43	0,28	1,63	2,42
P_2O_5	%	0,00	0,10	0,15	0,15	0,02	0,01	0,01	0,02	0,29	0,01	0,09	0,06
SO_3	%	1,04	0,20	0,06	0,07	0,27	0,23	0,21	0,32	0,44	0,37	0,20	0,22
K_2O	%	0,00	0,25	0,61	0,71	0,00	0,00	0,00	0,00	0,07	0,00	0,03	0,11
CaO	%	62,67	2,81	4,07	4,08	12,51	2,67	3,43	5,83	28,43	3,79	3,98	3,18
TiO_2	%	0,01	0,03	0,08	0,07	0,03	0,01	0,01	0,01	0,12	0,01	0,02	0,01
Cr_2O_3	%	0,00	0,00	0,00	0,00	0,03	0,00	0,00	0,00	0,00	0,00	0,00	0,00
MnO	%	0,00	0,02	0,02	0,02	0,00	0,01	0,01	0,01	0,02	0,01	0,02	0,02
Fe_2O_3	%	0,20	0,43	0,55	0,58	0,28	0,16	0,20	0,22	0,78	0,19	0,42	0,42
ZrO2	%	0,01	0,02	0,01	0,01	0,04	0,01	0,01	0,02	0,00	0,01	0,01	0,02
BaO	%	0,00	0,00	0,00	0,00	0,00	0,00	0,00	0,00	0,00	0,00	0,00	0,00
HfO_2	%	0,00	0,00	0,00	0,00	0,00	0,00	0,00	0,00	0,00	0,00	0,00	0,00
total	%	100,0	100,0	100,0	100,0	100,0	100,0	100,0	100,0	100,0	100,0	100,0	100,0
LECO													
S	%		0,000		0,000		0,000	0,000	0,000		0,000	0,000	0,000
SO_3	%		0,00		0,00		0,00	0,00	0,00		0,00	0,00	0,00

TABLE B-9: Statistical data

		1DOL			3DOLG			4DOLIME			7OHSAC			20INT			8UHSAC			13UPTAB			11FPT			15FST		
		mean	SD_{abs}	SD_{rel}	mean	SD_{abs}	SD_{rel}	mean	SD_{abs}	SD_{rel}	mean	SD_{abs}	SD_{rel}	mean	SD_{abs}	SD_{rel}	mean	SD_{abs}	SD_{rel}	mean	SD_{abs}	SD_{rel}	mean	SD_{abs}	SD_{rel}	mean	SD_{abs}	SD_{rel}
Na2O	%	0,02	0,02	111,99	0,05	0,02	53,45	0,04	0,01	21,83	0,07	0,01	15,55	0,06	0,01	13,61	0,10	0,02	15,79	0,06	0,02	34,12	0,07	0,01	17,01	0,06	0,01	25,34
MgO	%	40,16	0,14	0,36	40,15	0,05	0,13	40,20	0,18	0,44	96,46	0,25	0,26	40,00	0,21	0,53	76,60	1,93	2,51	95,94	0,40	0,42	97,10	0,26	0,27	97,66	0,15	0,15
Al2O3	%	0,10	0,00	4,92	0,08	0,01	16,27	0,13	0,02	14,93	0,11	0,01	12,58	0,09	0,00	0,00	0,74	0,05	6,76	0,14	0,02	11,83	0,12	0,01	11,78	0,04	0,01	15,81
SiO2	%	1,89	0,42	22,01	1,66	0,26	15,47	1,85	0,42	22,65	0,69	0,11	15,46	2,15	0,46	21,30	13,22	1,06	7,98	1,07	0,20	19,04	0,62	0,07	11,63	0,16	0,01	5,13
P2O5	%	0,01	0,00	25,34	0,01	0,00	0,00	0,02	0,00	23,28	0,02	0,00	25,69	0,00	0,00	141,42	0,06	0,01	16,67	0,02	0,00	17,20	0,02	0,00	20,33	0,01	0,00	81,65
SO3	%	0,11	0,02	20,16	0,05	0,03	56,57	0,12	0,02	17,11	0,28	0,04	15,90	0,09	0,01	15,71	0,32	0,03	7,94	0,33	0,08	22,94	0,27	0,07	27,84	0,24	0,03	12,09
K2O	%	0,01	0,01	43,45	0,03	0,00	0,00	0,03	0,00	15,89	0,02	0,00	29,45	0,03	0,01	28,28	0,22	0,03	11,63	0,01	0,01	60,85	0,00	0,00	0,00	0,00	0,00	0,00
CaO	%	57,47	0,27	0,46	57,49	0,26	0,45	57,37	0,23	0,40	2,09	0,14	6,91	57,33	0,22	0,38	8,40	0,86	10,24	2,13	0,23	10,80	1,54	0,14	9,01	1,61	0,11	6,96
TiO2	%	0,01	0,00	1,14	0,01	0,00	35,36	0,01	0,00	16,33	0,01	0,00	0,00	0,01	0,00	0,00	0,02	0,01	33,33	0,01	0,00	0,00	0,01	0,00	0,00	0,01	0,00	0,00
Cr2O3	%	0,01	0,01	79,79	0,00	0,00	0,00	0,01	0,03	235,86	0,00	0,00	0,00	0,00	0,00	0,00	0,00	0,00	0,00	0,00	0,01	238,05	0,00	0,00	0,00	0,00	0,00	0,00
MnO	%	0,00	0,00	84,90	0,00	0,00	141,42	0,01	0,00	53,67	0,01	0,00	0,00	0,00	0,00	141,42	0,01	0,00	0,00	0,01	0,00	0,00	0,01	0,00	0,00	0,01	0,00	0,00
Fe2O3	%	0,20	0,02	9,31	0,19	0,02	9,75	0,20	0,01	6,47	0,22	0,01	5,39	0,20	0,01	7,07	0,31	0,02	6,45	0,24	0,02	9,86	0,23	0,03	13,27	0,19	0,01	5,77
ZrO2	%	0,01	0,00	24,23	0,27	0,36	133,48	0,00	0,00	183,71	0,01	0,01	52,72	0,03	0,00	17,68	0,03	0,01	20,00	0,02	0,01	44,72	0,02	0,01	50,92	0,02	0,00	30,62
BaO	%	0,00	0,00	0,00	0,00	0,00	0,00	0,00	0,00	0,00	0,00	0,00	0,00	0,00	0,00	0,00	0,00	0,00	0,00	0,00	0,00	0,00	0,00	0,00	0,00	0,00	0,00	0,00
HfO2	%	0,00	0,00	141,42	0,00	0,00	141,42	0,00	0,00	244,95	0,00	0,00	287,48	0,00	0,00	0,00	0,00	0,00	0,00	0,00	0,00	223,61	0,00	0,00	0,00	0,00	0,00	0,00

Appendix C: Calculation of Mica and Quartz Content in Sample Material

Mica and quartz contents in the sample material were calculated as described below. For the calculation, these two minerals were defined as carriers of silicon and aluminium, whereby quartz contains only Si and mica contains both Si and Al. The molar ratio used for the calculation is shown in Table C-1. Since mica consists of phlogopite and annite, an average molar composition was defined as $K(Fe,Mg)_3(Si_3Al)O_{10}(OH,F)_2$. In a first step, total SiO_2 and Al_2O_3 levels from XRF-analysis were transferred to total Si and Al (Table C-2). Then the amount of mica was calculated based on aluminium. By subtracting Si contained in mica from total Si, silicon originated only from quartz as well as the quartz content were determined.

TABLE C-1: Molar ratios

elements	[g/mol]	composition	[g/mol]	ratio	[%]
K	39,098	SiO_2	60,084	Al/Al_2O_3	52,925
Mg	24,305	Al_2O_3	101,961	$Al/K(Fe,Mg)_3(Si_3Al)O_{10}(OH,F)_2$	5,795
Si	28,086	$KMg_3(Si_3Al)O_{10}(OH)_2$	417,260	Si/SiO_2	46,743
Al	26,982	$KFe_3(Si_3Al)O_{10}(OH,F)_2$	513,872	$Si/K(Fe,Mg)_3(Si_3Al)O_{10}(OH,F)_2$	18,098
O	15,999	$K(Fe,Mg)_3(Si_3Al)O_{10}(OH,F)_2$	465,566		
H	1,008				
F	18,999				
Fe	55,845				

TABLE C-2: Calculation of mica and quartz in material streams

property	content [%]																
	1DOL	3DOLG	4DOLIME	20INT	21HB	7OHSAC	8UHSAC	23U8M	9SSS	11FPT	13UPTAB	15FST	16FBF	17CBF	18UST	19CVF	22FVF
composition from XRF-analysis																	
Na2O	0,020	0,047	0,042	0,060	0,047	0,070	0,095	0,060	0,210	0,073	0,059	0,058	0,100	0,130	0,040	0,020	0,030
MgO	40,161	40,153	40,204	40,000	40,437	96,457	76,595	84,000	18,060	97,097	95,943	97,656	82,470	78,420	97,680	97,850	97,290
Al2O3	0,097	0,077	0,125	0,090	0,187	0,114	0,740	0,570	1,570	0,117	0,144	0,040	1,410	1,560	0,040	0,050	0,070
SiO2	1,886	1,657	1,854	2,147	0,880	0,691	13,215	8,790	60,650	0,620	1,068	0,156	11,740	15,260	0,190	0,180	0,290
P2O5	0,008	0,010	0,016	0,003	0,050	0,017	0,060	0,050	0,310	0,018	0,022	0,006	0,190	0,200	0,000	0,010	0,010
SO3	0,109	0,050	0,120	0,090	0,213	0,276	0,315	0,220	0,040	0,268	0,333	0,242	0,060	0,010	0,360	0,240	0,200
K2O	0,012	0,030	0,031	0,033	0,030	0,016	0,215	0,090	0,310	0,000	0,014	0,000	0,370	0,290	0,000	0,000	0,000
CaO	57,465	57,487	57,371	57,330	57,927	2,094	8,400	5,880	17,920	1,542	2,131	1,606	2,940	3,350	1,410	1,380	1,870
TiO2	0,010	0,013	0,011	0,010	0,010	0,010	0,015	0,030	0,120	0,010	0,010	0,010	0,080	0,100	0,010	0,010	0,010
Cr2O3	0,010	0,000	0,015	0,000	0,000	0,000	0,000	0,000	0,000	0,000	0,003	0,000	0,000	0,000	0,000	0,000	0,000
MnO	0,005	0,003	0,006	0,003	0,010	0,010	0,010	0,010	0,080	0,010	0,010	0,010	0,020	0,020	0,010	0,010	0,010
Fe2O3	0,196	0,193	0,197	0,200	0,203	0,221	0,310	0,280	0,720	0,225	0,236	0,190	0,580	0,640	0,220	0,230	0,210
ZrO2	0,012	0,267	0,002	0,027	0,003	0,015	0,025	0,010	0,010	0,015	0,017	0,016	0,030	0,020	0,030	0,010	0,010
BaO	0,000	0,000	0,000	0,000	0,000	0,000	0,000	0,000	0,000	0,000	0,000	0,000	0,000	0,000	0,000	0,000	0,000
HfO2	0,001	0,003	0,000	0,000	0,000	0,001	0,000	0,000	0,000	0,002	0,002	0,002	0,000	0,000	0,000	0,000	0,000
total	100,00	100,00	100,00	100,00	100,00	100,00	100,00	100,00	100,00	100,00	100,00	100,00	100,00	100,00	100,00	100,00	100,00
calculation																	
SiO2tot	1,886	1,657	1,854	2,147	0,880	0,691	13,215	8,790	60,650	0,620	1,068	0,156	11,740	15,260	0,190	0,180	0,290
Al2O3tot	0,097	0,077	0,125	0,090	0,187	0,114	0,740	0,570	1,570	0,117	0,144	0,040	1,410	1,560	0,040	0,050	0,070
Sitot	0,882	0,774	0,867	1,003	0,411	0,323	6,177	4,109	28,350	0,290	0,499	0,073	5,488	7,133	0,089	0,084	0,136
Altot	0,051	0,041	0,066	0,048	0,099	0,060	0,392	0,302	0,831	0,062	0,076	0,021	0,746	0,826	0,021	0,026	0,037
K(Fe,Mg)3(Si3Al)O10(OH,F)2	0,883	0,700	1,142	0,822	1,705	1,040	6,758	5,205	14,338	1,065	1,317	0,365	12,876	14,246	0,365	0,457	0,639
Si/K(Fe,Mg)3(Si3Al)O10(OH,F)2	0,160	0,127	0,207	0,149	0,309	0,188	1,223	0,942	2,595	0,193	0,238	0,066	2,330	2,578	0,066	0,083	0,116
delta Si	0,722	0,648	0,660	0,855	0,103	0,135	4,954	3,167	25,755	0,097	0,261	0,007	3,157	4,555	0,023	0,002	0,020
SiO2Quarz	1,544	1,386	1,412	1,828	0,220	0,289	10,599	6,775	55,099	0,208	0,559	0,015	6,755	9,744	0,049	0,003	0,043
mineral content																	
mica	0,883	0,700	1,142	0,822	1,705	1,040	6,758	5,205	14,338	1,065	1,317	0,365	12,876	14,246	0,365	0,457	0,639
quartz	1,544	1,386	1,412	1,828	0,220	0,289	10,599	6,775	55,099	0,208	0,559	0,015	6,755	9,744	0,049	0,003	0,043

Appendix D: Calculation of the Material Balance

To create a balance model for material streams in a process, the principles of correct balancing have to be applied. The most important rule of balancing is the conservation of unit inside the balance room (Formula D-2). This means, that the unit of property keeps constant. Since there were material conversions like calcining and slaking, the constant reference value through the process was defined as unit of SiO_2 respectively the SiO_2 bearing minerals, mica and quartz. Those minerals were assumed to be chemical inert for conversions. The unit $I_{i,j}$ of property i in material stream j is calculated as product of the mass of the material stream M_j and the grade of property $g_{i,j}$ in the stream (Formula D-1). The unit of a property in the streams of a single balance can be listed absolute in [t/h] or relative in [%].

$$I_{i,j} = M_j \cdot g_{i,j}$$

Formula D-1: Unit of property i

$$\sum_{j=1}^{n} M_j \cdot g_{i,j} = M_{feed} \cdot g_{i,feed}$$

Formula D-2: Conservation of units

$$r_{i,j} = \frac{I_{i,j}}{I_{i,feed}} \cdot 100 \qquad r_{i,j} = r_{m,j} \cdot \frac{g_{i,j}}{g_{i,feed}}$$

Formulas D-3 and D-4: Unit distribution or recovery

i	property
j	material stream
M_j	mass of the material stream [t/h]
$g_{i,j}$	grade of property i in material stream j [%]
$I_{i,j}$	unit of property i in material stream j [t/h]
r_{ij}	proportion of total units [%]
rm_j	proportion of material stream j by mass [%]

The material balance was calculated by using all available data. Chemical compositions from XRF-analysis (Appendix B, Table B-2 to B-8) as well as process data, measured solid contents (Chapter 5. Processing and Analysis, Table 4-5 or Appendix J, Table J-1 and J-2) and calculated mineral units (Appendix C, Table C-2) were used. The whole balance was divided in three single balances (I, II and III), which were calculated individually, before connecting them to a whole system. In the following paragraphs the calculation path is described in detail for SiO_2, which refers also to mica and quartz.

Balance I

Mass streams of dolomite and dolime were given from process data in t/h. With data of the chemical composition of each mass stream, the units of SiO_2 were calculated using Formula D-1. Since mass streams were only known for dolomite and dolime, the SiO_2 units in half burned material was calculated by subtracting the SiO_2 unit of dolime from dolomite. Now the total process feed was known and according to Formula D-2 defined as 100%. The unit distribution or recovery was calculated using Formula D-3. In Table D-1 the results are illustrated.

Balance II

For balance II only the mass stream of the feed and the SiO_2 grades in all three streams were known. By using Formula D-5, the mass stream distribution $rm_{i,j}$ can be calculated only knowing the SiO_2 grades. At this point it has to be mentioned, that the dry mass of the product streams was assumed to be constant for the slaking process. From a stoichiometric point of view, $Mg(OH)_2$ from seawater is precipitated, while $Ca(OH)_2$ from dolime is dissolved. Nevertheless, the total solid mass stream kept constant. The solid mass of the product from balance II (7OHSAC) equals the solid mass of the feed from balance III (13UPTAB), considering weak additional $Mg(OH)_2$ precipitation during seawater washing

$$rm_{1,j} = \frac{\left(g_{i,feed} - g_{i,2}\right)}{\left(g_{i,1} - g_{i,2}\right)} \cdot 100$$

Formula D-5: Calculation of mass distribution from grades

Since the mass stream of dolime was known from process data, the other dry mass streams could be calculated now in t/h with the mass stream distribution. With the solid content g_{solid} also the total mass streams could be calculated. The total unit and unit distribution of SiO_2, was calculated like in balance I. It was observed that there were small irregularities in the unit distribution of mica and quartz, likely to be originated from the assumption of an “average mica” for the calculation. In Table D-2 the results are illustrated.

Balance III

In balance III, the mass stream distribution rm_i was calculated in the same way as in balance II, by using SiO_2 grades. Since the total mass streams of primary thickener underflow and vacuum filter cake were known, only the band filter cake mass stream was calculated from rm_i. With the solid content g_{solid}, the dry material mass stream was derived. The total units and unit distributions were calculated same way as in balance I and II. Also in balance III it was observed that there were small irregularities in the contents of SiO_2, mica and quartz. In Table D-3 the results are illustrated.

To connect the single balances, the feed units of balance I of SiO_2, mica and quartz were defined as 100%. The product of balance I was also feed of balance II and the product of balance II was the feed of balance III. Therefore the distribution was adapted to the main feed units (see Table D-4).

Table D-1: Balance I

type	stream	M_{tot} [t/h]	M_{solid} [t/h]	rm [%]	g_{solid} [%]	SiO_2			mica			quartz		
						g_{SiO2} [%]	l_{SiO2} [t/h]	r_{SiO2} [%]	g_{mica} [%]	l_{mica} [t/h]	r_{mica} [%]	g_{quarz} [%]	l_{quarz} [t/h]	r_{quarz} [%]
Tailings fine	21HB	-	-	-	100,000	0,880	0,198	54,323	1,705	0,068	39,950	0,220	0,172	57,506
Product	4DOLIME	8,976	8,976	-	100,000	1,854	0,166	45,677	1,142	0,102	60,050	1,412	0,127	42,494
Feed	1DOL	19,317	19,317	100,000	100,000	1,886	0,364	100,000	0,883	0,171	100,000	1,544	0,298	100,000

Table D-2: Balance II

type	stream	M_{tot} [t/h]	M_{solid} [t/h]	rm [%]	g_{solid} [%]	SiO_2			mica			quartz		
						g_{SiO2} [%]	l_{SiO2} [t/h]	r_{SiO2} [%]	g_{mica} [%]	l_{mica} [t/h]	r_{mica} [%]	g_{quarz} [%]	l_{quarz} [t/h]	r_{quarz} [%]
Tailings coarse	9SSS	0,269	0,174	1,940	64,700	60,650	0,106	63,440	14,338	0,025	24,361	55,099	0,096	75,669
Product fine	7OHSAC	338,946	8,802	98,060	2,597	0,691	0,061	36,560	1,040	0,092	89,300	0,289	0,025	20,056
Feed	4DOLIME	8,976	8,976	100,000	100,000	1,854	0,166	100,000	1,142	0,102	113,662	1,412	0,127	95,725

Table D-3: Balance III

type	stream	M_{tot} [t/h]	M_{solid} [t/h]	rm [%]	g_{solid} [%]	SiO_2			mica			quartz		
						g_{SiO2} [%]	l_{SiO2} [t/h]	r_{SiO2} [%]	g_{mica} [%]	l_{mica} [t/h]	r_{mica} [%]	g_{quarz} [%]	l_{quarz} [t/h]	r_{quarz} [%]
Tailings coarse	17CBF	1,068	0,592	5,891	55,400	15,260	0,090	84,144	14,246	0,084	63,743	9,744	0,058	102,760
Product fine	19CVF	21,278	10,114	94,109	47,532	0,180	0,018	16,962	0,457	0,046	34,915	0,003	0,000	0,579
Feed	13UPTAB	54,582	10,047	100,000	18,407	1,068	0,107	101,106	1,317	0,132	98,659	0,559	0,056	103,339

Table D-4: Balance harmonisation

balance	type	stream	SiO2			mica			quarz		
			$r_{SiO2,balance}$ [%]	$r_{SiO2,harmonised}$ [%]	l [t/h]	$r_{mica,balance}$ [%]	$r_{mica,harmonised}$ [%]	l [t/h]	$r_{quartz,balance}$ [%]	$r_{quartz,harmonised}$ [%]	l [t/h]
I	Tailings	21HB	54,323	54,323	0,198	39,950	39,950	0,068	57,506	57,506	0,172
	Product	4DOLIME	45,677	45,677	0,166	60,050	60,050	0,102	42,494	42,494	0,127
	Feed	1DOL	100,000	100,000	0,364	100,000	100,000	0,171	100,000	100,000	0,298
II	Tailings	9SSS	63,440	28,978	0,106	24,361	14,629	0,025	75,669	32,155	0,096
	Product	7OHSAC	36,560	16,699	0,061	89,300	53,625	0,092	20,056	8,522	0,025
	Feed	4DOLIME	100,000	45,677	0,166	113,662	60,050	0,102	95,725	42,494	0,127
III	Tailings	17CBF	84,144	13,898	0,051	63,743	34,647	0,059	102,760	8,475	0,025
	Product	19CVF	16,962	2,802	0,010	34,915	18,978	0,032	0,579	0,048	0,000
	Feed	13UPTAB	101,106	16,699	0,061	98,659	53,625	0,092	103,339	8,522	0,025

Appendix E: Particle Size Analysis

Particle size analysis was performed by different methods, depending on the kind of sample material and purpose of the analysis. Dry sample material was sieved with standard test sieves (DIN 66165). Wet samples were wet sieved by Rhewum test sieves. The particle size analysis for particles smaller than 25µm was performed via sedimentation (see Appendix G: Preparation of Grain Size Classes via Sedimentation).

Table E-1: Dolomite

KG [mm]		rm [%]	R [%]	D [%]
20	25/20	1,224	1,224	98,776
14	20/14	5,322	6,546	93,454
10	14/10	12,437	18,983	81,017
6,3	10/6,3	13,830	32,813	67,187
5	6,3/5	3,735	36,549	63,451
3,15	5/3,15	5,328	41,877	58,123
2	3,15/2	3,038	44,915	55,085
1	2/1	5,066	49,981	50,019
0,5	1/0,5	14,188	64,169	35,831
0,315	0,5/0,315	11,130	75,298	24,702
0,2	0,315/0,2	8,611	83,909	16,091
0,1	0,2/0,1	7,710	91,620	8,380
0,063	0,1/0,063	2,950	94,569	5,431
0,05	0,063/0,05	1,207	95,776	4,224
0,025	0,05/0,025	1,780	97,556	2,444
0	<0,025	2,444	100,000	0,000
		100,000		

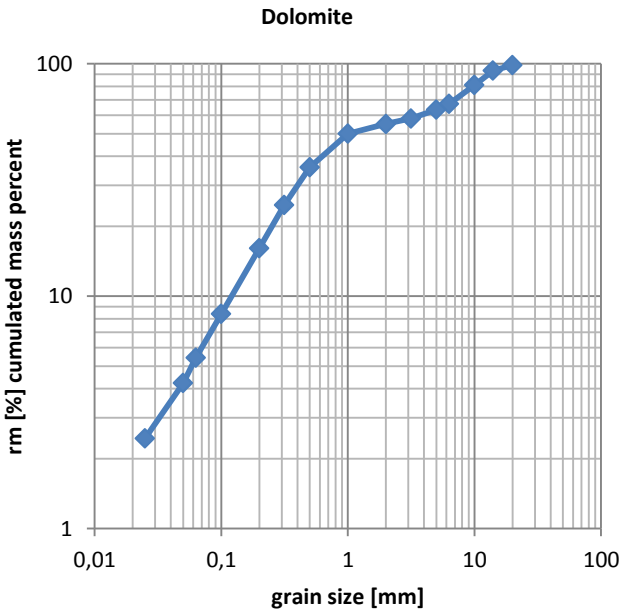

Table E-2: Sand separator

KG [mm]		rm [%]	R [%]	D [%]
2	>2	0,647	0,647	99,353
1	2/1	5,545	6,192	93,808
0,5	1/0,5	24,144	30,336	69,664
0,2	0,5/0,2	58,724	89,060	10,940
0,063	0,2/0,063	3,294	92,354	7,646
0,025	0,063/0,025	0,262	92,616	7,384
0	<0,025	7,384	100,000	0,000
		100,000		

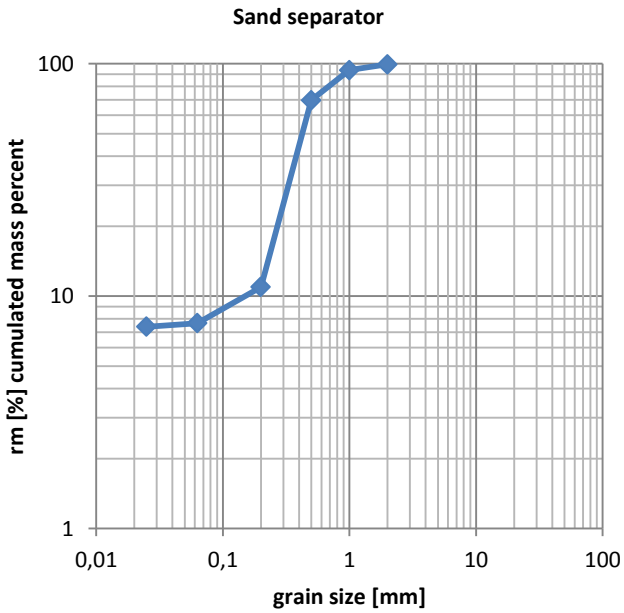

Table E-3: Overflow hydroseparator

KG [mm]		rm [%]	R [%]	D [%]
2	>2	0,000	0,000	100,000
1	2/1	0,000	0,000	100,000
0,5	1/0,5	0,000	0,000	100,000
0,2	0,5/0,2	0,343	0,343	99,657
0,063	0,2/0,063	8,597	8,940	91,060
0,025	0,063/0,025	12,202	21,142	78,858
0	<0,025	78,858	100,000	0,000
		100,000		

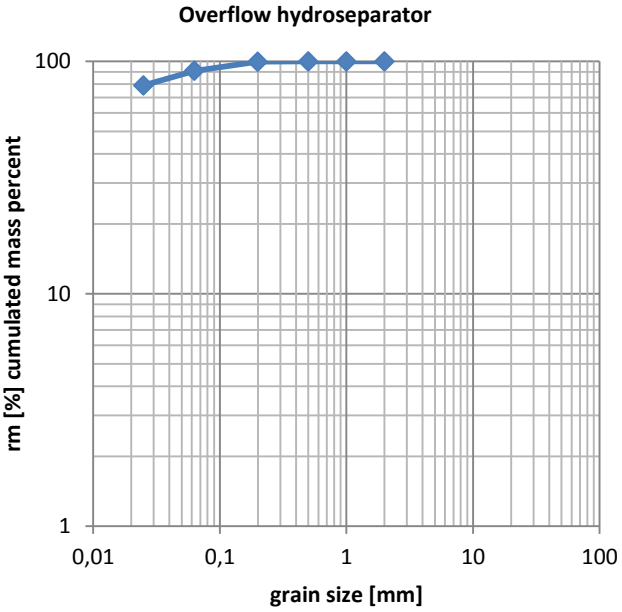

Table E-4: Underflow prim. thickener I (wet screening)

KG [mm]		rm [%]	R [%]	D [%]
2	>2	0,000	0,000	100,000
1	2/1	0,000	0,000	100,000
0,5	1/0,5	0,000	0,000	100,000
0,2	0,5/0,2	0,437	0,437	99,563
0,063	0,2/0,063	7,347	7,783	92,217
0,04	0,063/0,04	6,070	13,854	86,146
0,025	0,04/0,025	3,817	17,671	82,329
0	<0,025	82,329	100,000	0,000
		100,000		

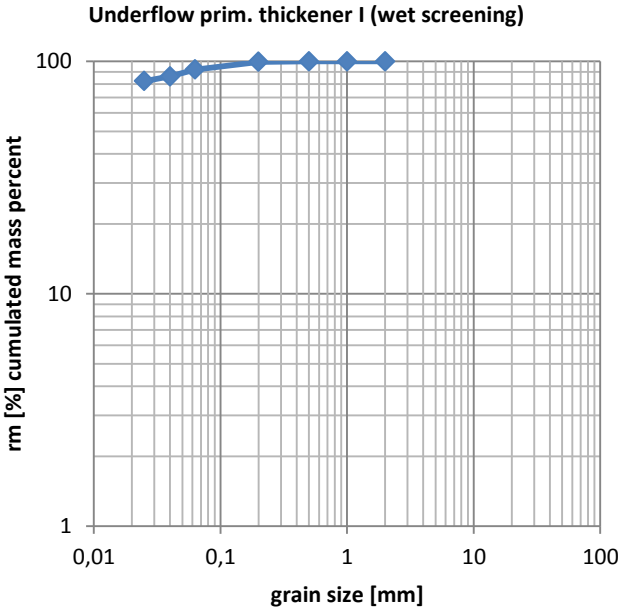

Table E-5: Cake band filter

KG [mm]		rm [%]	R [%]	D [%]
2	>2	0,000	0,000	100,000
1	2/1	0,025	0,025	99,975
0,5	1/0,5	0,215	0,240	99,760
0,2	0,5/0,2	5,184	5,424	94,576
0,063	0,2/0,063	28,814	34,238	65,762
0,04	0,063/0,04	21,671	55,908	44,092
0,025	0,04/0,025	11,354	67,262	32,738
0	<0,025	32,738	100,000	0,000
		100,000		

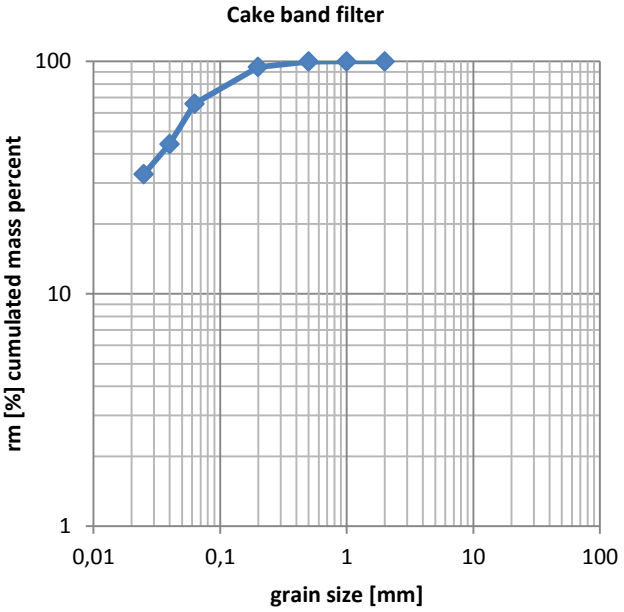

Table E-6: Slaked dolime

KG [mm]		rm [%]	R [%]	D [%]
2	>2	0,013	0,013	99,987
1	2/1	0,108	0,120	99,880
0,5	1/0,5	0,468	0,588	99,412
0,2	0,5/0,2	1,476	2,064	97,936
0,063	0,2/0,063	8,494	10,558	89,442
0,025	0,063/0,025	11,970	22,528	77,472
0	<0,025	77,472	100,000	0,000
		100,000		

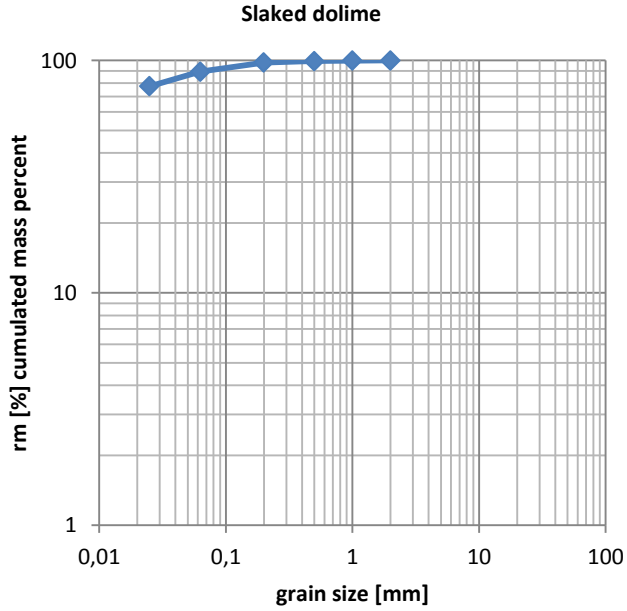

Table E-7: Underflow prim. thickener II (sedimentation)

KG [mm]		rm [%]	R [%]	D [%]
2	>2	0,000	0,000	100,000
1	2/1	0,000	0,000	100,000
0,5	1/0,5	0,000	0,000	100,000
0,2	0,5/0,2	0,437	0,437	99,563
0,063	0,2/0,063	7,347	7,783	92,217
0,04	0,063/0,04	6,070	13,854	86,146
0,025	0,04/0,025	3,817	17,671	82,329
0,02	0,025/0,020	18,408	36,079	63,921
0,015	0,020/0,015	29,949	66,027	33,973
0,01	0,015/0,010	32,491	98,519	1,481
0,005	0,010/0,005	0,768	99,287	0,713
0	<0,005	0,713	100,000	0,000
		100,000		

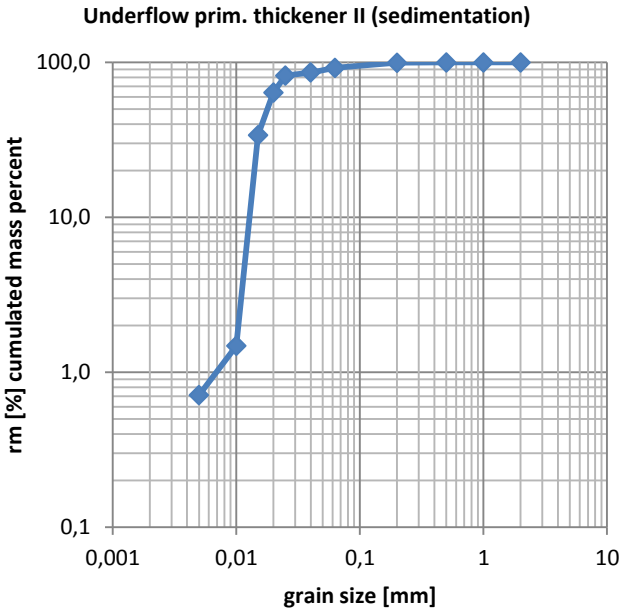

GS [mm]	K	m %	D [%] nass	D [%] trocken	n_{GGS}	$k_{äq}^3$	$k_{äq}$ [mm]
< 13,0 mm	13,000	71,9	100	100			8,8930
< 6,0 mm	6,000	3,8	28,1	100,0	1,64177	703,30	4,1646
< 3,15 mm	3,150	1,4	24,3	100,0	0,22549	72,23	2,4524
< 2,0 mm	2,000	1,7	22,9	97,7	0,13063	14,75	1,3401
< 1,0 mm	1,000	4,0	21,2	85,4	0,11128	2,41	0,6749
< 0,5 mm	0,500	4,2	17,2	63,0	0,30166	0,31	0,3907
< 0,315 mm	0,315	4,6	13,0	45,0	0,60593	0,06	0,2487
< 0,2 mm	0,200	4,3	8,4	27,6	0,96139	0,02	0,1389
< 0,1 mm	0,100	1,6	4,1	12,6	1,03477	0,00	0,0788
< 0,063 mm	0,063	2,5	2,5	7,9	1,07069	0,00	0,0000

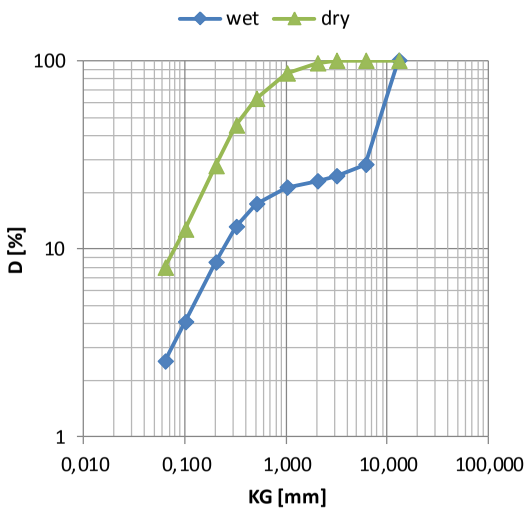

Inhomogeneity of grain size class 6,0-3,15 mm for 27.06.2014

j [mm]	xi-x0	$(xi-x0)^2$	mj [1]	ρ [kg/m³]	$k_{äq}^3$ [m³]	ci	Ii [kg%²]
13	28,1	789,6	0,719	2875,9	7,03303E-07	0,6	0,68898492
2	-71,9	5169,6	0,017	2875,9	2,40649E-09	0,6	0,00036494
1	-71,9	5169,6	0,04	2875,9	3,07392E-10	0,6	0,00010968
0,5	-71,9	5169,6	0,042	2875,9	5,96237E-11	0,6	2,2338E-05
0,315	-71,9	5169,6	0,046	2875,9	1,53832E-11	0,6	6,3123E-06
0,2	-71,9	5169,6	0,043	2875,9	2,67757E-12	0,6	1,0271E-06
0,1	-71,9	5169,6	0,016	2875,9	4,88816E-13	0,6	6,9767E-08
0,063	-71,9	5169,6	0,025	2875,9	0	0,6	0
						Summe	**0,68948929**

MW [mm]	K	xi [% SiO2]
> 2 mm	2,00	12,4000
2-1 mm	1,00	5,8700
1-0,5 mm	0,50	2,5400
500-315 mm	0,32	3,1400
315-200 mm	0,20	3,0100
200-100 mm	0,10	2,5800
100-40 mm	0,04	3,0700
< 40 mm	0,00	2,3600

Calculation of the sample mass

Δx	1	%-Pt
N	3	single sample amount
N-1	2	degree of freedome
α	0,05	
1-α/2	0,975	
$t_{0,975,2}$	4,303	
S	0,232	
S^2	0,054	
Mp	**12,764**	**bulk sample mass [kg]**
Ep	**4,255**	**single sample mass [kg]**

$$t_{1-\frac{\alpha}{2},N} = \frac{\Delta x}{\overline{S}}$$

$$\overline{S}^2 = \frac{I}{Mp}$$

Appendix G: Preparation of Grain Size Classes via Sedimentation

The sample preparation method via sedimentation is used, when a separation in very fine grain size classes is needed. Normally this is done for material smaller 25µm, when the limits of wet sieving are reached. In principle this method works by calculating the terminal or settling velocity of a sphere falling in a fluid based on Stokes' law (formula G-1). By defining a given grain size, the settling time ca be calculated (formula G-2). The separation is practically done in a sedimentation flask (see Figures G-1 to G-3), which is a big bottle with an outlet valve some centimetres above the bottom. The outlet valve is fixed to a tube that reaches into the centre of the flask.

$$v_e = \frac{h}{t} = \frac{k^2 \cdot g \cdot (\rho_s - \rho_l)}{18 \cdot \eta}$$

Formula G-1

$$t_{(k)} = \frac{h \cdot 18 \cdot \eta}{k^2 \cdot g \cdot (\rho_s - \rho_l)}$$

Formula G-2

v_e terminal or settling velocity [m/s]

h settling height [m]

t settling time [s]

k particle size [m]

g acceleration due to gravity [m/s^2]

ρ_s solid density [kg/m^3]

ρ_l liquid density [kg/m^3]

η dynamic viscosity [Pa s]

For sample preparation, material is fed to the bottle and filled up with fluid. It is important to use process fluid for the procedure, since several factors like salinity, viscosity and density influence the particle sedimentation. After homogenising the mixture in the bottle by shaking, the bottle is placed on a calm surface and not moved. Now the particles are settling according to their size faster or lower to the bottom. The bigger the grain size, the faster the grains settle. At the cut off grain size, the outlet valve on the bottom is opened after the calculated settling time. The drained suspension is collected for further processing. The flask with the precipitate is filled up again with process fluid and the procedure of homogenisation and settling is repeated until all particles smaller than the cut off grain size are removed. This is indicated by a clear liquid at the calculated settling time for the cut off grain size. All drained suspensions from the separation steps are then combined, filtrated, washed with distilled water and dried. After drying a sample for chemical analysis is prepared. Depending on the number of size classes, the whole procedure is repeated for other cut off grain sizes. Additionally to the preparation of size classes, the grain size distribution can be calculated with the masses from the size classes.

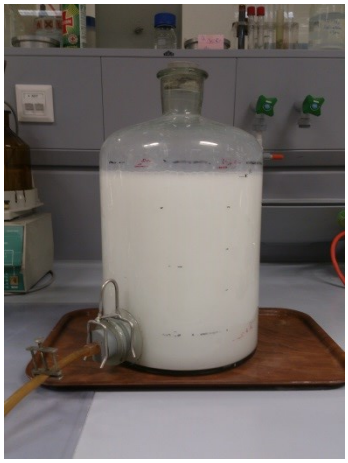

Figure G-1

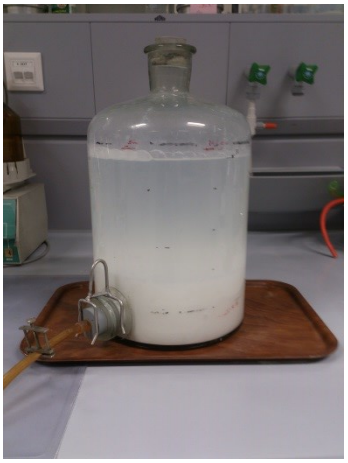

Figure G-2

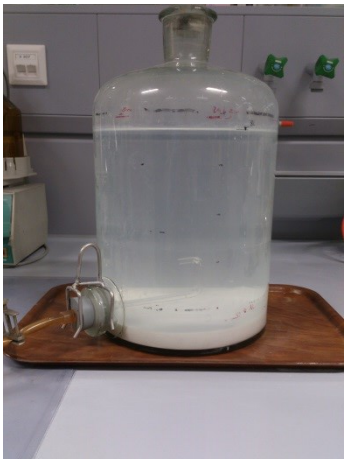

Figure G-3

Except of the great time consumption and the use of huge amounts of process liquid, the method is in general very easy to perform. When using liquids containing calcium hydroxide, air contact of the mixture should be reduced to a minimum, since calcium carbonate can be formed and precipitated with CO_2 from the air.

Appendix H: Classification of the Separation efficiency by Partition Numbers

To evaluate the separation efficiency of a purification step based on classification, partition numbers can be used. Partition numbers are theoretically the proportion of a property that was transferred from the feed to a product (Formula H-1). When grain size distributions are used, the property is size, therefore the partition number gives information about the amount of a grain size class that was transferred from the feed to the product. Illustrated in a partition curve (Figure H-1 and H-2), by combining partition numbers and grain size, an evaluation of the separation efficiency can be done. As separation size, normally the value of PN_{50} is used. That means that 50% of the property from the feed is transferred to the prduct. Also the gradient of the separation and the variation gives information about the separation efficiency. Therefore values like ecart probabe (EP_{ideal} = 0), imperfection (I_{ideal} = 0) and scattering range (X_{ideal} = 1) are calculated (Formulas H-2 to H-4).

$$PN_{i,j} = rm_j \cdot \frac{r_{i,j}}{r_{i,feed}}$$

Formula H-1: Partition number for property i in product j

i	grain size class
j	product
rm_j	proportion of product j by mass [%]
$r_{i,j}$	proportion of size class i in product j [%]
$r_{i,feed}$	proportion of size class i in feed [%]
$PN_{i,j}$	partition number for size class I in product j [%]

To calculate the separation efficiency of a separation process, first the particle size distributions of at least two of the three streams must be measured. If the mass distribution of the products is known (from balancing elemental grades or grades of size classes by solving an overdetermined set of equations) the partition numbers can be calculated (by using Formula 1) for each size class. By convention of area balancing along the x-axis, a continuous curve can be drawn, from which the values PN_{25}, PN_{50} and PN_{75} can be derived.

$$EP = \frac{PN_{75} - PN_{25}}{2}$$

Formula H-2

$$I = \frac{PN_{75} - PN_{25}}{2 \cdot PN_{50}}$$

Formula H-3

$$\chi = \frac{PN_{75}}{PN_{25}}$$

Formula H-4

Calculation of the partition numbers for the sand separator

Table H-1: Mass stream distribution

type	stream	rm [%]
coarse	9SSS	1,94
fine	7OHSAC	98,06
feed	sl. DOLIME	100,00

Table H-2: Calculation of partition numbers

grain size class i		r_{coarse}	r_{fine}	r_{feed}	$PN_{i,coarse}$
[mm]		[%]	[%]	[%]	[%]
2000	>2	0,647	0,000	0,013	100,000
1000	2/1	5,545	0,000	0,108	100,000
500	1/0,5	24,144	0,000	0,468	100,000
200	0,5/0,2	58,724	0,343	1,476	77,186
63	0,2/0,063	3,294	8,597	8,494	0,752
25	0,063/0,025	0,262	12,202	11,970	0,042
0	<0,025	7,384	78,858	77,472	0,185
		100,000	100,000	100,000	

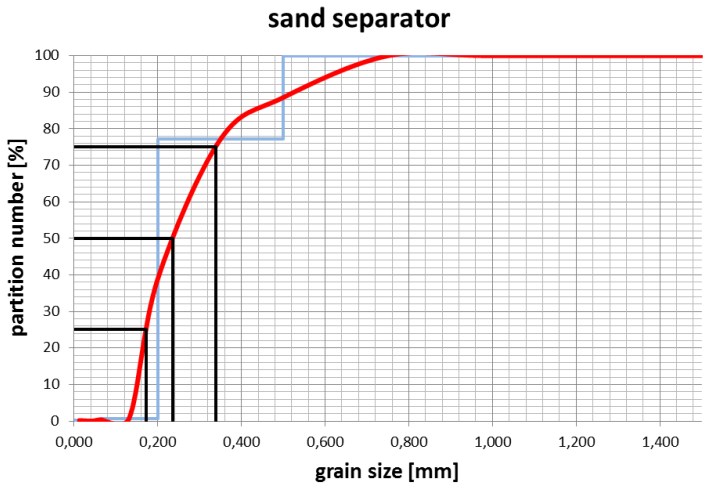

Table H-3: Separation efficiency

	[mm]	characterisation	
PN_{25}	0,172	EP	0,083
PN_{50}	0,235	Imp	0,353
PN_{75}	0,338	X	1,965

Calculation of the partition numbers for the cyclone system

Table H-4 Mass stream distribution

type	stream	rm [%]
coarse	17CBF	5,89
fine	19CVF	94,11
feed	13UPTAB	100,00

Table H-5: Calculation of partition numbers

grain size class i		r_{coarse}	r_{feed}	$PN_{i,coarse}$
[mm]		[%]	[%]	[%]
2000	>2	0,000	0,000	100,000
1000	2/1	0,025	0,000	100,000
500	1/0,5	0,215	0,000	100,000
200	0,5/0,2	5,184	0,437	69,896
63	0,2/0,063	28,814	7,347	23,104
40	0,063/0,04	21,671	6,070	21,030
25	0,04/0,025	11,354	3,817	17,522
0	<0,025	32,738	82,329	2,342
		100,000	100,000	

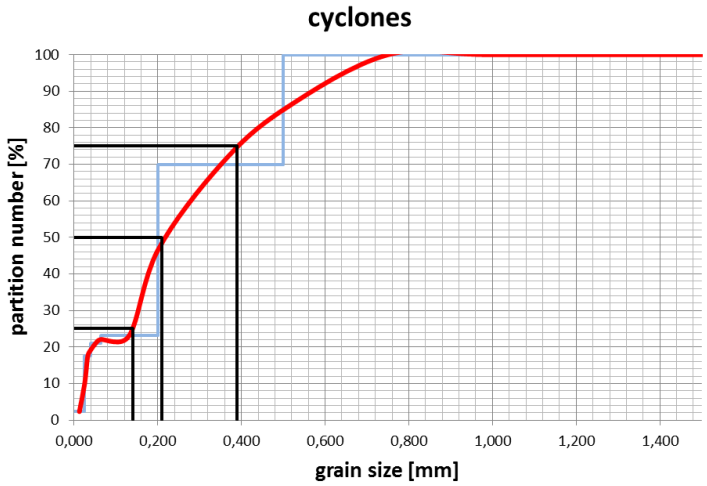

Table H-6: Separation efficiency

	[mm]	characterisation	
PN_{25}	0,140	EP	0,125
PN_{50}	0,210	Imp	0,595
PN_{75}	0,390	X	2,786

Appendix I: Intergrowth and distribution of SiO_2 grades over size classes visualised by Henry-Reinhardt Charts

To visualise enrichments of properties in grain size classes, Henry-Reinhardt charts can be used. To create this type of diagram for grain size classes, a sample has to be first separated by sieving or sedimentation. Then material of every size class is chemically analysed. To illustrate an enrichment of a property, the intergrowth and separation curves are calculated. In the following paragraph the calculation and illustration of a Henry Reinhard diagram is explained with the example of SiO_2 enrichment in the coarse fraction of primary thickener underflow (Figure I-1).

The Henry Reinhardt chart combines the information about liberation (intergrowth curve, purple line) and the best possible separation result with respect to the physical property tested. For the construction of the HR- chart the mass recovery (rmi, [%]) of each property class (in this case a size class) is depicted cumulatively versus the grade of a mineral phase (g_i, [%]) of interest in the assigned property class. Thus a stack of rectangles is created corresponding to the units (defined as the product of $rm_{i,j}$ x $g_{i,j}$, [%%], Formula I-1) of this phase in the order of increasing or decreasing property levels. By graphical area balancing, the discrete mass distribution of grades is transferred into a continuous one, called the "intergrowth curve". Each point of this curve (rm, g) corresponds to a mass fraction of a grade smaller than g. The degree of liberation can easily be assessed from the course of the curve, as the ratio of the units of the liberated mineral phase to the total mineral phase. The black, chain dotted line in the figure indicates the average grade of SiO_2 from which the total units of the phase can be deduced (I_{tot} = 140,76 [%%]). As no class consists only of SiO_2, the degree of liberation is zero [16].

The technical relevance of this chart becomes clear by drawing a horizontal line parallel to the abscissa intersecting the intergrowth curve (red dotted line). The line represents a separation cut of optimum efficiency at the level of the physical property (e.g. grain size of 85 µm). The mass split refers to the mass recoveries of the two products (5,9 % coarse and 94,1 % fine). The average grade of the products is attained by area balancing of the branches of the intergrowth curve above and below the separation line. By repeated construction at varying levels the cumulative curves are obtained depicting all possible average grades of the products [16].

$$I_{i,j} = rm_{i,j} \cdot g_{i,j}$$

Formula I-1: Units of property i in product j

i	property
j	grain size class
rm_j	proportion of grain size class j by mass [%]
$g_{i,j}$	grade of property i in grain size class j [%]
$I_{i,j}$	unit of property i in grain size class j [%]

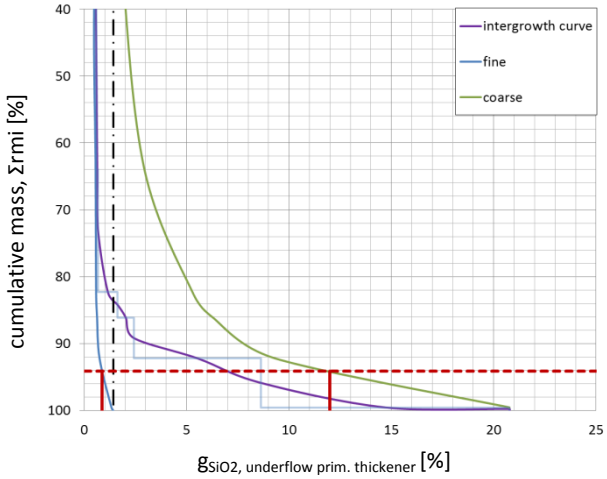

Figure I-1: Henry-Reinhard diagram for total SiO_2 in underflow prim. thickener

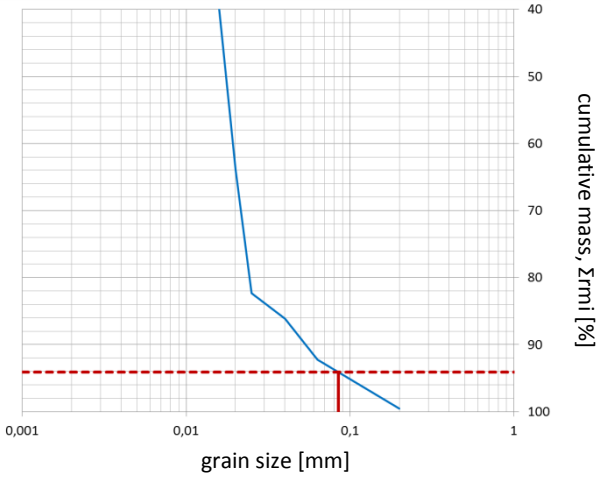

Figure I-2: Cumulative mass distribution of size for underflow prim. thickener

Table I-1: Calculation of Henry-Reinhardt diagram for total SiO_2 in underflow prim. thickener

GS [mm]		intergrowth			passing / fine			retained / coarse		
		rmi [%]	g_{SiO2} [%]	I [%%]	∑rmi [%]	g_{SiO2} [%]	∑I [%%]	100-∑rmi [%]	g_{SiO2} [%]	I_{tot}-∑I [%%]
0	<0,005	0,713	1,330	0,949	0,713	1,330	0,949	99,287	1,408	139,807
0,005	0,010/0,005	0,768	1,070	0,822	1,481	1,195	1,770	98,519	1,411	138,985
0,01	0,015/0,010	32,491	0,480	15,596	33,973	0,511	17,366	66,027	1,869	123,389
0,015	0,020/0,015	29,949	0,590	17,670	63,921	0,548	35,036	36,079	2,930	105,720
0,02	0,025/0,020	18,408	0,670	12,333	82,329	0,575	47,369	17,671	5,285	93,386
0,025	0,04/0,025	3,817	1,630	6,222	86,146	0,622	53,591	13,854	6,292	87,165
0,04	0,063/0,04	6,070	2,420	14,690	92,217	0,740	68,281	7,783	9,311	72,474
0,063	0,2/0,063	7,347	8,630	63,400	99,563	1,323	131,682	0,437	20,770	9,074
0,2	0,5/0,2	0,437	20,770	9,074	100,000	1,408	140,756	0,000		0,000
		100,000	1,408	140,756						

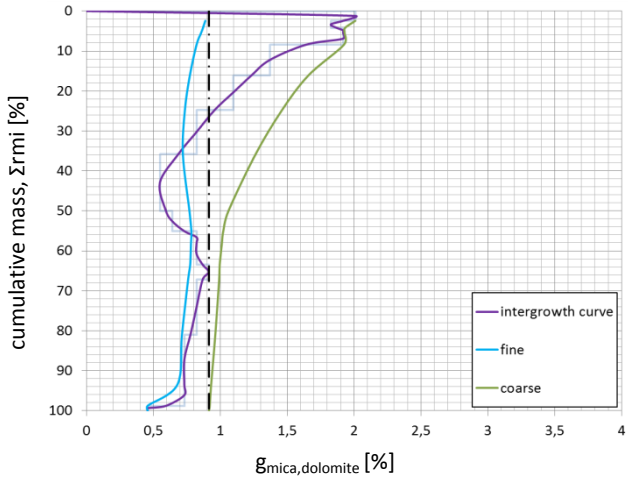

Figure I-3: Henry-Reinhardt diagram for mica in dolomite

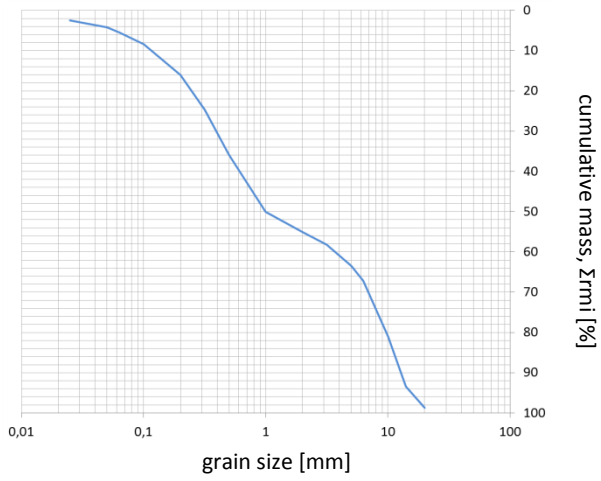

Figure I-4: Cumulative mass distribution of size for dolomite

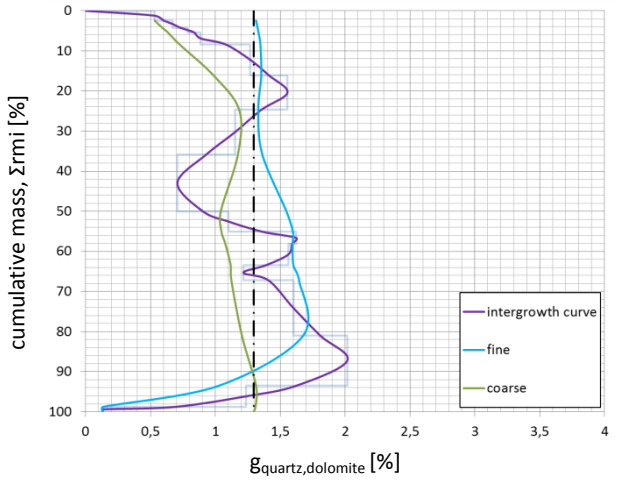

Figure I-5: Henry-Reinhardt diagram for quartz in dolomite

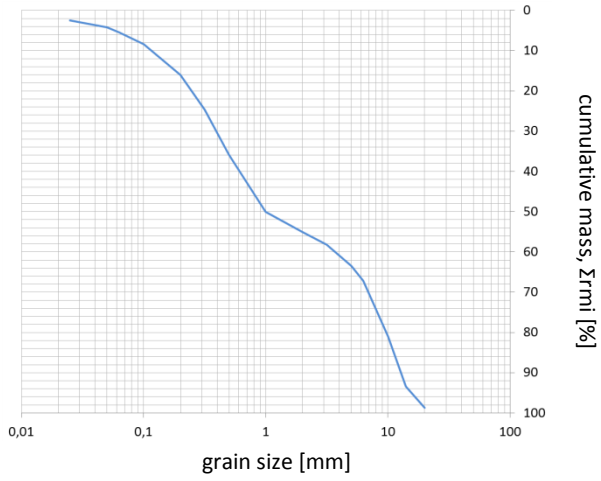

Figure I-6: Cumulative mass distribution of size for dolomite

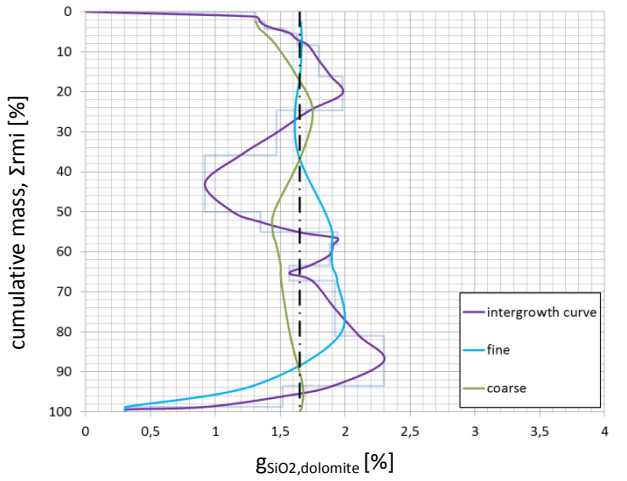

Figure I-7: Henry-Reinhardt diagram for total SiO_2 in dolomite

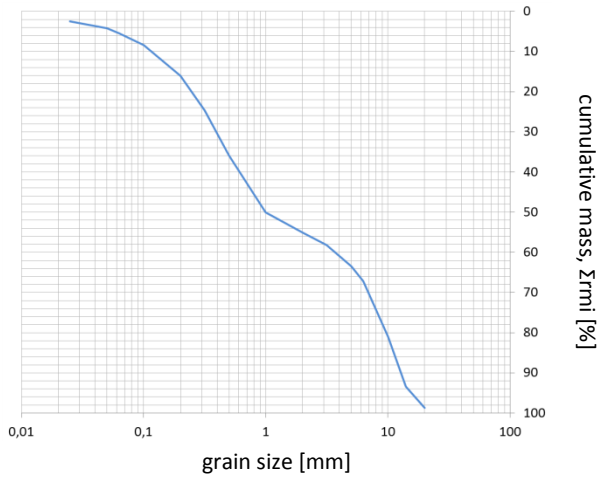

Figure I-8: Cumulative mass distribution of size for dolomite

Table I-2: Calculation of Henry-Reinhardt diagram for mica in dolomite

GS [mm]		intergrowth			passing / fine			retained / coarse		
		rmi [%]	g_{mica} [%]	I [%%]	∑rmi [%]	g_{mica} [%]	∑I [%%]	100-∑rmi [%]	g_{mica} [%]	I_{tot}-∑I [%%]
0	<0,025	2,444	2,009	4,909	2,444	2,009	4,909	97,556	0,887	86,569
0,025	0,05/0,025	1,780	1,826	3,251	4,224	1,932	8,161	95,776	0,870	83,317
0,05	0,063/0,05	1,207	1,918	2,315	5,431	1,929	10,476	94,569	0,857	81,002
0,063	0,1/0,063	2,950	1,918	5,657	8,380	1,925	16,132	91,620	0,822	75,346
0,1	0,2/0,1	7,710	1,370	10,562	16,091	1,659	26,694	83,909	0,772	64,784
0,2	0,315/0,2	8,611	1,096	9,436	24,702	1,463	36,130	75,298	0,735	55,348
0,315	0,5/0,315	11,130	0,822	9,148	35,831	1,264	45,278	64,169	0,720	46,200
0,5	1/0,5	14,188	0,548	7,774	50,019	1,061	53,052	49,981	0,769	38,426
1	2/1	5,066	0,639	3,238	55,085	1,022	56,290	44,915	0,783	35,188
2	3,15/2	3,038	0,822	2,497	58,123	1,011	58,787	41,877	0,781	32,691
3,15	5/3,15	5,328	0,822	4,379	63,451	0,996	63,166	36,549	0,775	28,312
5	6,3/5	3,735	0,913	3,411	67,187	0,991	66,578	32,813	0,759	24,900
6,3	10/6,3	13,830	0,822	11,367	81,017	0,962	77,944	18,983	0,713	13,533
10	14/10	12,437	0,731	9,086	93,454	0,931	87,031	6,546	0,679	4,447
14	20/14	5,322	0,731	3,888	98,776	0,920	90,919	1,224	0,457	0,559
20	25/20	1,224	0,457	0,559	100,000	0,915	91,478		0,457	
		100,000	0,915	91,478						

Table I-3: Calculation of Henry-Reinhardt diagram for quartz in dolomite

GS [mm]		intergrowth			passing / fine			retained / coarse		
		rmi [%]	g_{quartz} [%]	I [%%]	∑rmi [%]	g_{quartz} [%]	∑I [%%]	100-∑rmi [%]	g_{quartz} [%]	I_{tot}-∑I [%%]
0	<0,025	2,444	0,532	1,300	2,444	0,532	1,300	97,556	1,314	128,178
0,025	0,05/0,025	1,780	0,673	1,198	4,224	0,591	2,498	95,776	1,326	126,981
0,05	0,063/0,05	1,207	0,788	0,951	5,431	0,635	3,449	94,569	1,333	126,030
0,063	0,1/0,063	2,950	0,888	2,618	8,380	0,724	6,066	91,620	1,347	123,412
0,1	0,2/0,1	7,710	1,270	9,789	16,091	0,985	15,856	83,909	1,354	113,623
0,2	0,315/0,2	8,611	1,556	13,396	24,702	1,184	29,252	75,298	1,331	100,227
0,315	0,5/0,315	11,130	1,152	12,819	35,831	1,174	42,071	64,169	1,362	87,408
0,5	1/0,5	14,188	0,708	10,043	50,019	1,042	52,114	49,981	1,548	77,365
1	2/1	5,066	1,103	5,585	55,085	1,047	57,699	44,915	1,598	71,780
2	3,15/2	3,038	1,622	4,927	58,123	1,077	62,626	41,877	1,596	66,852
3,15	5/3,15	5,328	1,562	8,321	63,451	1,118	70,947	36,549	1,601	58,531
5	6,3/5	3,735	1,216	4,544	67,187	1,124	75,491	32,813	1,645	53,987
6,3	10/6,3	13,830	1,602	22,153	81,017	1,205	97,644	18,983	1,677	31,835
10	14/10	12,437	2,017	25,088	93,454	1,313	122,732	6,546	1,031	6,747
14	20/14	5,322	1,237	6,584	98,776	1,309	129,316	1,224	0,133	0,163
20	25/20	1,224	0,133	0,163	100,000	1,295	129,479		0,133	
		100,000	1,295	129,479						

Table I-4: Calculation of Henry-Reinhardt diagram for total SiO_2 in dolomite

GS [mm]		intergrowth			passing / fine			retained / coarse		
		rmi [%]	g_{SiO2} [%]	I [%%]	∑rmi [%]	g_{SiO2} [%]	∑I [%%]	100-∑rmi [%]	g_{SiO2} [%]	I_{tot}-∑I [%%]
0	<0,025	2,444	1,310	3,201	2,444	1,310	3,201	97,556	1,657	161,695
0,025	0,05/0,025	1,780	1,380	2,457	4,224	1,340	5,658	95,776	1,663	159,239
0,05	0,063/0,05	1,207	1,530	1,847	5,431	1,382	7,505	94,569	1,664	157,392
0,063	0,1/0,063	2,950	1,630	4,808	8,380	1,469	12,312	91,620	1,665	152,584
0,1	0,2/0,1	7,710	1,800	13,879	16,091	1,628	26,191	83,909	1,653	138,705
0,2	0,315/0,2	8,611	1,980	17,049	24,702	1,751	43,240	75,298	1,616	121,656
0,315	0,5/0,315	11,130	1,470	16,361	35,831	1,663	59,601	64,169	1,641	105,295
0,5	1/0,5	14,188	0,920	13,053	50,019	1,453	72,654	49,981	1,846	92,242
1	2/1	5,066	1,350	6,839	55,085	1,443	79,493	44,915	1,901	85,403
2	3,15/2	3,038	1,940	5,894	58,123	1,469	85,387	41,877	1,899	79,509
3,15	5/3,15	5,328	1,880	10,017	63,451	1,504	95,404	36,549	1,901	69,493
5	6,3/5	3,735	1,570	5,865	67,187	1,507	101,268	32,813	1,939	63,628
6,3	10/6,3	13,830	1,920	26,554	81,017	1,578	127,822	18,983	1,953	37,074
10	14/10	12,437	2,300	28,606	93,454	1,674	156,428	6,546	1,294	8,469
14	20/14	5,322	1,520	8,089	98,776	1,666	164,517	1,224	0,310	0,380
20	25/20	1,224	0,310	0,380	100,000	1,649	164,896		0,310	
		100,000	1,649	164,896						

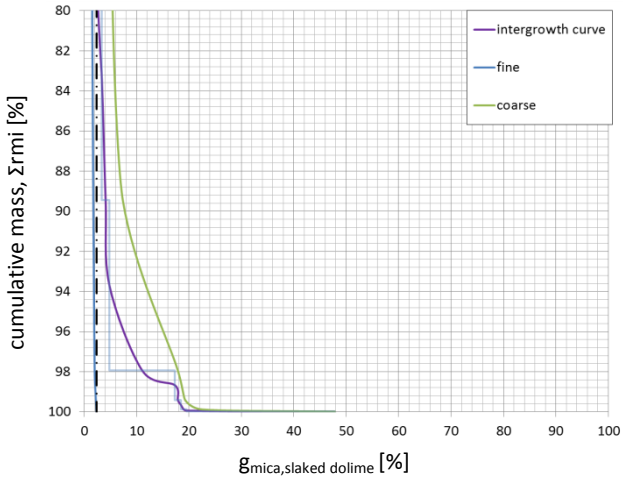

Figure I-9: Henry-Reinhardt diagram for mica in slaked dolime

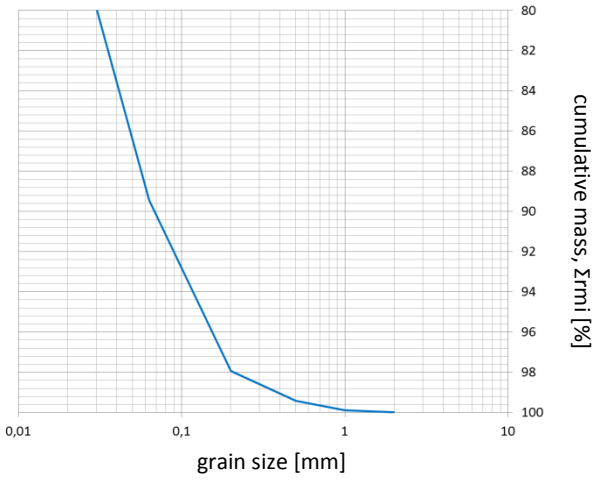

Figure I-10: Cumulative mass distribution of size for slaked dolime

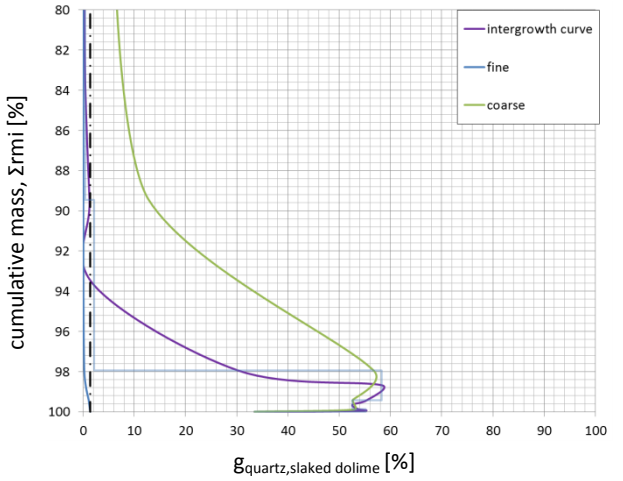

Figure I-11: Henry-Reinhardt diagram for quartz slaked dolime

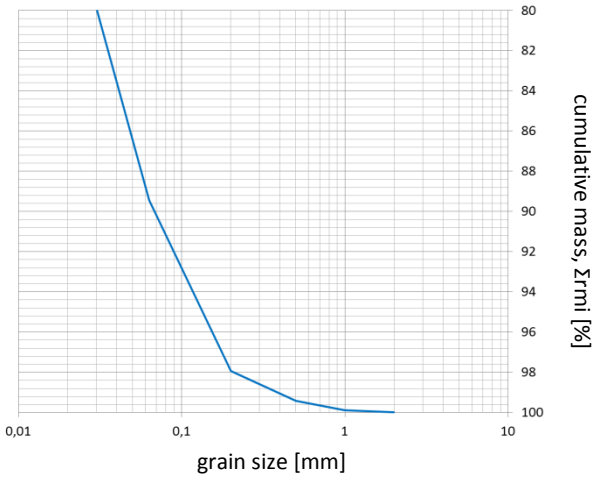

Figure I-12: Cumulative mass distribution of size for slaked dolime

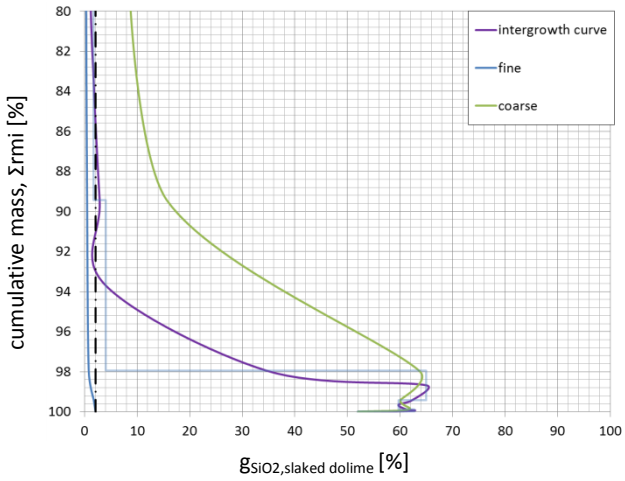

Figure I-13: Henry-Reinhardt diagram for total SiO_2 in slaked dolime

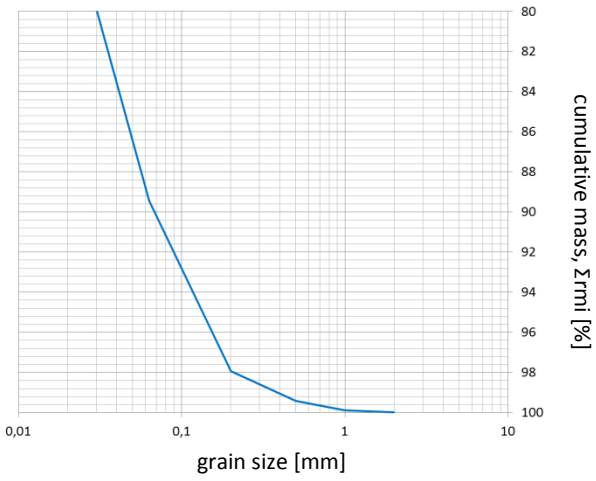

Figure I-14: Cumulative mass distribution of size for slaked dolime

Table I-5: Calculation of Henry-Reinhardt diagram for mica in slaked dolime

GS [mm]		intergrowth			passing / fine			retained / coarse		
		rmi [%]	g_{mica} [%]	I [%%]	∑rmi [%]	g_{mica} [%]	∑I [%%]	100-∑rmi [%]	g_{mica} [%]	I_{tot}-∑I [%%]
0	<0,025	77,472	1,495	115,787	77,472	1,495	115,787	22,528	5,255	118,397
0,025	0,063/0,025	11,970	3,386	40,529	89,442	1,748	156,316	10,558	7,375	77,868
0,063	0,2/0,063	8,494	4,822	40,961	97,936	2,014	197,277	2,064	17,881	36,907
0,2	0,5/0,2	1,476	17,325	25,566	99,412	2,242	222,843	0,588	19,274	11,341
0,5	1/0,5	0,468	18,447	8,639	99,880	2,318	231,482	0,120	22,500	2,702
1	2/1	0,108	19,543	2,102	99,987	2,336	233,584	0,013	47,853	0,600
2	>2	0,013	47,853	0,600	100,000	2,342	234,184	0,000	0,000	0,000
		100,000	2,342	234,184						

Table I-6: Calculation of Henry-Reinhardt diagram for quartz in slaked dolime

GS [mm]		intergrowth			passing / fine			retained / coarse		
		rmi [%]	g_{quartz} [%]	I [%%]	∑rmi [%]	g_{quartz} [%]	∑I [%%]	100-∑rmi [%]	g_{quartz} [%]	I_{tot}-∑I [%%]
0	<0,025	77,472	0,000	0,000	77,472	0,000	0,000	22,528	6,212	139,950
0,025	0,063/0,025	11,970	0,402	4,815	89,442	0,054	4,815	10,558	12,799	135,135
0,063	0,2/0,063	8,494	2,134	18,130	97,936	0,234	22,945	2,064	56,687	117,005
0,2	0,5/0,2	1,476	58,304	86,037	99,412	1,096	108,982	0,588	52,631	30,968
0,5	1/0,5	0,468	52,558	24,613	99,880	1,338	133,595	0,120	52,916	6,355
1	2/1	0,108	55,184	5,935	99,987	1,395	139,530	0,013	33,473	0,420
2	>2	0,013	33,473	0,420	100,000	1,400	139,950	0,000	0,000	0,000
		100,000	1,400	139,950						

Table I-7: Calculation of Henry-Reinhardt diagram for total SiO_2 in slaked dolime

GS [mm]		intergrowth			passing / fine			retained / coarse		
		rmi [%]	g_{SiO2} [%]	I [%%]	∑rmi [%]	g_{SiO2} [%]	∑I [%%]	100-∑rmi [%]	g_{SiO2} [%]	I_{tot}-∑I [%%]
0	<0,025	77,472	0,277	21,449	77,472	0,277	21,449	22,528	8,247	185,790
0,025	0,063/0,025	11,970	1,713	20,507	89,442	0,469	41,956	10,558	15,654	165,283
0,063	0,2/0,063	8,494	4,001	33,988	97,936	0,775	75,944	2,064	63,610	131,294
0,2	0,5/0,2	1,476	65,012	95,936	99,412	1,729	171,880	0,588	60,093	35,359
0,5	1/0,5	0,468	59,700	27,957	99,880	2,001	199,837	0,120	61,627	7,402
1	2/1	0,108	62,750	6,749	99,987	2,066	206,586	0,013	52,000	0,652
2	>2	0,013	52,000	0,652	100,000	2,072	207,238	0,000	0,000	0,000
		100,000	2,072	207,238						

Feed cyclones

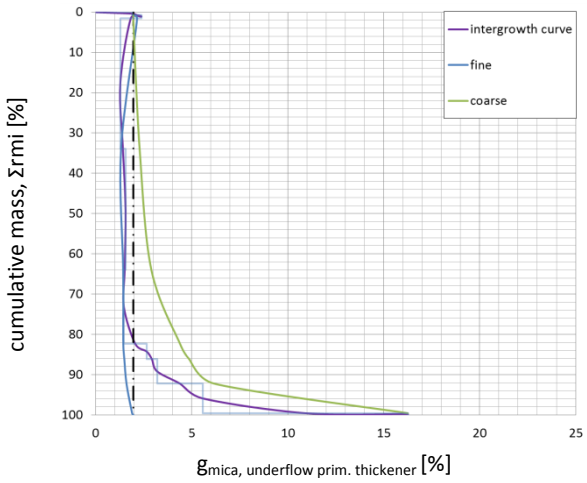

Figure I-15: Henry-Reinhardt diagram for mica in dolomite

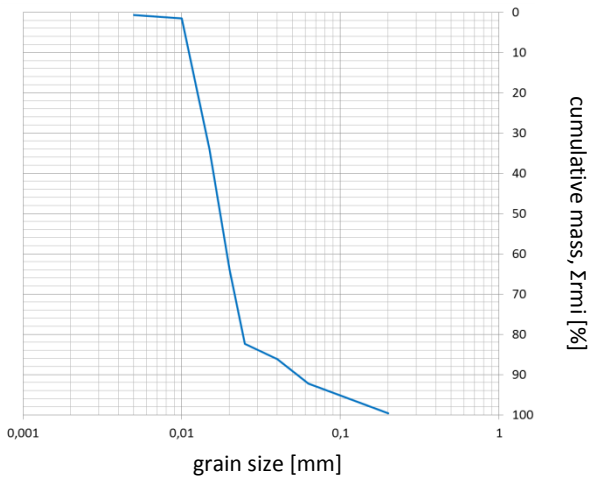

Figure I-16: Cumulative mass distribution of size for underflow prim. thickener

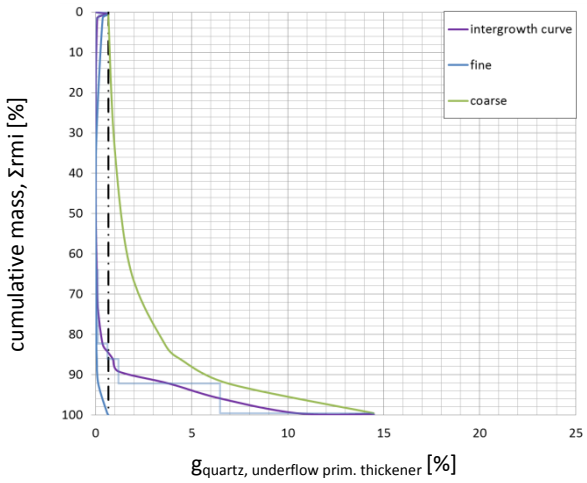

Figure I-17: Henry-Reinhardt diagram for quartz in dolomite

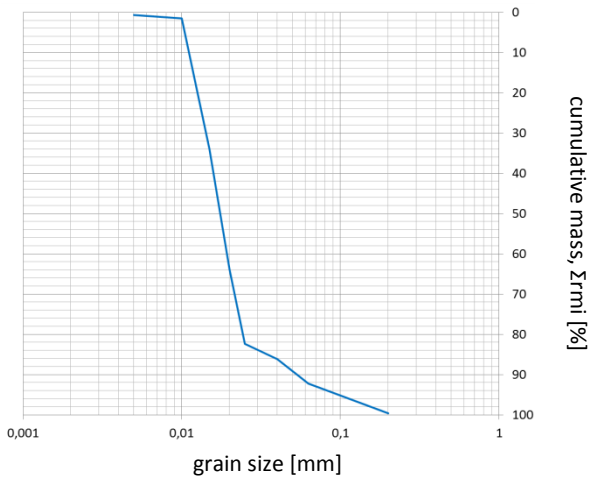

Figure I-18: Cumulative mass distribution of size for underflow prim. thickener

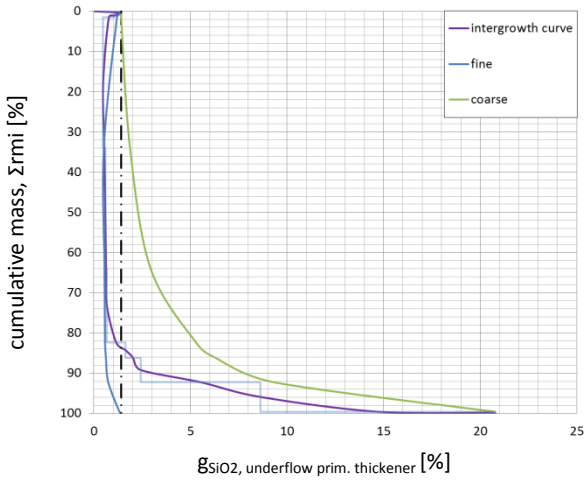

Figure I-19: Henry-Reinhardt diagram for total SiO_2 in dolomite

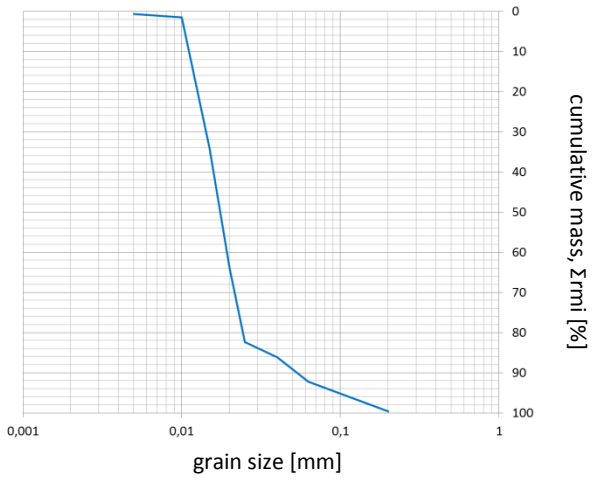

Figure I-20: Cumulative mass distribution of size for underflow prim. thickener

Table I-8: Calculation of Henry-Reinhardt diagram for mica in underflow prim. thickener

GS [mm]		intergrowth			passing / fine			retained / coarse		
		rmi [%]	g_{mica} [%]	I [%%]	∑rmi [%]	g_{mica} [%]	∑I [%%]	100-∑rmi [%]	g_{mica} [%]	I_{tot}-∑I [%%]
0	<0,005	0,713	1,918	1,368	0,713	1,918	1,368	99,287	1,957	194,293
0,005	0,010/0,005	0,768	2,374	1,823	1,481	2,154	3,191	98,519	1,954	192,470
0,01	0,015/0,010	32,491	1,279	41,541	33,973	1,317	44,732	66,027	2,286	150,929
0,015	0,020/0,015	29,949	1,552	46,495	63,921	1,427	91,227	36,079	2,895	104,435
0,02	0,025/0,020	18,408	1,461	26,897	82,329	1,435	118,123	17,671	4,388	77,538
0,025	0,04/0,025	3,817	2,648	10,109	86,146	1,489	128,232	13,854	4,867	67,429
0,04	0,063/0,04	6,070	3,196	19,403	92,217	1,601	147,635	7,783	6,170	48,027
0,063	0,2/0,063	7,347	5,571	40,925	99,563	1,894	188,559	0,437	16,255	7,102
0,2	0,5/0,2	0,437	16,255	7,102	100,000	1,957	195,661	0,000		0,000
		100,000	1,957	195,661						

Table I-9: Calculation of Henry-Reinhardt diagram for quartz in underflow prim. thickener

GS [mm]		intergrowth			passing / fine			retained / coarse		
		rmi [%]	g_{quartz} [%]	I [%%]	∑rmi [%]	g_{quartz} [%]	∑I [%%]	100-∑rmi [%]	g_{quartz} [%]	I_{tot}-∑I [%%]
0	<0,005	0,713	0,588	0,419	0,713	0,588	0,419	99,287	0,659	65,402
0,005	0,010/0,005	0,768	0,151	0,116	1,481	0,361	0,535	98,519	0,663	65,286
0,01	0,015/0,010	32,491	0,000	0,000	33,973	0,016	0,535	66,027	0,989	65,286
0,015	0,020/0,015	29,949	0,000	0,000	63,921	0,008	0,535	36,079	1,810	65,286
0,02	0,025/0,020	18,408	0,104	1,920	82,329	0,030	2,455	17,671	3,586	63,366
0,025	0,04/0,025	3,817	0,605	2,308	86,146	0,055	4,762	13,854	4,407	61,058
0,04	0,063/0,04	6,070	1,183	7,178	92,217	0,129	11,941	7,783	6,922	53,880
0,063	0,2/0,063	7,347	6,473	47,556	99,563	0,598	59,496	0,437	14,476	6,324
0,2	0,5/0,2	0,437	14,476	6,324	100,000	0,658	65,821	0,000		0,000
		100,000	0,658	65,821						

Table I-10: Calculation of Henry-Reinhardt diagram for total SiO_2 in underflow prim. thickener

GS [mm]		intergrowth			passing / fine			retained / coarse		
		rmi [%]	g_{SiO2} [%]	I [%%]	∑rmi [%]	g_{SiO2} [%]	∑I [%%]	100-∑rmi [%]	g_{SiO2} [%]	I_{tot}-∑I [%%]
0	<0,005	0,713	1,330	0,949	0,713	1,330	0,949	99,287	1,408	139,807
0,005	0,010/0,005	0,768	1,070	0,822	1,481	1,195	1,770	98,519	1,411	138,985
0,01	0,015/0,010	32,491	0,480	15,596	33,973	0,511	17,366	66,027	1,869	123,389
0,015	0,020/0,015	29,949	0,590	17,670	63,921	0,548	35,036	36,079	2,930	105,720
0,02	0,025/0,020	18,408	0,670	12,333	82,329	0,575	47,369	17,671	5,285	93,386
0,025	0,04/0,025	3,817	1,630	6,222	86,146	0,622	53,591	13,854	6,292	87,165
0,04	0,063/0,04	6,070	2,420	14,690	92,217	0,740	68,281	7,783	9,311	72,474
0,063	0,2/0,063	7,347	8,630	63,400	99,563	1,323	131,682	0,437	20,770	9,074
0,2	0,5/0,2	0,437	20,770	9,074	100,000	1,408	140,756	0,000		0,000
		100,000	1,408	140,756						

Table J-1: Total composition of material streams

		1DOL	3DOLG	20INT	21HB	4DOLIME	6SW	14FW	7OHSAC	8UHSAC	23U8M	9SSS	11FPT	13UPTAB	15FST	16FBF	17CBF	18UST	19CVF	22FVF
water	[%]	0,00	0,00	0,00	0,00	0,00	96,73	100,00	94,17	92,45	94,10	35,16	94,74	78,93	92,14	95,63	44,37	74,62	52,30	99,72
insoluble rest	[%]	97,57	97,91	97,35	98,08	97,45	0,00	0,00	2,56	3,62	2,70	19,77	2,03	18,06	6,80	3,51	42,11	25,11	47,31	0,26
mica	[%]	0,88	0,70	0,82	1,70	1,14	0,00	0,00	0,03	0,30	0,16	9,28	0,02	0,24	0,02	0,56	7,89	0,09	0,22	0,00
quartz	[%]	1,54	1,39	1,83	0,22	1,41	0,00	0,00	0,01	0,46	0,21	35,65	0,00	0,10	0,00	0,29	5,40	0,01	0,00	0,00
soluble (salt)	[%]	0,00	0,00	0,00	0,00	0,00	3,27	0,00	3,23	3,17	2,83	0,14	3,20	2,66	1,03	0,01	0,23	0,17	0,17	0,02
total	[%]	100,00	100,00	100,00	100,00	100,00	100,00	100,00	100,00	100,00	100,00	100,00	100,00	100,00	100,00	100,00	100,00	100,00	100,00	100,00

Table J-2: Composition of washed and dried material

		1DOL	3DOLG	20INT	21HB	4DOLIME	7OHSAC	8UHSAC	23U8M	9SSS	11FPT	13UPTAB	15FST	16FBF	17CBF	18UST	19CVF	22FVF
CaO	[%]	57,47	57,49	57,33	57,93	57,37	2,09	8,40	5,88	17,92	1,54	2,13	1,61	2,94	3,35	1,41	1,38	1,87
MgO	[%]	40,16	40,15	40,00	40,44	40,20	96,46	76,60	84,00	18,06	97,10	95,94	97,66	82,47	78,42	97,68	97,85	97,29
mica	[%]	0,88	0,70	0,82	1,70	1,14	1,04	6,76	5,21	14,34	1,07	1,32	0,37	12,88	14,25	0,37	0,46	0,64
quartz	[%]	1,54	1,39	1,83	0,22	1,41	0,29	10,60	6,77	55,10	0,21	0,56	0,01	6,75	9,74	0,05	0,00	0,04
total	[%]	100,00	100,00	100,00	100,00	100,00	100,00	100,00	100,00	100,00	100,00	100,00	100,00	100,00	100,00	100,00	100,00	100,00